

2010

Lipid Chemistry and Mechanical State of the Membrane Modulate Ion Channel Function

Daniel Schmidt

Follow this and additional works at: http://digitalcommons.rockefeller.edu/student_theses_and_dissertations

 Part of the [Life Sciences Commons](#)

Recommended Citation

Schmidt, Daniel, "Lipid Chemistry and Mechanical State of the Membrane Modulate Ion Channel Function" (2010). *Student Theses and Dissertations*. Paper 102.



LIPID CHEMISTRY AND MECHANICAL STATE OF THE MEMBRANE
MODULATE ION CHANNEL FUNCTION

A Thesis Presented to the Faculty of
The Rockefeller University
in Partial Fulfillment of the Requirements for
the degree of Doctor of Philosophy

by
Daniel Schmidt
June 2010

Lipid Chemistry and mechanical state of the membrane modulate ion channel function

Daniel Schmidt, Ph.D.

The Rockefeller University 2010

My research focused on voltage-dependent K^+ (K_v) channels. K_v channels serve many different functions in different cells, but most notably underlie action potentials in electrically excitable cells, such as neurons and muscle (Hodgkin and Huxley, 1952, 1945). K_v channel gating is governed by the transmembrane voltage, they are therefore voltage-dependent switches for ionic current (Hille, 2001). Changes in the transmembrane voltage are sensed by the channel's voltage sensor domains, which contain charged amino acids (most often arginines) called gating charges.

Shortly before I started to work on my PhD project, the crystal structure of the eukaryotic $K_v1.2$ channel had been solved. This structure reinforced the idea that the voltage sensors are arranged as independent domains at the perimeter of a K_v channel facing the lipid membrane, thus exposing some of the gating charges to the lipid. The obvious question to ask at that time was, given the energetic penalty for placing charged amino acids inside the hydrophobic core of the membrane, how does the lipid membrane stabilize the arginine residues? By studying the recombinantly-expressed archæal K_v channel KvAP in an artificial membrane system that allowed me to create a defined lipid environment, I could show that the lipid membrane provides an environment that is suitable for voltage sensors because the lipid's phosphate groups serve as countercharges for the voltage sensor's arginine residues. I came to the conclusion that a direct interaction between the arginine side chains and lipid phosphodiester stabilizes the voltage sensor through multidentate hydrogen bonding. I suggested that the usage of positively charged amino acids in voltage sensors is an adaptation to the phospholipid composition of the cell membrane.

Prompted by these results, I studied the gating properties of KvAP in different lipid systems and was able to derive the first quantitative kinetic gating model for KvAP. I found that, unlike the well studied eukaryotic Shaker K_v channel, KvAP possesses an inactivated state that is accessible from the pre-open state of the channel. Changing the lipid composition of the membrane influences multiple gating transitions in the model, but most dramatically the rate of recovery from this inactivated state. I also showed that inhibition by the spider toxin VSTx1 is most easily explained if VSTx1 binds only to the depolarized conformation of the voltage sensor. By delaying the voltage sensor's return to the hyperpolarized conformation VSTx1 favors the inactivated state of KvAP.

Aside from varying the chemical composition, I also studied how the mechanical state of lipid membranes influences K_v channel gating. I found that K_v channels are mechanosensitive proteins and that a model in which membrane tension influences a single parameter (the equilibrium constant governing pore-opening after the voltage sensors have moved) can account quantitatively for complex changes in voltage-dependent gating, that are caused by the formation of tight lipid/glass seal in patch clamp recordings. The mechanical state of the membrane also governs the apparent affinity of spider toxins for K_v channels. This unexpected relationship between voltage sensor toxin affinity and the mechanical state of the membrane suggests that the toxin modifies the membrane mechanical forces experienced by the K_v channel.

In summary, my thesis research describes how both the chemical and mechanical properties of lipid membranes regulate K_v channel function and pharmacology. These results demonstrate that the lipid membrane is not solely a passive solvent for membrane proteins, but that its composition and structure might be considered a source for functional diversity, enabling a membrane protein's function to be tuned to the requirements of a particular cell type.

To my mentor Rod MacKinnon.

Acknowledgements

I would like to thank Professor Rod MacKinnon for his support, enthusiasm and extraordinary mentorship.

I am greatly indebted to all members of the MacKinnon lab, particularly my co-workers Qiu-Xing Jiang and Sam Cross for collaborating with me on several projects as well as Alice MacKinnon and Xiao Tao for technical assistance and advice.

Special thanks go to the members of my thesis committee, Professors Brian Chait, Tom Muir and Fred Sigworth, for their time and attention. I am filled with gratitude for the kindness of Professor Günter Blobel to enable my first scientific endeavors as visiting student in his laboratory.

I gratefully acknowledge the fantastic support I received from the Boehringer Ingelheim Fonds.

Disclaimer

Qiu-Xing Jiang performed the KvAP recordings in planar lipid bilayer made of DOGS, DOG and DOPA (Chapter 2.1.2). Samuel R. Cross performed the global fitting in Chapter 2.2.2 and collected the experimental data for Figures 2.13.g and 2.14.g.

Table of Contents

	iii
Acknowledgements	iv
Disclaimer	v
1 Background	1
1.1 Membrane Models	1
1.2 Lipid Diversity	2
1.3 Lipids Organize the Membrane into Microdomains	4
1.4 The Nature of Protein-Lipid Interactions	6
1.5 Influence of Headgroup Chemistry on Lipid Binding	8
1.6 Influence of Acyl Chain Length on Lipid Binding	8
1.7 Lipid Microdomains as Signaling Platforms	9
1.8 Ion channels can be Localized to Microdomains	10
1.9 Membrane Properties alter Ion Channel Function	11
1.10 ‘Design’ Principles of Mechanosensitivity	12
1.10.1 The Composite Structure of the Cell Boundary	13
1.10.2 The Modes of Bilayer Deformation	15
2 Thesis Research	21
2.1 Phospholipids and Cationic Gating Charges	21
2.1.1 Introduction	21
2.1.2 Results	22
2.1.3 Discussion	29
2.2 KvAP’s Refractory State	33
2.2.1 Introduction	33
2.2.2 Results	34
2.2.3 Discussion	47
2.3 Gating Comparison of K_v Channels	49

2.3.1	Introduction	49
2.3.2	Results	49
2.3.3	Discussion	72
3	Conclusions and Outlook	75
3.1	The origin of cationic gating charges	75
3.1.1	The lipid membrane stabilizes voltage sensor conformation during gating	76
3.1.2	Molecular Evolution of Voltage Sensors	76
3.1.3	Voltage sensors enrich phospholipids in the protein vicinity	78
3.2	Voltage Sensor Toxins	79
3.3	Intrinsic Mechanosensitivity	82
3.3.1	Precedent for mechanosensitivity in eukaryotic ion channels	83
3.3.2	Artifacts from lipid glass interaction - increased membrane tension	88
3.3.3	Mechanoprotective role of the cytoskeleton	90
3.3.4	The biological relevance of tension regimes	92
4	Material and Methods	95
4.1	Protein purification and reconstitution	95
4.1.1	KvAP	95
4.1.2	MthK	96
4.1.3	K _v 1.2 and Paddle Chimæra	97
4.2	Electrophysiology	97
4.2.1	Bilayer Recordings	97
4.2.2	Whole Oocyte Recordings	98
4.2.3	Patch Clamp Recordings	98
4.3	Kinetic Modeling	99
5	Appendices	101
5.1	Tension Scaling	101
5.2	K _v channel open probability derivation	102
	References	104

List of Figures

1.1	Chemical diversity of Lipids	3
1.2	Lipid composition of cell membranes and signaling lipids.	5
1.3	Relative lipid binding constants for OmpF, KcsA and Ca ²⁺ -ATPase.	7
1.4	Lipid effects on Ca ²⁺ -ATPase activity.	19
1.5	Modes of Bilayer Deformation	19
2.1	Assessment of KvAP function in phospholipid and DOTAP membranes.	23
2.2	Assessment of MthK function in DOTAP membranes.	24
2.3	KvAP function depends on membrane lipid composition.	25
2.4	KvAP function depends on membrane lipid composition (DOTAP titration).	26
2.5	KvAP function depends on membrane lipid composition (DOGS & GlucCer).	27
2.6	A Phosphate group is important for KvAP voltage-dependent gating (Acyl chain length).	28
2.7	Phosphate group is important for KvAP voltage-dependent gating (DOG & DOPA).	30
2.8	Role of the negative charge on the phosphate group.	31
2.9	Assessment of MthK function in EDOPC membranes.	32
2.10	Multidentate hydrogen-bonding between lipid phosphodiester and voltage sensor arginines.	33
2.11	A Comparison of inactivation in KvAP and Shaker K _v channels.	35
2.12	The accumulation of inactivation between pulses follows a geometric series.	37
2.13	A detailed kinetic gating scheme for KvAP in DPhPC decane bilayers.	38
2.14	A detailed kinetic gating scheme for KvAP in POPE:POPG decane bilayer.	42
2.15	Voltage sensor toxin VSTx1 and nature of the inactivated state.	45
2.16	Voltage sensor toxin VSTx1 and nature of the inactivated state (<i>cont.</i>).	46

2.17	The membrane regulates gating.	50
2.18	The membrane regulates toxin sensitivity.	51
2.19	The membrane regulates gating (<i>cont.</i>).	52
2.20	The effect of lipid composition.	53
2.21	The effect of membrane configuration (oocytes).	55
2.22	The effect of membrane configuration (SF9).	56
2.23	The effect of membrane forces (Paddle Chimæra).	57
2.24	The effect of membrane forces (Open probability).	58
2.25	The effect of membrane forces (Shaker K_v).	59
2.26	The effect of membrane forces ($K_v2.1$).	60
2.27	Lipid-Glass Adhesion.	62
2.28	A structural description.	63
2.29	Global fit for tension scaling.	66
2.30	Tension sensitivity at different membrane voltages.	68
2.31	Membrane mechanics and voltage sensor toxins.	70
2.32	Pore-blocking toxin CTX affinity.	71
2.33	Membrane mechanics and voltage sensor toxins (<i>cont.</i>).	73

List of Tables

1.1	Lipid association constants	6
2.1	Fitting parameters for tension scaling	69

Chapter 1

Background

1.1 Membrane Models

The cell membrane is a structural scaffold that ensures the physical integrity of the cell while at the same time is flexible to allow for the growth and changes in cell shape. The primary role of biological membranes is to separate the cellular components from the external environment. Because of this separation, it is possible to create and maintain gradients of molecules between the cell and its surroundings. By the virtue of membrane components that allow for selective transport processes across the membrane, cells use such gradients for a variety of processes, for example cell signaling, nutrient uptake and the production of energy equivalents. The molecules that make up biological membranes reflect these requirements. The chemical structure of lipid molecules facilitates their self-assembly into a lipid bilayer with a hydrophobic region sandwiched between two hydrophilic outer layers. The hydrophobic layer forms an insurmountable barrier to the free diffusion of hydrophilic molecules. This barrier can only be overcome by specific protein carriers and transport systems. It is estimated that in the absence of specific transport systems 4000 water molecules per second and per phospholipid molecule can pass the lipid bilayer compared to only one sodium ion every 70 hours (Deamer and Bramhall, 1986). Another defining property of biological membranes is their extremely large aspect ratio. This again is due to the lipid molecules' self-assembly into a bilayer with lateral dimensions that are typically much larger than the bilayer thickness of 5 nm. As a consequence, the elastic models that describe membrane deformations are two-dimensional and focus on stretching & bending of a planar sheet (Wiggins and Phillips, 2005). Early models of biological membranes such as the Singer-Nicolson (S-N) fluid mosaic membrane model (Singer and Nicolson, 1972) approximate them to be a “two-dimensional solution of integral

membrane proteins... in the viscous phospholipid bilayer". The S-N model assumes macroscopically uniform lipid composition, easy lateral movement of membrane proteins that are distributed randomly across the membrane and cannot move out of the plane of the bilayer. However, this description does not consider the compositional complexity of biological membranes. Membranes can contain hundreds of different lipid species, peripheral and integral membrane proteins, all of which can be modified by various carbohydrates. Both lipid and protein often associate with other cellular components such as the cytoskeleton or the extracellular matrix. Experimental data support the idea that this compositional heterogeneity gives rise to a great deal of structural heterogeneity (Dowhan, 1997; Edidin, 2003). In recent years the S-N model has been modified to shift its emphasis away from fluidity towards mosaicity. Mosaicity has mostly been studied through optical methods, like confocal microscopy or single particle tracking (Edidin, 2003). These studies congruently support the notion of a mosaic distribution of membrane proteins and lipids into microdomains, *aka* lipid rafts (see Chapter 1.3).

1.2 Lipid Diversity

It is estimated that 5% of a cell's genes are involved in the synthesis of the more than 1000 different lipid species (Dowhan, 1997). The connected energetic cost of gene upkeep implies that both cellular structure and function must depend on this diversity. Lipid molecules are chemically very diverse (see Figure 1.1), but can be broadly characterized as belonging to two groups. Glycerophospholipids consist of a hydrophilic headgroup and a hydrophobic diacylglycerol that contains saturated or *cis*-unsaturated fatty acyl chains of varying length. Phosphatidylcholine (PC), phosphatidylethanolamine (PE), phosphatidylinositol (PI), phosphatidylserine (PS) and phosphatidic acid (PA) make up the five structural lipids in eukaryotes. PC accounts for more than 50% in most membranes and most PC molecules contain at least one *cis*-unsaturated acyl chain to ensure that the planar bilayer remains in the liquid crystalline phase over a biologically relevant temperature range (i.e. 0 – 45 °C) (Figure 1.2). Because of their almost perfect cylindrical shape, PC molecules self-organize into planar bilayers. Conversely, the conically shaped PE and cardiolipin (CL) introduce curvature stress, as does the asymmetric distribution of various lipids between the leaflets of a lipid bilayer. Regions of local curvature stress are called frustrated bilayers; they are important in many biological processes such as membrane fission, fusion and folding (Marsh, 2007). They are also important for accom-

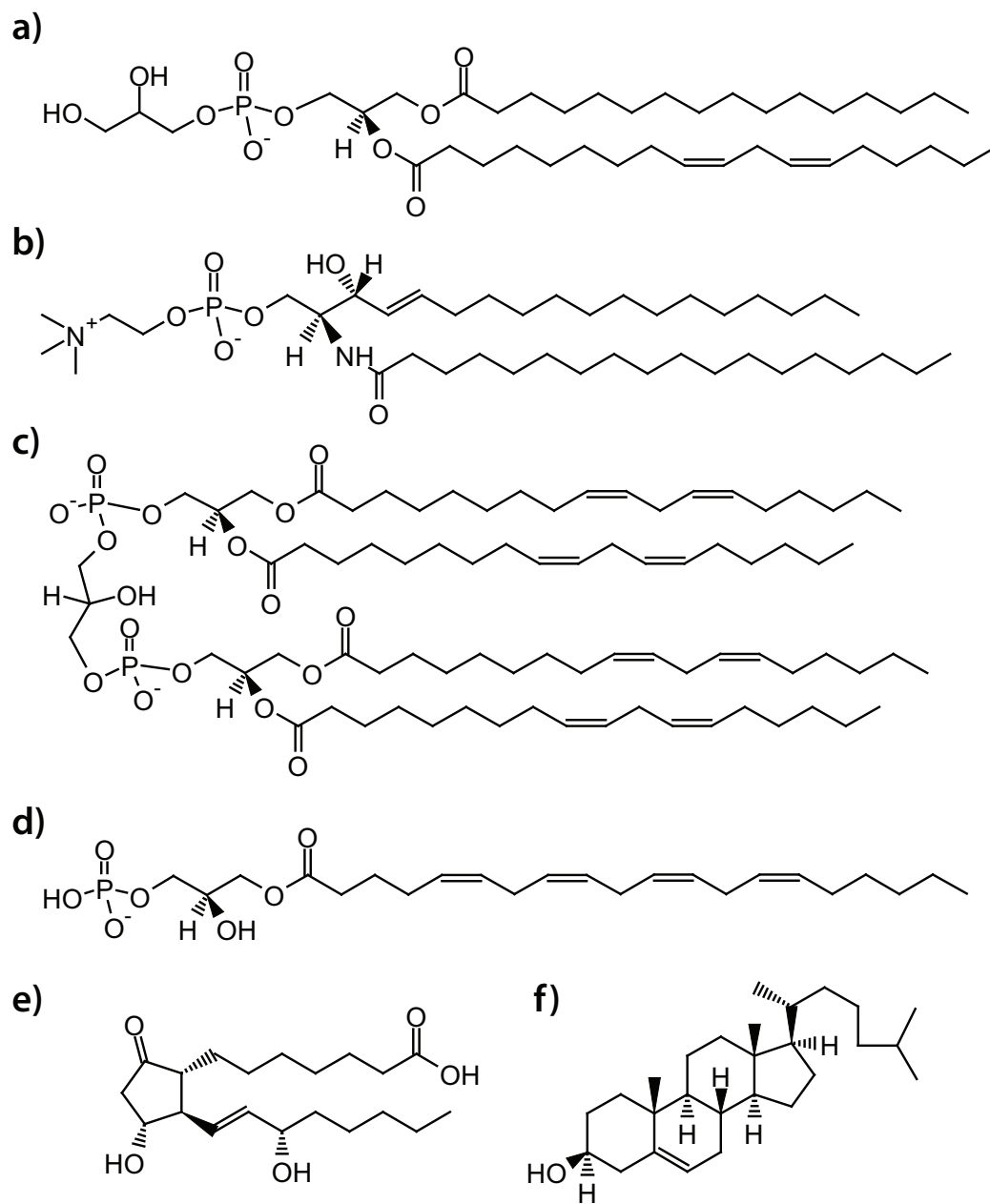


Figure 1.1: **Chemical diversity of structural and signaling lipids.** a, Phosphatidylglycerol b, Sphingomyelin c, Cardiolipin d, Lyso-Phosphatidic Acid e, Cholesterol f, Prostaglandin E.

modating and modulating the activity of peripheral membrane proteins (Dowhan and Bogdanov, 2002; Marsh, 2007). The other main class of structural lipids is sphingolipids. Their hydrophobic backbone is made up of ceramide (Cer) which is a condensation product of one fatty acyl chain and sphingosine, both of which can be saturated or *trans*-unsaturated. The major mammalian sphingolipids are sphingomyelin (Sm) and glycosphingolipids, which make up the majority of the lipid in neuronal tissue. Due to the absence of *cis*-unsaturated bonds in sphingolipids, they can pack more tightly and by themselves would form a lipid gel phase. Hydrophobic molecules such as sterols (cholesterol in mammals and ergosterol in fungi) fluidize sphingolipid-containing membrane phases. A large battery of signaling lipids can be generated from both glycerophospho- and sphingolipids: *lyso*-PC (LPC), *lyso*-PA (LPA), diacylglycerol (DAG), sphingosine (Sph), ceramide-1-phosphate (C1P) and many others (Wymann and Schneider, 2008). Some of them readily partition into the aqueous environment and can communicate paracrine cell-to-cell signals (Meyer zu Heringdorf and Jakobs, 2007). Another class of important signaling lipids are phosphorylated derivatives of PI, that can recruit both soluble and membrane proteins to specific membranes, thus defining organelle identity (Munro, 2002).

1.3 Lipids Organize the Membrane into Microdomains

What chemical and physical forces give rise to the observed microdomains? Some focus has been put on the very nature of the lipid molecules themselves and the reason why there is such a variety of them. It was suggested that lipids and other membrane-associated small molecules like cholesterol tend to form multiple types of *microdomains* with lateral dimension of 4 to 700 nm in fluid-mixed bilayers governed by their chemical properties, molecular shape and the charge distribution (Edidin, 2003; Simons and Ikonen, 1997; Somerharju et al., 1999; Virtanen et al., 1998; Volonte et al., 1999). It was proposed that these microdomain structures do not cover all of the membrane but are in rapid equilibrium with other membrane areas in which the lipids are distributed randomly. Lipid probes with saturated acyl chains spend an average of 13 milliseconds in a given local microdomain (Schütz et al., 2000). In freshly fused cell it takes certain membrane protein components approximately 20 minutes to intermix, while other membrane components mix quickly (Nagy et al., 2001). This suggests a hierarchy of membrane organization with some membrane areas at fast and some at slow equilibrium with the bulk lipid phase.

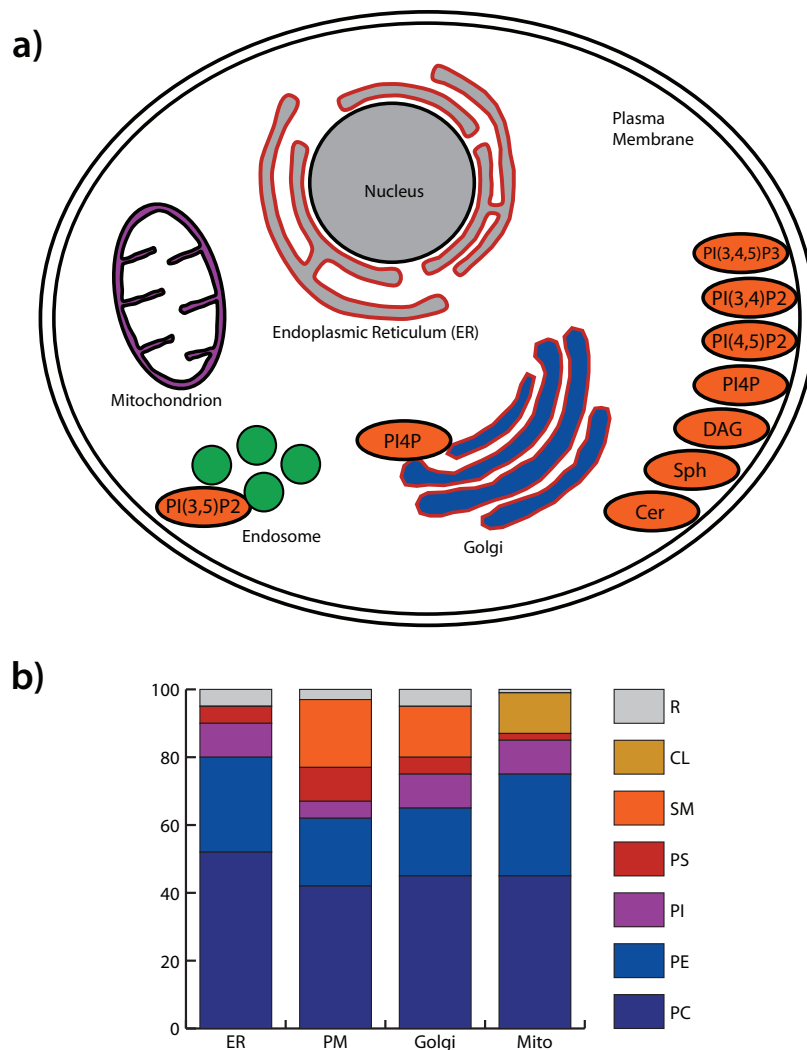


Figure 1.2: **Steady-state lipid composition of cell membranes and signaling lipids.** The cellular membrane compartments vary in lipid composition. **a**, Cell compartments and the localization of signaling lipids (orange circles). Except for Ceramide (Cer) the levels of signaling lipids is below 1% of the total lipid content of the cell. **b**, Composition of subcellular membranes according to headgroup chemistry. The majority of cell lipids are synthesized at the Endoplasmic reticulum and Golgi (red lining). The exception is the Mitochondrion which synthesizes some lipids autonomously, in particular Cardiolipin (CL). Modified from (van Meer et al., 2008).

Membrane proteins themselves could alter the structure of microdomains through a free energy optimization of protein-lipid interaction profiles. It was shown experimentally that the composition of an α -helix can determine the specific lipid environment it prefers (Lewis et al., 2001). Other examples of selective lipid accumulation that best matches the transmembrane segment of an integral membrane protein are described for the *E. coli* lactose-permease reconstituted into liposomes (Lehtonen and Kinnunen, 1997) and bacteriorhodopsin in a binary Didodecyl-PC/Dioleoyl-PC (DDo-decPC/DOPC) lipid system (Dumas et al., 1997). When a membrane consists of two or more lipid phases, the free energy of embedding a membrane protein can be lowered by surrounding it with the lipid phase that provides the lowest protein-lipid interaction potential. This preferred phase is said to wet the protein (Gil et al., 1997). Sharing the wetting layer between two or more proteins can give rise to capillary condensation: membrane proteins can aggregate and thus reduce the surface area that is interacting unfavorably with another phase. Capillary condensation has been demonstrated to drive the oligomerization and activity of bacteriorhodopsin (Botelho et al., 2006). Wetting and capillary condensation are means to organize membrane proteins in lipid membranes of complex composition (Gil et al., 1998).

1.4 The Nature of Protein-Lipid Interactions

Electron spin resonance studies (ESR) employ spin-labeled lipids that can be incorporated into both native and reconstituted lipid membranes; they provide information about the mobility of lipid molecules. ESR spectra of spin-labeled lipids in native membrane or reconstituted lipid-protein systems show that a number of labeled lipids are immobilized when compared to protein-free membranes (Brotherus et al., 1981; Jost and Griffith, 1978; Marsh and Horváth, 1998; Marsh et al., 1982; Powl et al., 2005). The presence of this subpopulation can be explained by the reduced motional freedom of a lipid molecule that has to pack against the uneven exterior of a membrane protein in order to maintain the integrity of the lipid membrane as a permeability barrier. These lipid molecules adopt a disordered conformation to maximize the contact area with the protein. The ensemble of distorted lipid molecules around the exterior of a membrane protein is called the annular lipid shell.

ESR studies can be used to estimate the number of annular lipids around a membrane protein such as the Ca^{2+} -ATPase. The measured number of annular lipids, 32, agrees well the minimal number of lipid molecules required to form a bilayer shell one

Table 1.1: Lipid association constants relative to Phosphatidylcholine

Protein	Association Constants				
	CL	PA	PS	PG	PE
Cytochrome c oxidase	2.7	1.9	1.0	1.0	1.0
Cytochrome c reductase	0.7	2.4	1.8	1.7	1.3
Na ⁺ ,K ⁺ -ATPase	1.9	1.5	1.7	0.9	0.9
Acetylcholine Receptor	-/-	2.7	0.7	-/-	1.1
Bacteriorhodopsin	1.0	1.0	1.0	1.0	1.0

lipid wide around the circumference of the protein (Marsh and Horváth, 1998). This indicates that the annular lipid shell does not extend much beyond one or two lipid molecules into the surrounding bulk lipid phase. Apart from annular lipids binding at the exterior of the protein, there are specific binding pockets for lipid molecules within the core of the protein. These pockets are called non-annular sites and most lipids that bind in such sites fulfill a specialized function (oligomerisation, catalytic activity etc.), acting as a prosthetic group (de Foresta et al., 1989; Simmonds et al., 1984, 1982). In fact, a wide range of hydrophobic molecules can bind in these non-annular sites, as shown in the case of the Ca²⁺-ATPase (de Foresta et al., 1989; Froud et al., 1986), bacteriorhodopsin (Cartailler and Luecke, 2003; Luecke et al., 1998), acetylcholine receptor (Jones and McNamee, 1988) and the Photosystems I&II (Guskov et al., 2009; Jordan et al., 2001).

ESR studies, together with studies of the quenching of protein fluorescence by spin-labelled or brominated phospholipids can also provide an estimate of relative binding constant for various lipid species (Brotherus et al., 1981; East and Lee, 1982; Jost and Griffith, 1978; London and Feigenson, 1981a,b; Marsh and Horváth, 1998). Assuming that lipid-protein interactions can be described as a competitive binding equilibrium of different lipid species at a number of sites on the protein, there will be an association constant K_A that can express the relative lipid affinities. Table 1.1 reproduces the association constants of several lipid species to membrane proteins.

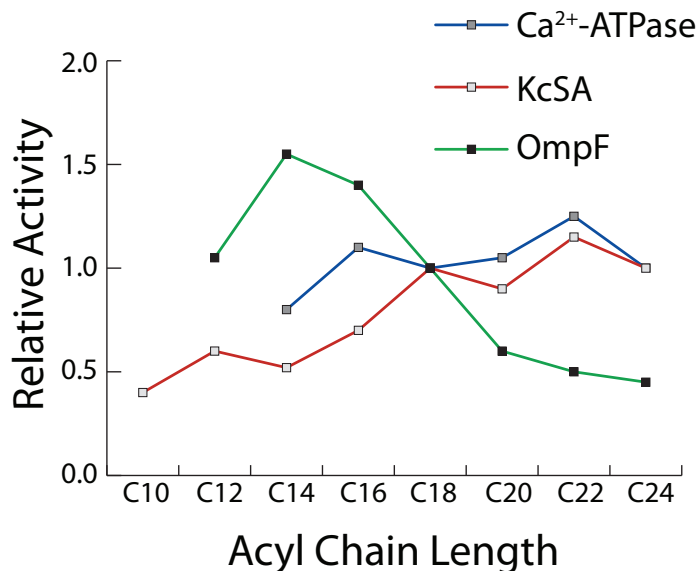


Figure 1.3: **Relative Lipid Binding Constants for OmpF, KcsA and Ca²⁺-ATPase.** Relative binding constant of Phosphatidylcholines with varying acyl chain length compared to DOPC. Modified from (East and Lee, 1982; O’Keeffe et al., 2000; Williamson et al., 2002).

1.5 Influence of Headgroup Chemistry on Lipid Binding

As apparent from Table 1.1, most investigated proteins do not have a strong selectivity for a particular annular lipid headgroup chemistry. The small preferences for anionic phospholipids can be decreased with increasing ionic strength indicating an important electrostatic component of the interaction (Marsh and Horváth, 1998). It is important to point out, however, that the presence of some mol-fraction of anionic phospholipid together with zwitterionic phospholipids is often required for high protein activity (Bell and Burns, 1991; Valiyaveetil et al., 2002). While it is not trivial to distinguish whether these anionic phospholipids bind to annular as opposed to non-annular sites, they can increase the protein activity by acting as a prosthetic group. For example, studies with the bovine heart cytochrome c oxidase have shown that sequential and increasingly harsher detergent washes can remove different lipid populations: 40 lipid molecules are loosely associated, 8 more tightly bound and 3 very tightly bound; those very tightly bound lipids were found to be cardiolipin (Robinson, 1982). Other examples of membrane proteins that require a tightly bound anionic lipid for function are NADH dehydrogenase, cytochrome bc1, ATP synthase, the KcsA K⁺ channel and the acetylcholine receptor AchR (Heginbotham et al., 1998;

Heimpel et al., 2001; Jiang et al., 2000; Rankin et al., 1997; Sunshine and McNamee, 1994; Valiyaveetil et al., 2002).

1.6 Influence of Acyl Chain Length on Lipid Binding

A lipid membrane of a given lipid composition will have an equilibrium hydrophobic thickness that has to match to the thickness of the hydrophobic exterior of membrane proteins. There are two ways the thickness can be matched: First, since membrane proteins are usually much more rigid than lipid molecules, the lipid molecules adjacent to the membrane protein can distort to locally thicken or thin the bilayer. Alternatively, if the membrane protein contains relatively flexible α -helical elements, those can tilt to reduce their effective length across the bilayer. Figure 1.3 illustrates the relative association constant of lipids with different acyl chain length (East and Lee, 1982; London and Feigenson, 1981a,b; O’Keeffe et al., 2000; Williamson et al., 2002) to the β -barrel containing OmpF and the mainly α -helical KcsA or Ca^{2+} -ATPase. In principle, a lipid species that can bind to a membrane protein without an energetically costly bilayer deformation should have the highest affinity. In the case of OmpF this is Dimyristoyl-PC (DMPC). Shorter or longer acyl chains clearly bind less strongly. Interestingly, KcsA and the Ca^{2+} -ATPase, both mainly α -helical proteins, do not show a strong preference for a particular acyl chain length. This could reflect the inherently greater flexibility of α -helical proteins to adopt to different bilayer thicknesses when compared to β -barrel proteins.

Such flexibility in response to an altered bilayer thickness will not be without a functional consequence. Interestingly, the lipid acyl chain length has a marked effect on the *activity* of the Ca^{2+} -ATPase with a maximum for Dioleoyl-PC (DOPC) (Figure 1.4)(Lee, 1998). The differences in apparent lipid affinity and protein activity as a function of acyl chain length indicate that while a protein can be biochemically behaved over a wide range of bilayer thicknesses, it is adopting a functional conformation only in specific bilayer conditions. Studies with bilayers that contain varying mol-fractions of lipids with different acyl chain length indicate that the underlying conformational change is highly cooperative (Figure 1.4b)(Lee, 1998). Such cooperativity most likely reflects an energetic cost of conformational change being balanced

by the associated summed differences in free energy of 30 bound lipid molecules (see Chapter 1.4).

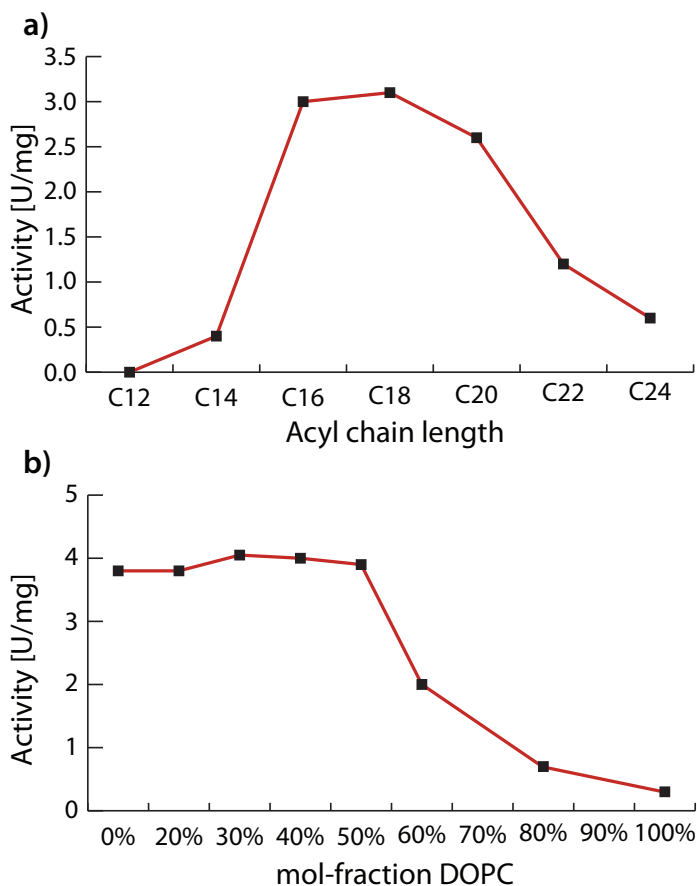


Figure 1.4: **Lipid Effects on Ca^{2+} -ATPase Activity.** **a**, ATPase activity as a function of acyl chain length. All lipids are monounsaturated and in liquid crystalline state at 25 °C. **b**, Dependence of ATPase activity on mol-fraction of DOPC. Modified from (Lee, 1998).

1.7 Lipid Microdomains as Signaling Platforms

Lipid-protein interactions can give rise to secondary lipid-mediated protein-protein interactions. These induced interactions can in theory be seen as a way to indirectly organize the protein components of the membrane into distinct functional units. In fact, the ability to sequester specific lipids and proteins while excluding others is proposed to play a role in a range of cellular processes, such as signal transduction (Damjanovich et al., 1997; Field et al., 1997; Simons and Toomre, 2000; Young et al., 2003), lipid sorting (Anderson, 1998; Anderson and Jacobson, 2002; Hooper, 1999;

Kurzchalia and Parton, 1999; Okamoto et al., 1998; Simons and Toomre, 2000; Simons and van Meer, 1988), protein trafficking (Ikonen, 2001; Sharma et al., 2003) and organization of the cytoskeleton (Caroni, 2001; Laux et al., 2000).

Lipid-protein interactions also influence the localization of peripheral membrane proteins. Their binding to microdomains can depend on the mol-fraction of cholesterol in the membrane (Benachir and Lafleur, 1995), lipid acyl chain composition (Başaran et al., 1999; Giorgione et al., 1998; Pande et al., 2005) and the charge of the lipid headgroup (van den Brink-van der Laan et al., 2001). Some peripheral proteins, such as G proteins, target preferentially to microdomains because of covalently attached saturated acyl chains that interact strongly with liquid-ordered lipids in microdomains through *van der Waals* forces (Khan et al., 2003; Moffett et al., 2000; Schroeder et al., 1997).

1.8 Ion channels can be Localized to Microdomains

There is extensive literature on the differential localization of ion channels to multiple types of lipid microdomains (for a review see (Martens et al., 2004)). The experimental evidence is usually footed on biochemical colocalization of certain marker lipids and membrane proteins; $K_v2.1$ for example is shown to be enriched in biochemically isolated detergent-resistant membranes from transfected fibroblasts and rat brain tissue (Martens et al., 2000). Often times, the functional dependence of a specific ion channel on localization can also be shown; again, the example of $K_v2.1$, whose steady-state inactivation is shifted to hyperpolarized voltages by the treatment of transfected fibroblast with cyclodextrin, a cholesterol-depleting agent (Brown and London, 2000). Other K_v channels, such as $K_v4.2$ expressed in fibroblasts are unaffected, suggesting that they are localizing to a different membrane environment. The list can easily be expanded: $K_v1.5$ resides in caveolæ (Martens et al., 2001), whereas $K_v2.1$, $K_v1.4$ and $Kir2.1$ target to non-caveolar microdomains, and $K_v4.2$ is not microdomain associated (Martens et al., 2000; Romanenko et al., 2004; Wong and Schlichter, 2004). The same holds true for other voltage-dependent and ligand-gated channels: $Kir3.1$ associated with microdomains in CHO cells and neuronal cell culture (Delling et al., 2002). $TRP1$, Na_v and L-type Ca_v channels are localized to caveolæ; $TRP1$'s activity is altered by cholesterol depletion; so is that of olfactory cyclic-nucleotide-gated channels (Brady et al., 2004; Darby et al., 2000; Lockwich et al., 2000; Yarbrough et al., 2002). Cholesterol-rich microdomains and the $\alpha7$ nico-

tinic acetylcholine receptor become progressively colocalized during synaptogenesis in somatic spines of ciliary neurons (Brusés et al., 2001).

Why these ion channels localize with lipid microdomains is not always known; the channel-microdomain localization might occur through direct protein-lipid interaction (see Chapter 1.4), or they could occur through protein-protein interactions with auxiliary protein subunits that have a preferential localization to these microdomains themselves (see Chapter 1.7). Examples are “K⁺ channel interacting proteins” (KChIPs), which are a class of EF-hand containing Ca²⁺ binding proteins. They require proper palmitoylation to efficiently enhance the cell-surface expression of K_v channels (Takimoto et al., 2002).

1.9 Membrane Properties alter Ion Channel Function

The functional importance of microdomain localization is evident from cholesterol-depletion experiments that dramatically change the gating properties of some ion channels (Barrantes, 2002; Hajdú et al., 2003; Romanenko et al., 2004). There could be, however, other biophysical properties, other than the presence of cholesterol, that set microdomains apart from the surrounding bulk lipid phase; parameters like bilayer fluidity & thickness, surface charge and bending rigidity, for example. These parameters can theoretically contribute to the membrane deformation free energy associated with the conformational change of an ion channel during gating (see Chapter 1.10.2).

There are many other examples of how the lipid membrane influences ion channel function. They can be categorized into (a) specific lipid molecules acting as prosthetics groups or (b) the material properties of the lipid membrane, e.g. bilayer stiffness and thickness, that modulate some property of the ion channel.

Inward-rectifying K⁺ channels, such as IRK1 and ROMK are directly activated by binding phosphatidylinositol-4,5-bisphosphate (PIP₂). For G protein-coupled channels like GIRK1/4, PIP₂ binding acts synergistically with the activation by Gβγ (Huang et al., 1998). The interaction with PIP₂ also mediates the mechanosensitivity of GIRK4 (Zhang et al., 2004). Similarly, it has been shown that binding of PIP₂

is necessary to maintain the function of voltage-dependent Ca^{2+} channels (Ca_v (Wu et al., 2002)).

Aside from activation, the inactivation properties of K_v channels can be regulated by membrane lipids as well. The application of PIP_2 to the cytoplasmic side of excised membrane patches can remove the fast N-type inactivation in $\text{K}_v1.1$ and $\text{K}_v3.4$; addition of the fatty arachidonic acid reintroduces the fast inactivation. Through its negatively charged headgroup the addition of PIP_2 leads to electrostatic trapping of the positively charged inactivation peptide. Arachidonic acid is also implicated in altering mechanical membrane properties (Oliver et al., 2004).

Microdomains are thought to be enriched with sphingomyelin (Samsonov et al., 2001); as described in Chapter 1.8 some K_v channels are enriched in these domains. It recently has been reported that certain K_v channels are activated through the enzymatic modification of sphingomyelin by sphingomyelinase (Ramu et al., 2006). Taken together these observations make a strong case for the possibility that cell excitability may be regulated by altering the chemical properties of lipids in the plasma membrane, possibly by either modification of lipid chemistry or by altered membrane protein targeting.

It also has been suggested that various channels respond to changes in the mechanical state of the membrane: the cardiac muscarinic K^+ channel (GIRK1/4) (Ji et al., 1998), the S-type K^+ channels (Patel et al., 1998), the NMDA receptor (Casado and Ascher, 1998), the Shaker K_v channel (Gu et al., 2001), the BK channel (Naruse et al., 2009), N- and L-type Ca^{2+} channels (Calabrese et al., 2002; Lyford et al., 2002), and the Skm Na^+ channel (Tabarean et al., 1999). As of yet, the changes at the lipid membrane that underlie this mechanosensitivity are not well understood and as I will discuss in detail in a later section of my thesis, Chapter 3.3.2, using patch clamp measurements might in fact be inappropriate to study mechanosensitivity for the majority of these studies.

Small molecule toxin blockers and modifiers of ion channels are influenced by the lipid membrane as well. Some toxins partition into the lipid membrane before they interact with their binding site on the voltage sensor of ion channels, thus increasing their effective concentration (Lee and Mackinnon, 2004; Milescu et al., 2007). Other toxins partition into the bilayer but can interact with their target as both *L*- and

D-enantiomer, suggesting that they act through perturbing of the lipid packing and line tension adjacent to the channel as opposed to direct protein-protein interaction (Suchyna et al., 2004). In either case, the partition coefficient depends on the lipid composition of the membrane (Posokhov et al., 2007).

1.10 ‘Design’ Principles of Mechanosensitivity

Ever since the first cells were fully encapsulated in a semipermeable lipid membrane, they must have had mechanosensitive processes that provide mechanisms for cell protection against changes in osmotic conditions of the surrounding environment. At first there may have been large non-selective pores that open in response to osmotic swelling of the cell and reduce the intracellular pressure and membrane tension by literally spewing out the cell’s contents. Over time these processes may have evolved to be part of the cell’s signaling repertoire. A survey of the literature suggests that mechanosensitive processes are part of hearing (Hackney and Furness, 1995; Howard et al., 1988), arterial vessel tone (Burnstock, 1999; Davis and Hill, 1999), touch and pain sensation (Burnstock and Wood, 1996; Nakamura and Strittmatter, 1996; Tavernarakis and Driscoll, 1997), cell volume regulation (Nilius et al., 1997; Wang et al., 1996) and tissue growth (Lammerding et al., 2004).

Several well established genetic systems seem amenable to study mechanosensitive processes in multicellular organisms: *Caenorhabditis elegans* (nematode) movement relies of touch sensation, *Drosophila melanogaster* (fruit fly) have mechanosensitive hair bristles, and the lateral-line organelles in *Danio rerio* (zebrafish) enables them to detect directional water movement (Duggan et al., 2000; Gillespie and Walker, 2001). Nevertheless, while some researchers claim that over the last two decades the molecular nature of specific mechanosensitive membrane processes have been identified, closer inspection of the actual data often reveals unidentified activities that need very specific experimental conditions to be studied. Arguably, the most serious problem with such studies is that pressure difference (J/m^3) across the membrane is taken as the important input variable, when in fact tension (J/m^2) is the membrane parameter that governs mechanosensitivity. The fact remains, for most mechanosensitive processes, we do not know the clonal nature of the involved proteins or the underlying cellular framework.

1.10.1 The Composite Structure of the Cell Boundary

The Cytoskeleton

The structural basis of mechanosensation in animal cells is the composite structure of extracellular matrix, lipid bilayer, and cytoskeleton. By the virtue of membrane proteins these three layers form an integrated composite structure. Any externally applied force produces strains in multiple elements within these three layers.

The cytoskeleton provides shear rigidity to a lipid bilayer. It is anchored to the lipid bilayer by interactions between ankyrin and other cytoskeletal proteins with various integral membrane proteins. Because it is localized directly below the plasma membrane, it also allows the cell to assume non-spherical shapes by acting as a scaffold and to increase the surface area for a given volume beyond that of a smooth sphere. The amount of membrane excess area can range between 40-1,000% depending on the cell type and typically is achieved by membrane folds such as micro- and macrovilli or caveolæ (Dulhunty and Franzini-Armstrong, 1975; Zhang and Hamill, 2000). The cytoskeleton is a viscoelastic structure that is highly expandable. During mechanical deformations of the cell, cytoskeleton-stabilized excess membrane reservoirs can smooth out. This process provides additional surface area before significant tensions can build up in the bilayer (Hochmuth et al., 1996; Sens and Turner, 2006, 2004). Additional support for this idea comes from capacitance measurements of mast cells that can inflate four-fold in volume with little-increase in membrane capacitance (Solsona et al., 1998). Also, Sheetz and colleagues (Raucher and Sheetz, 1999) found that the tether force on an optically trapped bead did not depend on the tether length over a wide range of tether lengths, indicating that the material for the membrane tether is supplied by flattening out a membrane reservoir and not by stretching the membrane. When cells were treated with the cytoskeleton-disrupting drugs cytochalasin B or D, the tether length increased dramatically, indicating that it is the cytoskeleton that creates folds in the plasma membrane which can contribute to this membrane reservoir.

The cytoskeletal meshwork is highly integrated with cells-spanning microfilaments and microtubule support and has been proposed to behave as a *tensegrity* structure in which mechanical deformation can be communicated cell-wide (Ingber, 1997, 1993).

The Extracellular Matrix

The external extracellular matrix of animal cells is made of various proteins and carbohydrate components; it serves as the bonding material between the cells of tissues and is connected to the intracellular cytoskeleton through integral membrane proteins such as integrins. The extracellular matrix allows external force cues to be filtered or focused and communicated effectively to specialized cells within a tissue. Merkel cells, the pacinian cell capsule at the tip of certain neurons or hair cells of the inner ear are examples for such specialized cells that often possess unique structures that confer high directionality and vibrational sensitivity on the mechanotransduction process (Boulais and Misery, 2008).

The Lipid Bilayer

The lipid bilayer can be considered an elastic solid (Dan and Safran, 1998; Helfrich, 1973; Nielsen et al., 1998; Rawicz et al., 2000); one of its most important features is *in-plane fluidity*, which would allow the equilibration of membrane tension throughout the whole area of the membrane, were it not for the cytoskeleton. The cytoskeleton effectively compartmentalizes the lipid membrane into smaller areas with different amounts of in-plane tension. Each leaflet of the bilayer resists change in the angle between adjacent lipid molecules, giving rise to *bending stiffness* of the membrane. The specific chemistry of lipid molecules also gives them a preferred *in-plane spacing*, which will cause them to resist any changes in spacing due to external tension. Lastly, the lipid composition of the lipid bilayer will give rise to an equilibrium *hydrophobic thickness*, which for embedded membrane proteins can lead to an energetically costly hydrophobic mismatch.

These four properties are described by four elasticity constants (moduli) that describe the response of a bilayer to shear, bending, expansion and compression (Evans and Hochmuth, 1978). The larger a modulus, the more the bilayer resists that form of deformation. Because these deformation are elastic, they follow the application of external forces instantaneously. Mechanical forces and their corresponding deformations constitute the most important class of external cues for mechanosensitive processes.

1.10.2 The Modes of Bilayer Deformation

Two models have been suggested for how a membrane can sense external mechanical cues: (a) through physical linkers that pull or push on some part of the protein resulting in gating or (b) the surrounding bilayer directly communicating mechanical forces to alter the protein conformation. They are called tether-based or bilayer model for mechanosensitivity, respectively.

While the mechanical manifestation of a tether-based model is straightforward to understand (Hooke’s Law), a convenient way to explain the bilayer model is to consider the channel as a two-state system with an open and a closed state. A simple model describes how the elastic properties of a lipid bilayer can be used to determine the bilayer’s contribution to the energy of these two states. Boltzmann statistics can be used to calculate the open probability (P_o) of the channel:

$$P_o = \frac{1}{1 + e^{\left(\frac{\Delta G_{tot}}{k_B T}\right)}} \quad (1.1)$$

The total change in free energy ΔG_{tot} is defined as the total free energy difference between the closed and open state. Changes in electrostatic gating energy (ΔG_{elect}), internal protein conformation free energy (ΔG_{prot}) and bilayer deformation free energy (ΔG_{memb}) all contribute to ΔG_{tot} of channel gating.

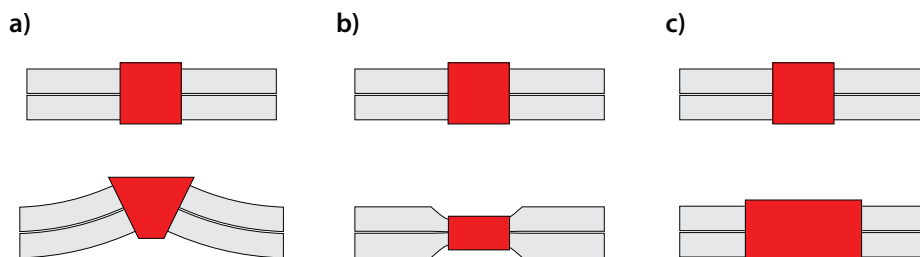


Figure 1.5: **Modes of Bilayer Deformation** **a**, Midplane Bending. **b**, Bilayer Compression. **c**, Footprint Dilation. Modified from (Ursell et al., 2008).

How large is the membrane contribution ΔG_{memb} to the free energy change of channel gating? The bilayer deformations that a transmembrane protein can produce are broadly split in three main classes (see Figure 1.5): those that deform the midplane of the bilayer (*midplane bending*), those that deform the leaflet thickness (*bilayer compression*) and those deformations that accompany a change on the cross sectional area of the membrane protein (*footprint dilation*).

As analysed elsewhere (Ursell et al., 2008), in the midplane deformation model, the shape of the membrane protein can influence the slope of the bilayer at the protein-lipid interface which, in addition to the protein radius, will give the deformation energy:

$$G^{mid}(R, \tau) = \pi R \sqrt{\kappa_b \tau} (\theta)^2 \quad (1.2)$$

where R is the radius of the protein, θ is the interface tilt angle, κ_b is the bending modulus and τ is the membrane tension. As is obvious from Equation (1.2), for a given interface tilt angle and protein radius, an increase in membrane tension will make midplane bending deformations more costly. Therefore, increased membrane tension will prefer a flatter membrane (i.e. θ towards 0°) or a smaller protein radius. In the case of midplane deformation, the deformation free energy scales to the square root of tension.

The basis for hydrophobic mismatch deformation is the fact that compared to lipid molecules proteins are relatively rigid. Hence, the lipid will undergo the majority of deformation when the hydrophobic transmembrane regions of a protein are matched with the hydrophobic core of the bilayer. The deformation energy due to thickness variation of the surrounding lipids that is induced by embedding a membrane protein is given by:

$$G^{thick}(R, \tau) = \pi \kappa_b \left(\frac{u_0}{\lambda} + \frac{\tau l}{K_A \lambda} \right)^2 \left(1 + \sqrt{2} \frac{R}{\lambda} \right) \text{ with } \lambda = \left(\frac{l^2 \kappa_b}{K_A} \right)^{\frac{1}{4}} \simeq 1 \text{ nm} \quad (1.3)$$

Where K_A is the bilayer stretch modulus, u_0 is the hydrophobic mismatch, l is the leaflet hydrophobic thickness, R is the radius of the protein, κ_b is the bending modulus and τ is the membrane tension.

Like midplane deformation, hydrophobic mismatch deformation prefers a smaller protein radius. While for midplane deformation increased tension always increase the deformation energy, in the case of hydrophobic thickness deformation the tension can either increase or decrease the deformation energy depending on the sign of the hydrophobic mismatch (u_0), i.e. the protein can be either thicker or thinner than the bilayer. Given very small values of τ/K_A , the thickness free energy scales approximately with tension.

The most straightforward derived expression for free energy is that of the footprint dilation. If the protein footprint area increases, the membrane will yield to external tension τ . Therefore, the free energy of the footprint dilation can be expressed in

terms of a change in channel area:

$$G^{dil} = -\tau \overbrace{\pi R^2}^A \quad (1.4)$$

with τ is the membrane tension and R being protein radius.

Again the footprint dilation free energy scales linearly with applied membrane tension.

If one had to cast the above equations into basic design principles of how to make a membrane protein sensitive to mechanical bilayer deformations then it would be the following: under non-zero membrane tension, a increase in protein radius is always favored. Conversely, midplane and hydrophobic mismatch deformation prefer a smaller channel radius, because this will lead to a smaller annulus of deformed lipid, hence a smaller free energy penalty. These two competing interests on protein radius allow for the existence of several stable energy states associated with different protein conformations (i.e. different radii, interfacial slopes etc.) that a protein can occupy in response to changes in external mechanical force caused by tension.

Chapter 2

Thesis Research

2.1 Phospholipids and Cationic Gating Charges

2.1.1 Introduction

K_v channels open and close in response to changes in transmembrane voltage. These changes are sensed by the channel's voltage sensor domains, which contain charged amino acids called gating charges (Sigworth, 1994). Upon membrane depolarization all four voltage sensors of a K_v channel undergo a conformational change that is moving the equivalent of 14 elementary charges across the lipid membrane; they are electromechanical force transducers (Aggarwal and MacKinnon, 1996; Schoppa et al., 1992). The voltage sensors are connected to the K_v channel pore through a linker domain that couples the movement of the voltage sensor to the opening and closing of the pore. Various atomic structures have suggested that the voltage sensor is located at the protein-lipid interface and that the arginine gating charges may be exposed to the membrane (Jiang et al., 2004, 2003a,b; Lee et al., 2005; Long et al., 2005a,b). This raises the possibility that the interaction of the voltage sensors with the membrane is important to K_v channel function and leads to the question of how the membrane is creating a suitable environment to accommodate positively charged arginines. Why do voltage sensors use positively charged amino acids, in particular why arginine, to sense voltage in the first place? Could the selection of arginine for this purpose represent an adaptation to a ubiquitous feature of most cell membranes: the presence of the anionic phosphodiester of phospholipids? The positive charge and multidentate hydrogen bonding capacity of arginine's guanidinium group makes it an excellent chemical match for favorable electrostatic and hydrogen bonding interactions with the lipid phosphodiester.

To gain an understanding of the lipid-dependent aspects of K_v channel function and to test the ideas mentioned above, I began to study the voltage-gated potassium K^+ channel KvAP from the Archæa *Aeropyrum pernix* in an artificial membrane system, the planar lipid bilayer (PLB) (Ruta et al., 2003). Only in this system the lipid bilayer composition can be directly controlled; other heterologous expression systems such as *Xenopus laevis* oocytes and mammalian cell lines are limited in their capacity for lipid modification.

2.1.2 Results

Figure 2.1 shows voltage-dependent KvAP K^+ channels in three different experimental conditions. In each condition the membrane voltage was held at -100 mV and then stepped to more positive depolarizing voltages to open the channels. When KvAP channels were present in phospholipid membranes the channels opened in a voltage-dependent manner (Figure 2.1b). By contrast, when channels were present in membranes consisting of a lipid known as 1,2-Dioleoyl-3-Trimethylammonium-Propane (DOTAP)(Campbell et al., 2001), which contains a positively charged trimethylammonium group instead of a negatively charged phosphodiester (Figure 2.1a), no channel activity was observed (Figure 2.1d). The absence of channel activity is not due an irreversible change of KvAP when reconstituted into DOTAP vesicles. When channels were first reconstituted into pure DOTAP lipid vesicles, which were then fused with a planar lipid membrane of phospholipids, KvAP functioned in the regular voltage-dependent manner (Figure 2.1c). The presence of functional channels in this phospholipid membrane means that functional KvAP channels had to be present in the DOTAP lipid vesicles that were used to deliver channels to the planar membrane.

As a control I looked at the Ca^{2+} -dependent K^+ channel, MthK, and asked whether it is able to function in pure DOTAP membranes. MthK has a pore that is similar to KvAP but contains a gating ring structure in the cytoplasm (instead of voltage sensors in the membrane) that enables intracellular Ca^{2+} to open the pore (Jiang et al., 2002). In DOTAP membranes MthK is activated by Ca^{2+} and inhibited by the scorpion toxin charybdotoxin (CTX) (Figure 2.2). This control experiment shows that DOTAP vesicles can indeed fuse with DOTAP planar membranes and that DOTAP membranes do not prevent the pore of a K^+ channel from functioning. The control also implies that the inability of DOTAP membranes to support KvAP function is related to the voltage sensing mechanism.

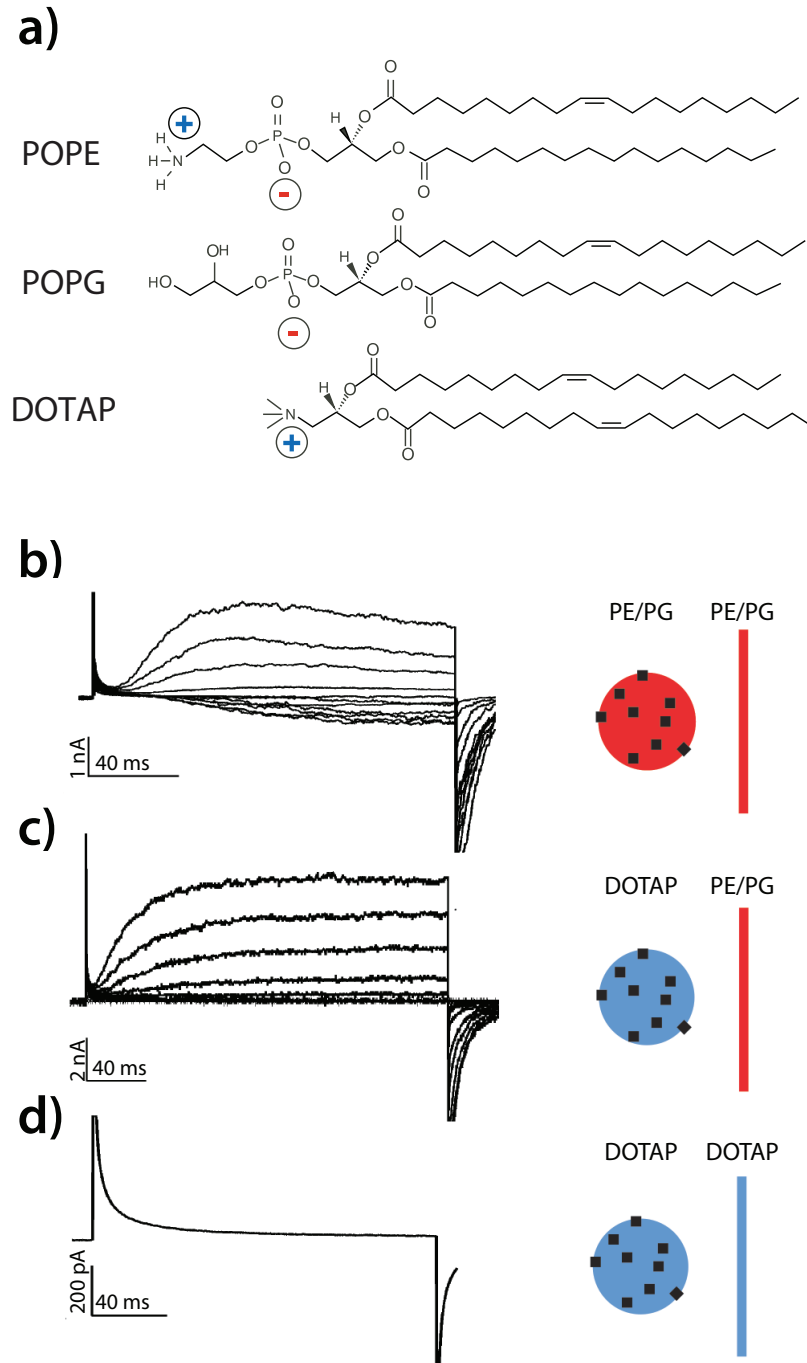


Figure 2.1: **Assessment of KvAP function in phospholipid and DOTAP membranes.** **a**, Chemical structures of POPE, POPG and DOTAP. **b**, KvAP (black squares in cartoon) in 3:1 POPE:POPG (PE/PG) vesicles (red circle) fused into a 3:1 POPE:POPG bilayer (red) yielded voltage-dependent currents (left traces). **c-d**, KvAP in DOTAP vesicles (blue circles) gave functional channels (trace in **c**) after fusion into a POPE:POPG bilayer (red line), but failed to function (trace **d**) after fusion into a DOTAP bilayer (blue line). Voltage pulses in (**b-c**): -100 to 40 mV, $\Delta V = 10$ mV, holding potential (h.p.) -100 mV. The pulse in (**d**) was from h.p. -100 mV to 100mV

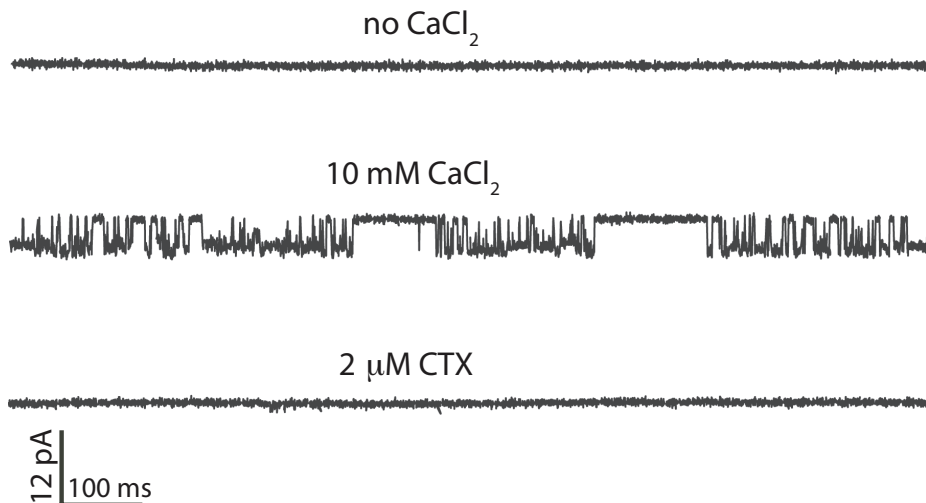


Figure 2.2: **Assessment of MthK function in DOTAP membranes.** Single channel recordings of MthK in DOTAP membranes with no CaCl_2 (top), 10 mM CaCl_2 (middle), and after the addition of 2.0 μM CTX (bottom). h.p. is -150 mV, and channels open downward.

The inability of KvAP to function in pure DOTAP membranes could in principle be due to either the inability of DOTAP vesicles to fuse with DOTAP membranes or DOTAP not supporting KvAP function. By adding phospholipids to the silent DOTAP membranes, it might be possible to “wake-up” inactive KvAP channels, distinguishing these two possibilities. Several minutes after fusing channel-containing DOTAP vesicles with DOTAP planar membranes empty phospholipid vesicles (without KvAP) were fused, resulting in channel activity (Figure 2.3). Since the phospholipid vesicles themselves did not contain KvAP channels, the channels were presumably present in the DOTAP planar membrane but were not functional. In these experiments the number of active channels was always small and in several respects their function were altered compared to pure phospholipid bilayers. Most importantly, however, the channels began to function in a voltage-dependent manner only *after* phospholipids were delivered to the membrane, that is, in the context of a DOTAP planar membrane KvAP is a “phospholipid-activated” voltage-dependent K^+ channel.

If DOTAP membranes fail to support channel function then we might expect to observe channels exhibiting intermediate behavior between normal and nonfunctional in composite membranes containing DOTAP and phospholipids at different molar percentages. I therefore studied the effect on voltage-dependent gating of systemati-

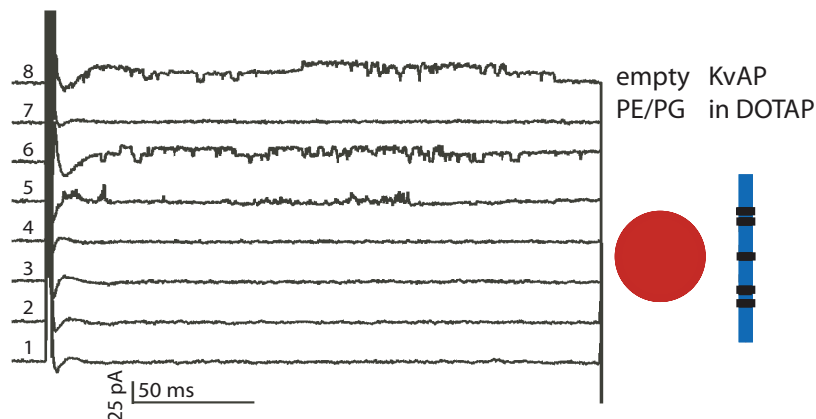


Figure 2.3: **KvAP function depends on membrane lipid composition.** KvAP-containing DOTAP vesicles were fused into a DOTAP bilayer. Channel activity was monitored with pulses from -100 mV to 100 mV every two minutes. Empty POPE:POPG vesicles were introduced between traces 3 and 4. A triple-exponential function was used to subtract capacitance transients. Traces 2-8 were shifted upward successively by 50 pA.

cally decreasing the mol-fraction of phospholipids (Figure 2.4a-c). A dilute solution of phospholipid vesicles containing KvAP channels at a high protein-to-lipid ratio was used for fusion: this condition best ensured that after fusion the lipid composition of the planar membrane was dominated by the planar membrane lipids (the phospholipid-DOTAP mixture) rather than the vesicle lipids. As the mol-fraction of phospholipids was decreased, successively larger depolarization voltages were required to open the channels, and the activation curve became less steep (Figure 2.4a,b). It is clear that gating becomes progressively more abnormal as the mol-fraction of phospholipids is decreased (Figure 2.4b,c). The absence of function in pure DOTAP membranes (Figure 2.1d) appears to represent the limit of the dilution experiment (Figure 2.4a-c), and the restoration of voltage-dependent activity upon addition of phospholipids (Figure 2.3) appears to reflect the fulfillment of a phospholipid requirement for voltage-dependent channel function.

The inability of DOTAP to support KvAP function could be related to the absence of a negatively charged phosphodiester or to the presence of a positively charged trimethylammonium group (Figure 2.1a). To distinguish these two possibilities I studied additional non-phospholipid membranes, 1,2-Dioleoyl-Glycero-3-Succinate (DOGS) and soy Glucocerebrosides (GlucCer), which do not have a trimethylammonium group (Figure 2.5a,b). DOGS is a carboxyl-containing anionic lipid at neutral pH. DOGS

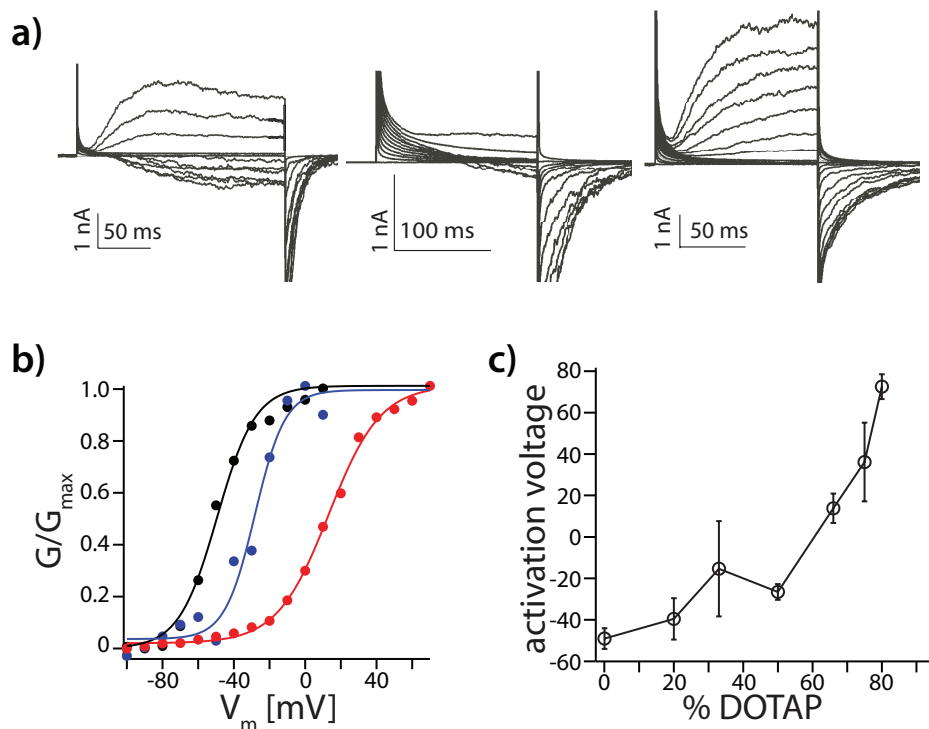


Figure 2.4: **KvAP function depends on membrane lipid composition.** **a**, KvAP in POPE:POPG vesicles at a protein-lipid ratio (PLR, w/w) of 1.0 was fused into bilayers of mixed DOTAP and POPE:POPG with DOTAP% 0 (1st panel), 50 (2nd), and 67 (3rd). Voltage pulses: h.p. -100 mV to 20 mV (1st and 2nd panels) and h.p. -80 mV to 70 mV (3rd), $\Delta V = 10$ mV. **b**, Boltzmann functions (solid lines) fit data from (a) with $V_{0.5}$ (mV) and Z (mV^{-1}): -42, 3.1 (0%, blue); -25, 1.9 (50%, green); 14, 1.7 (67%, red). **c**, $V_{0.5}$ (mean \pm s.e.m. or range of mean, $n = 2-5$) versus DOTAP%.

forms large unilamellar vesicles into which KvAP can be reconstituted and in which KvAP is functional when fused into POPE:POPG planar membranes. DOGS also forms stable planar membranes, however, no channel activity is observed. GlucCer is a neutral lipid with a ceramide backbone and sugar head group. Rare (1 to 3 channels) opening events are observed at very positive membrane voltages (Figure 2.5b). One has to keep on mind that this lipid preparation is very heterogenous and when I performed a thin-layer chromatography phosphate assay with this lipid, I could detect trace amounts of phosphate, suggesting contamination with phospholipids. I can also not exclude the possibility that this lipid may exhibit complex phase behavior. Therefore I cannot be certain whether GlucCer or contaminant lipids support the rare openings at very positive voltages. In either case, KvAP function in this membrane is very abnormal. DOTAP, DOGS, and GlucCer are chemically very different from

each other. None of them appear to create a suitable environment for normal KvAP function.

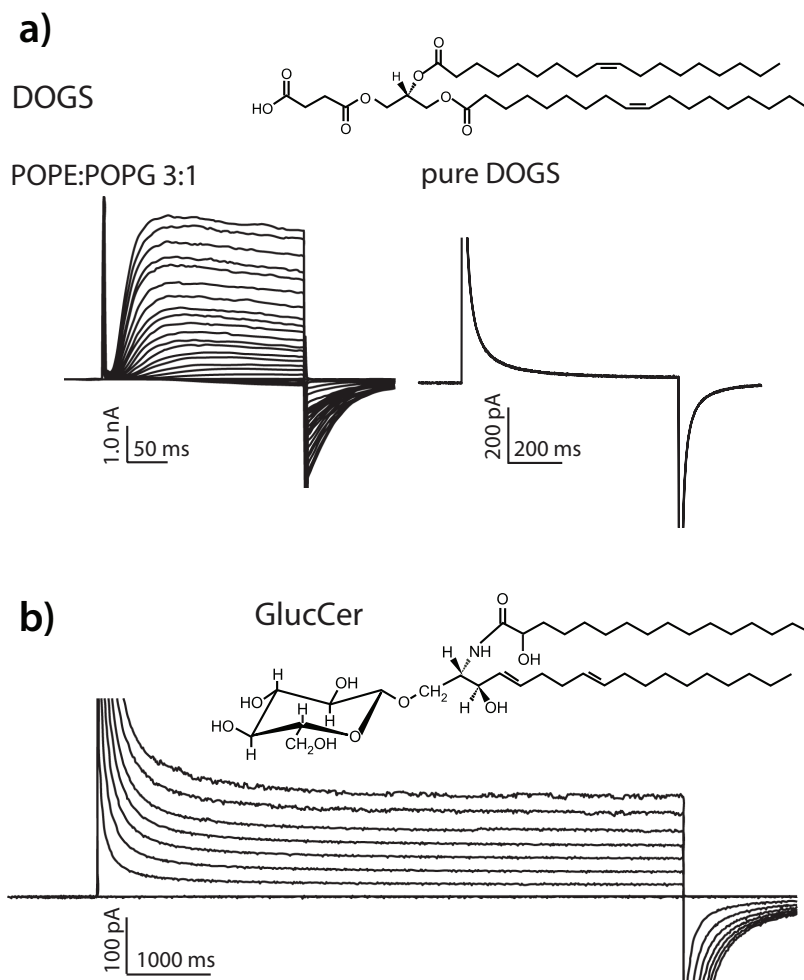


Figure 2.5: **KvAP function depends on membrane lipid composition.** **a**, KvAP in DOGS vesicles fused into bilayers of POPE:POPG (left) and DOGS (right). Voltage pulses: -80 to $+180$ mV, $\Delta V = 10$ mV, h.p. -100 mV (left); from h.p. -100 to 120 mV (right). **b**, KvAP in DOTAP vesicles fused into a glucosyl-cerebroside bilayer. Voltage pulses: -150 to 130 mV, $\Delta V = 40$ mV, h.p. -150 mV.

In an effort to further investigate which part of phospholipid membranes is needed for K_v channel function, I examined membranes composed of DOTAP and phospholipids containing acyl chains of varying length. In DOTAP bilayers that were supplemented with either Dioleoyl-phosphatidylcholine (DOPC), Dimyristoyl-phosphatidylcholine (DMPC) or Didecyl-phosphatidylcholine (DDecPC) (Figure 2.6a) I could record voltage-dependent KvAP function (Figure 2.6b-d). Of note, DMPC and

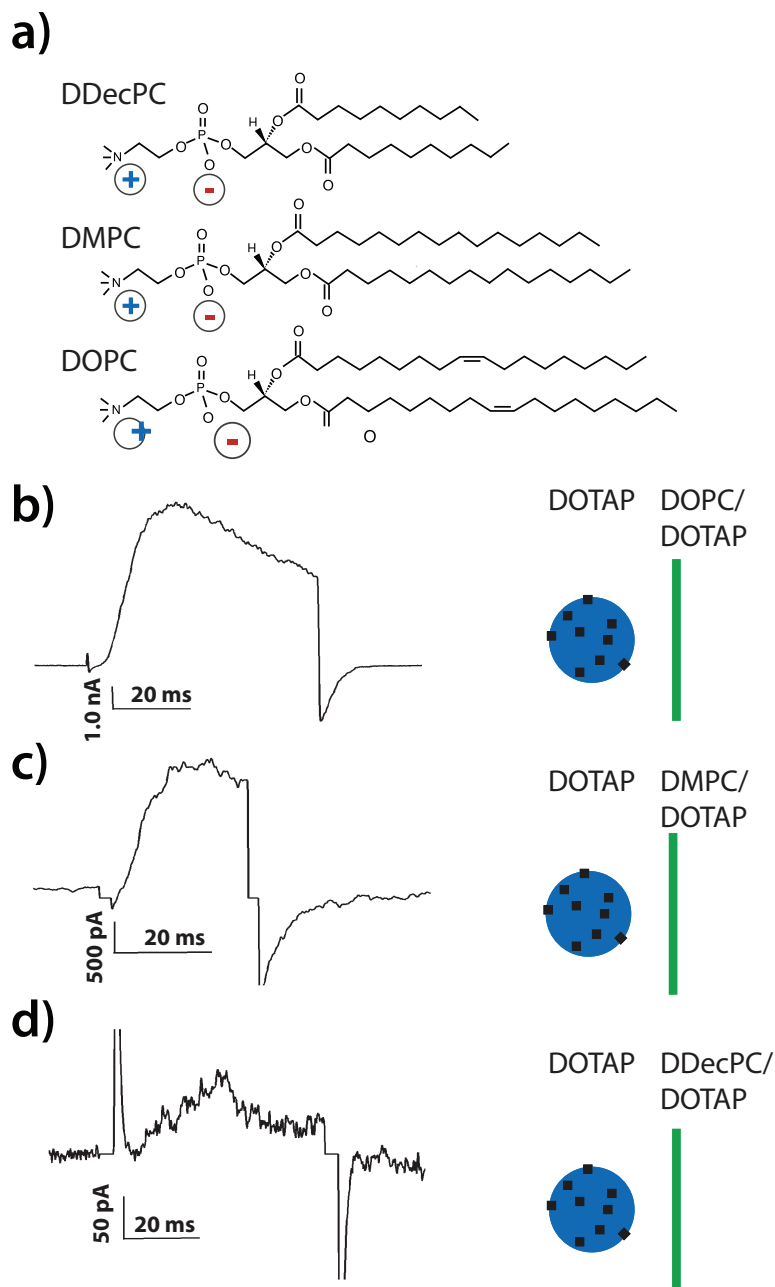


Figure 2.6: **Phosphate group is important for KvAP voltage-dependent gating.** **a**, Chemical structures of DOPC, DMPC and DDecPC. **(b)-(d)** Channels in DOTAP vesicles were fused into bilayers of 1:1 ratio of DOTAP and DOPC (**b**), DMPC (**c**) and DDecPC (**d**). Voltage pulses: -100 to 100 mV, $\Delta V = 20$ mV, h.p. = -100 mV. Recordings of CTX (200 nM) treated bilayers were used to subtract capacitance transients from the original traces. The residual peaks at the beginning and end of the pulse are due to the incomplete subtraction of capacitance components.

DDecPC do not form stable bilayers in the planar bilayer system by themselves. I could conclude from this experiment that it is not the acyl chain length that is crucial for KvAP function, but the headgroup requirement that these short chain lipids fulfill by plugging into the lipid bilayer.

Figure 2.7 demonstrates the requirement of a charged phosphate group in a different lipid system. Dioleoyl-Glycerol (DOG) is an uncharged (neutral) lipid that does not contain a phosphate group and Dioleoyl-Phosphate (DOPA) is the phosphorylated derivative of DOG (Figure 2.7a). KvAP channels do not function in membranes containing only DOG (Figure 2.7b) even though they can exist in such membranes, as demonstrated by the fusion of KvAP containing DOG vesicles into phospholipid planar membranes (Figure 2.7c). DOPA membranes support voltage-dependent channel function (Figure 2.7d). Channels also function in 1:1 mixtures of DOG and DOPA but the midpoint of activation is shifted approximately 65 mV positive compared to POPE:POPG membranes and 55 mV compared to DOPA membranes (data not shown). Here again, a charged phosphodiester group appears to be important for voltage-dependent channel function.

Next I investigated the chemical properties of the phosphate ester that are required for voltage sensor function. The phospholipid 1,2-Dioleoyl-Glycero-3-Ethylphosphocholine (EDOPC) is similar to DOPC with respect to many of its physical properties, however, due to ethylation the resulting phosphotriester is uncharged and it does not participate in intermolecular hydrogen bonding with itself (Figure 2.8) (MacDonald et al., 1999). EDOPC does not support KvAP function, and furthermore, as normal phospholipids (POPE : POPG) are diluted by increasing the mol-fraction of EDOPC the effects on gating are qualitatively similar to those observed in DOTAP membranes (Figure 2.4a-c and Figure 2.8b-d). In control experiments with EDOPC membranes the MthK channel conducts K^+ , is Ca^{2+} -activated, and inhibited by CTX (Figure 2.9). Therefore EDOPC membranes support the function of a non-voltage-dependent K^+ channel. I concluded that the negative charge on the lipid phosphodiester and possibly its hydrogen bonding potential is specifically important for the function of the KvAP voltage-dependent K^+ channel.

2.1.3 Discussion

KvAP channels function in a variety of different lipid membranes including those presented here and in lipids not presented here (e.g. Diphytanoyl-PC, Dioleoyl-

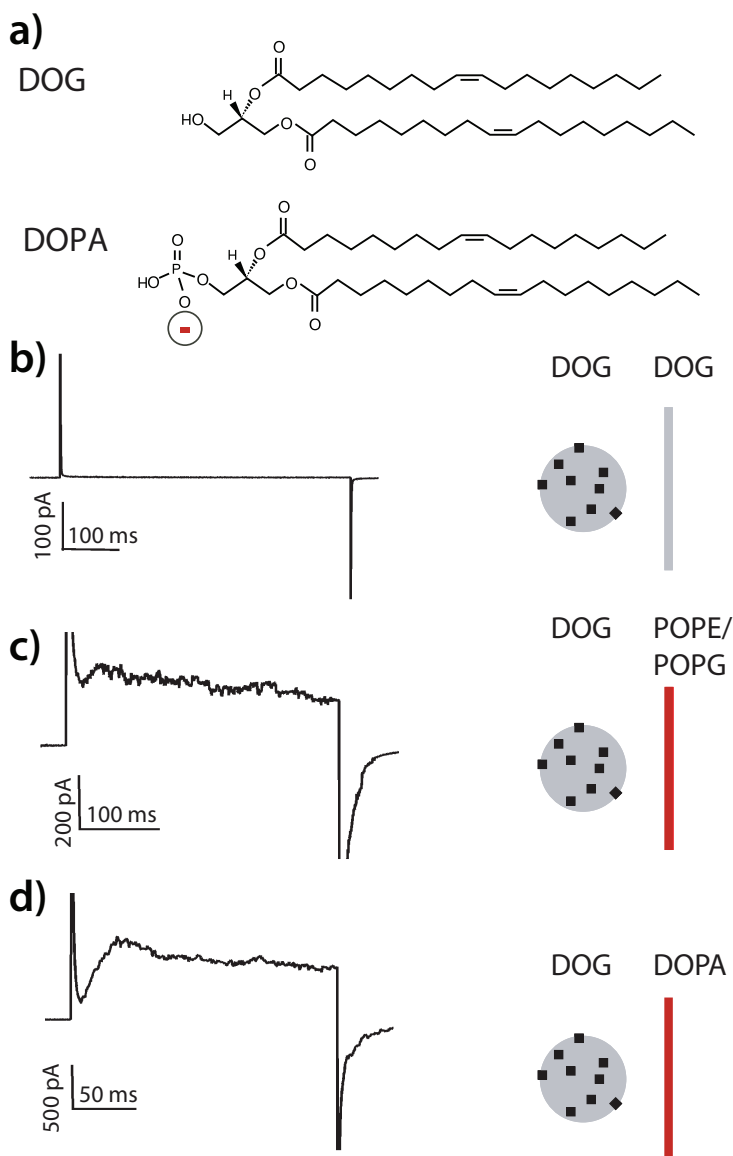


Figure 2.7: **Phosphate group is important for KvAP voltage-dependent gating.** **a**, The chemical structure of DOG and DOPA. **b**, DOG planar membranes do not support channel activity, whereas channels in DOG vesicles fused into PE/PG planar membranes (**c**) or DOPA planar membranes (**d**) give rise to channel activity. Voltage pulses: step to 100 mV, h.p. = -100 mV.

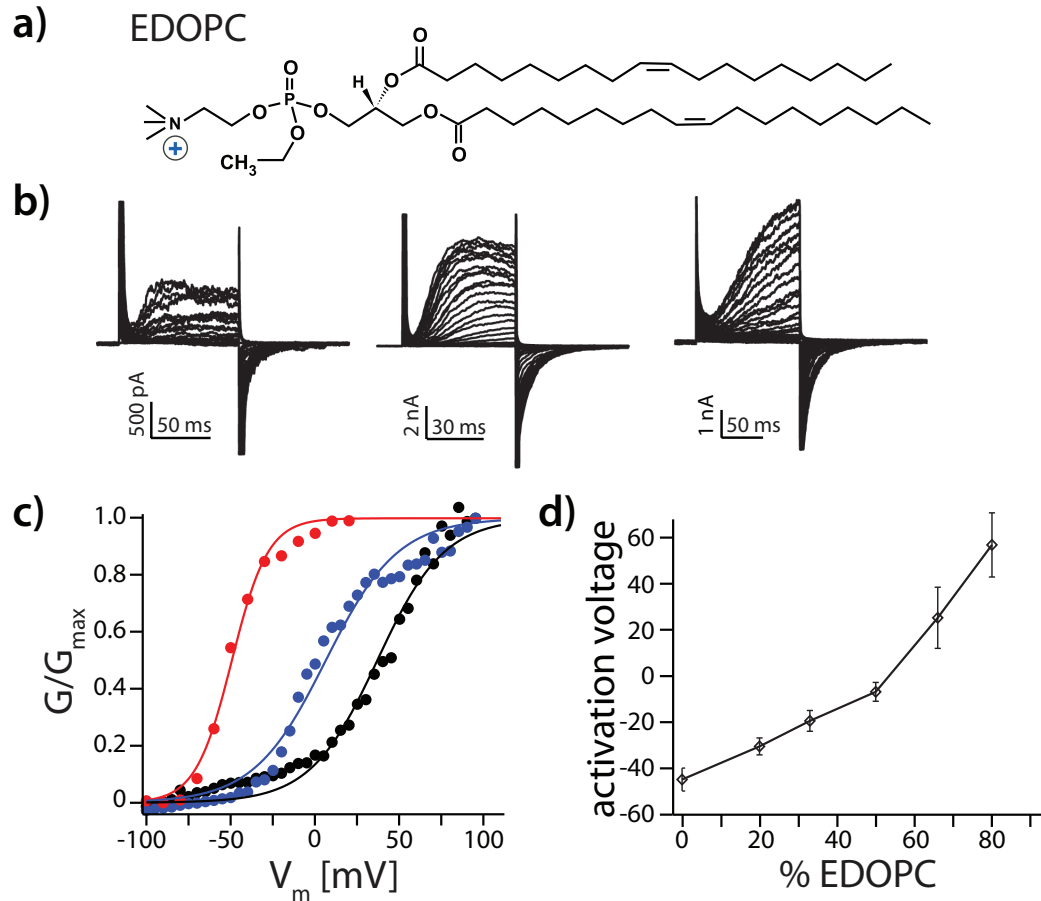


Figure 2.8: **Role of the negative charge on the phosphate group.** **a**, Chemical structure of EDOPC. **b**, KvAP in POPE:POPG vesicles (PLR 1.0) fused into bilayers of mixed EDOPC and POPE:POPG with EDOPC% 33 (1st panel), 66 (2nd) and 80 (3rd). Voltage pulses: -100 to 100 mV, $\Delta V = 5$ or 10 mV, h.p. -100 mV. **c**, Boltzmann functions (continuous lines) from normalized tail currents (black dots) measured from traces in (b) with $V_{0.5}$ (mV) and Z (mV^{-1}): -25, 2.0 (33%, blue); 19, 1.7 (66%, green); and 70, 1.5 (80%, red). **d**, "Activation voltage" $V_{0.5}$ (mean \pm s.e.m., $n=3$) versus EDOPC%.

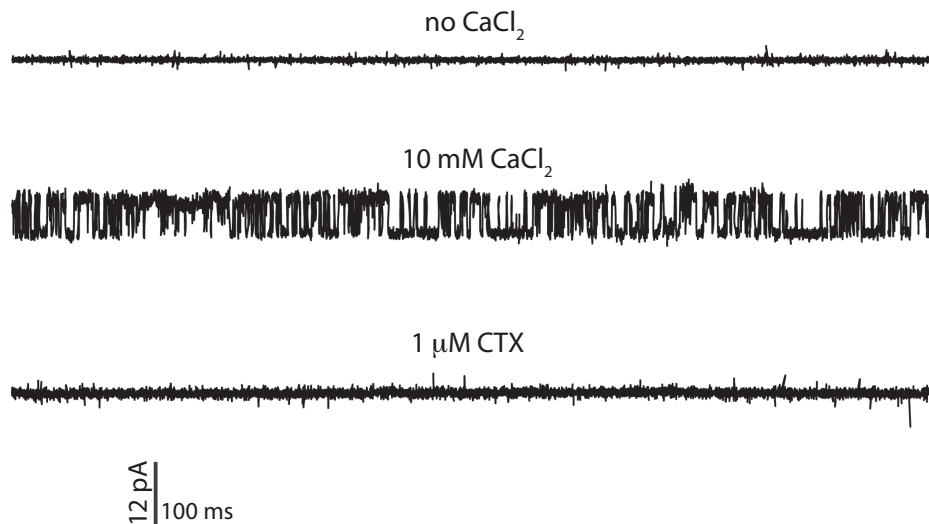


Figure 2.9: **Assessment of MthK function in EDOPC membranes.** Single channel recordings of MthK in EDOPC membranes with no CaCl_2 (top), 10 mM CaCl_2 (middle), and after the addition of 1 μM CTX (bottom). h.p. is +150 mV, and channels open upward.

PC, Dieicosenoyl-PC, Phosphatidylserine). Rates of opening and closing and mid-points of activation vary among membranes of different composition, but in all cases voltage-dependent gating is fundamentally intact. These observations suggest that the voltage-dependent mechanism is sensitive to but fairly tolerant of significant chemical variation in the lipid head group and acyl chains. However, the negatively charged phosphodiester seems to be a requirement for KvAP channel function.

The crystal structures of voltage-dependent K^+ channels KvAP, $\text{K}_v1.2$ and Paddle Chimæra revealed that voltage sensor arginine residues probably interact to some extent with the lipid membrane (Jiang et al., 2004, 2003a,b; Lee et al., 2005; Long et al., 2005a,b, 2007). The experiments presented here suggest that these interactions play an energetically significant role in voltage sensor function. Among the various properties of a lipid bilayer the presence negatively charged phosphodiester is of utmost importance. I envision that phospholipid molecules surrounding a voltage-dependent channel, even if not specifically bound to it, could mediate transient ionized hydrogen bonds (i.e. salt bridges) between the phosphodiester and the arginine guanidinium groups of the voltage sensor (Figure 2.10). Such interactions, by stabilizing specific conformations of the voltage sensor, would render the membrane a functionally important component of the voltage sensing machinery. I would argue that the usage of

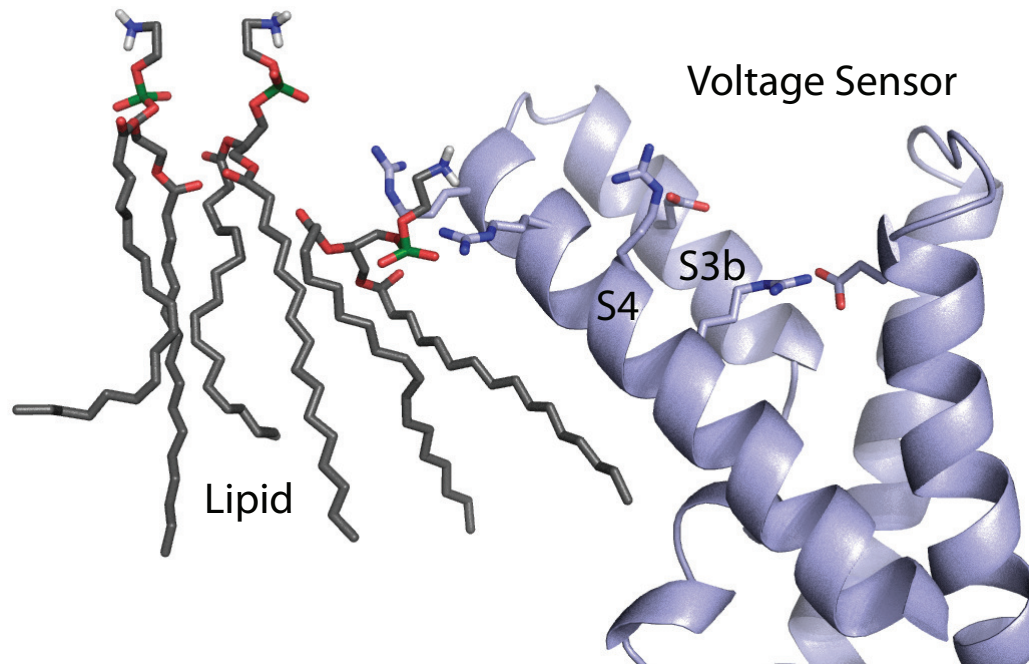


Figure 2.10: **Multidentate hydrogen-bonding between lipid phosphodiester and voltage sensor arginines.** The hypothesized interaction between the side chains of Arginine residues (R117 and R120) in the voltage sensor (PDB 1ORS) and lipid phosphodiester groups. Notice the deformation of lipid molecules directly adjacent to the voltage sensor.

positively charged amino acids with a preference toward arginine in voltage sensors is an adaptation to the phospholipid composition of the cell membrane.

2.2 KvAP's Refractory State

2.2.1 Introduction

For historical reasons most studies on the function of K_v channels have been performed on the eukaryotic Shaker K_v channel (Hoshi et al., 1994; Schoppa and Sigworth, 1998b,c,a; Zagotta et al., 1994a,b). All models assume that upon membrane depolarization, the four voltage sensors undergo a conformational change independently from each other. This conformational change is detectable as a transient gating current that results from the motion of charged amino acids across the membrane electric field. Only after all four voltage sensor have moved to their depolarized

conformation, the pore opens in a concerted manner allowing for ions to conduct. The ion conduction (i.e. current) turns on with a sigmoidal shape in the Shaker channel after membrane depolarization due to the multiple transitions that must occur.

Even if the membrane is kept at a depolarized voltage, inactivation occurs spontaneously. As such, inactivation does not represent a return to the closed conformation, because the voltage sensors remain in their depolarized conformation and the pore's gate remains opened. The pore itself, however, becomes plugged by the channel's N-terminus, thus blocking the ion permeation pathway (Hoshi et al., 1990). This mechanism is termed *N-type inactivation* and distinct from the remaining *C-type inactivation* that occurs in channels where the N-terminal peptide has been removed. C-type inactivation is not well understood, but thought to originate at the selectivity filter itself (Hoshi et al., 1991). In recent years K_v channels have been discovered in the most unlikely organisms. A K_v channel called KvAP from the thermophilic archæa *æropyrum pernix* yielded the first atomic structural information on any voltage-dependent channel (Jiang et al., 2003a). The KvAP channel, which can be synthesized by *E.coli* and is biochemically robust, has become a focus of study in many laboratories. It is known to open upon membrane depolarization, inactivates, and interacts with well-known K_v channel toxins (Ruta and Mackinnon, 2004; Ruta et al., 2003).

2.2.2 Results

The relationship between activation and inactivation

Figure 2.11a show the K^+ current response to a paired depolarization pulse carried by KvAP. During the first pulse, after the capacitive transient, KvAP channels start to open with a sigmoid-shaped time course, and inactivate after reaching a maximum current level. A second depolarization pulse elicits the same response except that the total number of active channels seems to be reduced below the level of remaining active channels in the first pulse (dotted line, Figure 2.11a). When this paired depolarization pulse is recorded with the Shaker K_v channel (a version with the N-terminal inactivation gate removed) a more typical response is observed: the current level at the beginning of the second pulse starts where the end of the first pulse left off (Figure 2.11b). The current level in the second pulse remains low, because the time in between the pulses is not sufficient for the channels to recover from inactivation. The unusual aspect of KvAP is that there are fewer active channels in the second pulse than were present at the end of the first pulse. Other differences include the rates

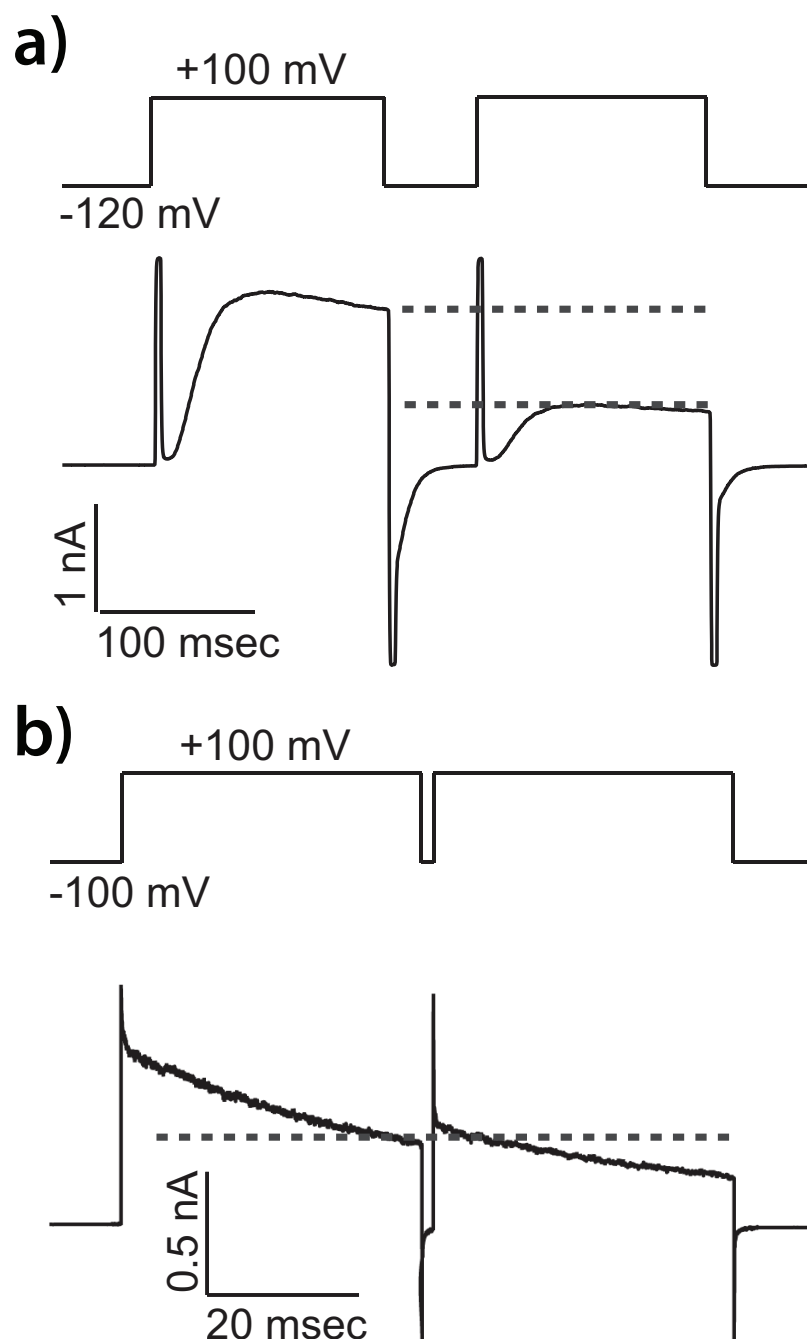


Figure 2.11: **A Comparison of Inactivation in KvAP and Shaker K_v Channels.** DPhPC vesicles containing KvAP (a) or $K_v1.2$ - $K_v2.1$ Paddle Chimæra (b) were fused into DPhPC bilayers. The current response to a paired depolarization pulse from a holding voltage -120 mV (KvAP, a) -100 mV (Paddle Chimæra, b) to +100 mV was recorded. The dotted lines indicated the current levels at the end of the first and the beginning of the second depolarization pulse.

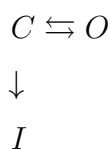
of opening and inactivation. While the sigmoid-shaped activation can be observed with KvAP, it occurs too rapidly in the Shaker channel and thus is obscured by the capacitive transient. How is it possible that for KvAP there are fewer channels open in the seconds pulse than at the end of the first pulse? This observation is explicable if KvAP can open *or* inactivate rather than open *and then* inactivate. On elaboration, if upon membrane depolarization, channels move from the closed to the open and then to the inactivated state according to this scheme:

Scheme 1.



then the fraction of the active channels in the second depolarization pulse can never be smaller than in the first pulse because all channel would have to move through the open state in order to inactivate, a process that would not happen as the membrane is held at hyperpolarized voltages in between the two pulses. If, on the other hand, channels can either open or inactivate according to this scheme:

Scheme 2.



then the fraction of open channels can be smaller in the second pulse than at the end of the first pulse. In scheme 2, as the channel moves from the closed conformation upon membrane depolarization it has the choice to either open or to inactivate.

In fact, given sufficiently brief time periods in between the pulse and sufficiently brief pulses, Scheme 2 predicts that the fractional current after the n th pulse will be given by:

$$\frac{I_n}{I_0} = A^n \tag{2.1}$$

In this expression the constant A is a function of the rate constant governing the transitions from $C \rightleftharpoons O$ or $C \rightleftharpoons I$. Figure 2.12a shows the current elicited by a series of four pulses $n=0$ to 3; Figure 2.12b graphs the fraction of initial current ($n=0$) remaining as a function of n pulses. The solid curve shows Equation (2.1) fit to the data. From this simple analysis I conclude that KvAP, upon membrane depolarization, can either open or inactivate directly from a closed conformation.

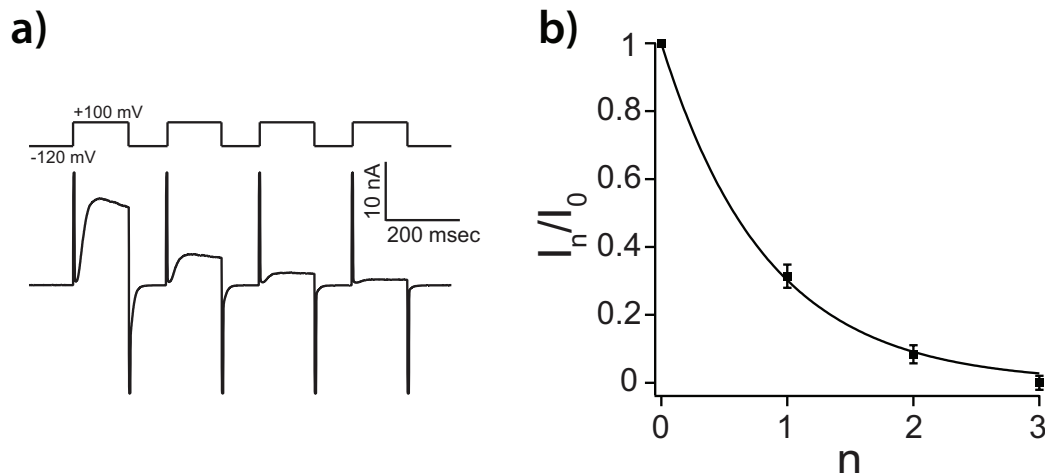
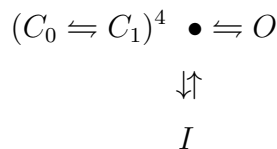


Figure 2.12: **The accumulation of inactivation between pulses follows a geometric series.** **a**, Repetitive pulse from holding voltage -120 mV to $+100$ mV. Accumulation of inactivation can be seen between pulses as a fractional decrease in current that is larger than the inactivation that occurred during the previous pulse. **b**, The fractional decrease in peak current (mean $I_n/I_0 \pm$ s.e.m, $n=5$) during depolarization as function of number of pulses (n) can be fitted to a geometric progression $I_n/I_0 = A^n$ with $A = 0.302 \pm 0.01$.

A minimal scheme for KvAP gating

I modified Scheme 2 to account for the sigmoid-shaped time course of opening and arrived at a more general form:

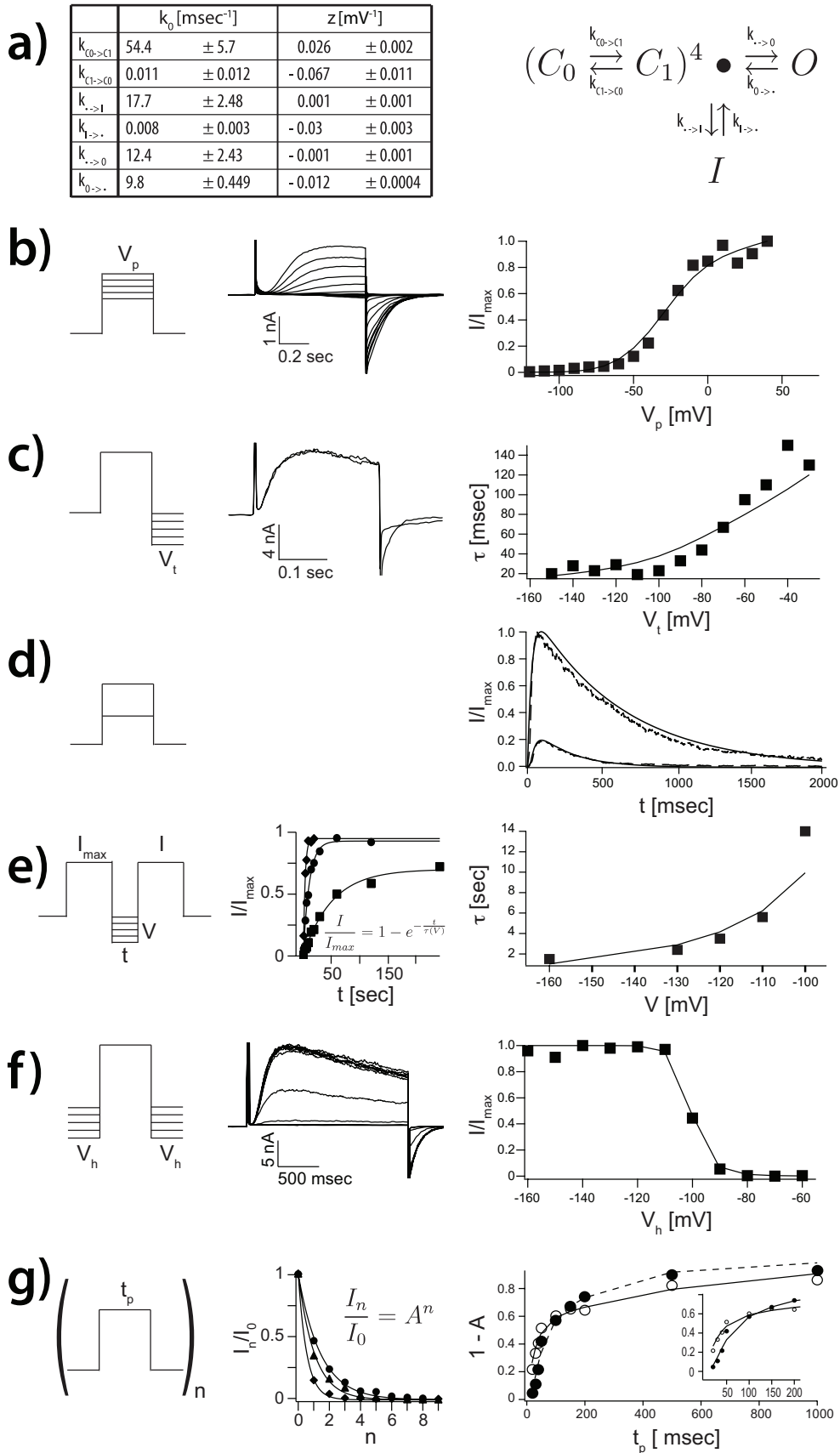
Scheme 3.



in which the closed state is represented by the state C_0 and C_1 raised to the power of 4. This form expresses the general idea that four voltage sensors must first undergo and conformational change before the pore can open (Hoshi et al., 1994; Schoppa and Sigworth, 1998b,c,a; Zagotta et al., 1994a,b). From atomic structures of K_v channels we know that the voltage sensors are arranged as independent domains surrounding and being attached to the central pore. Implicit in Scheme 3 is the idea that each voltage sensor can independently undergo a conformational change $C_0 \rightleftharpoons C_1$; once all four voltage sensors have reached the conformation representing C_1 , the channel

is in a *pre-open* state represented by the dot in Scheme 3 primed to open or to inactivate. This scheme represents the simplest gating model possible and is omitting various steps of a necessarily more complex molecular process, but can it explain the experimental recording of KvAP in planar lipid bilayers?

Figure 2.13 (*following page*): **A detailed kinetic gating scheme for KvAP in DPhPC decane bilayers.** **a**, The rate constants and their voltage dependences (\pm estimated standard deviations, see Chapter 2.2.2) as derived from fitted data below for gating scheme 3 (see text). **b-g**, The solid lines in each right panel represent numerically modeled data using parameters from table in **(a)**. Unless otherwise noted data points represent mean values of at least three independent measurements. **b**, G/V data: A representative family of currents is shown (middle panel) for voltage pulses from a common holding voltage (-120 mV) to increasingly more positive depolarization voltages (final +40 mV, ΔV 10 mV). Corresponding tail currents (I/I_{max}) are plotted (right panel). **c**, Voltage dependence of deactivation: Currents were elicited by stepping from a common holding voltage to a common depolarization voltage. Open channels were closed (deactivated) by stepping back to increasingly negative hyperpolarization voltages (-30 mV to -150 mV, ΔV 10 mV). Two representative examples are shown, -50 mV and -140 mV. Tail currents were fitted to single exponential functions and the fitted values for τ were plotted as a function of hyperpolarization voltage (right panel, $n=1$). **d**, Fractional current response (I/I_{max} , dotted lines) after prolonged depolarization to +20 mV and +100 mV respectively. **e**, Recovery from inactivation: Paired 200 ms depolarization pulses to +100 mV with increasing interpulse length were used to determine the fractional recovery of channel activity (I/I_{max}) at different holding voltages (-100 mV to -160 mV) during the interpulse. All channels were completely inactivated at the end of the first of the paired pulses. The fractional recovered currents are plotted as a function of interpulse length (representative examples, middle panel) and fitted to single exponential functions. The fitted values for τ are plotted as a function of interpulse holding voltage (right panel). **f**, Steady State inactivation: From increasingly more negative holding voltages (-60 mV to -160 mV, ΔV 10 mV), currents were elicited by stepping to a common depolarization voltage of +100 mV. Representative recordings are shown (middle panel). Fractional elicited currents (I/I_{max}) are plotted as a function of holding voltage (right panel). **g**, Repetitive pulse of varying length t_p from a holding potential of -120 mV to +20 mV or +100 mV. Exemplary data for the fractional decrease in peak current I/I_{max} during depolarization as function of number of pulses (n) is shown (middle panel) for pulses to +20 mV and three different pulse lengths (20, 30 and 50 ms). The solid line represents a fit to $I_n/I_0 = A^n$. The fraction of inactivated channel $1 - A$ is plotted against pulse length t_p for depolarization pulse to +20 mV (closed circles) and +100 mV (open circles).



All of the experiments were carried out in planar lipid bilayers with 150 mM KCl in the internal and external solutions. Figure 2.13 shows examples of raw current traces as well as graphs of quantities extracted from multiple current measurements for a set of conventional voltage protocols. Smooth solid curves correspond to the model prediction, with rate constants (k_0) and degree of voltage-dependence (z) for each step, derived through global fitting to the Scheme 3, shown in Figure 2.13a.

The activation curve (Figure 2.13b), the rate of deactivation (Figure 2.13c), the rate of recovery from inactivation (Figure 2.13e), the voltage dependence of steady state inactivation (Figure 2.13f), and the fraction of channels that inactivate after a given time as a function of voltage (Figure 2.13g) all demonstrate the voltage dependence of KvAP gating. Fits of the six rate constants and their voltage dependence suggest that all transitions exhibit some degree of voltage dependence, with the strongest in the $C_0 \rightleftharpoons C_1$ transitions. The existence of some voltage dependence in the transition between the pre-open state and the open state gives rise to a continued increase of current after an initial plateau in the activation curve (Figure 2.13b). The very strong voltage dependence in the rate of deactivation can be account for by the fact that the voltage dependence of the $C_0 \rightleftharpoons C_1$ transition occurs mostly in the $C_1 \rightarrow C_0$ direction (Figure 2.13c). Such asymmetry in the distribution of voltage dependence over a forward and backward reaction is common and does not imply that the reaction necessarily follows a different pathway in the two directions. The asymmetry is explicable if the transition state is offset to one side of the reaction pathway, in this case toward C_0 .

The inactivation process is also voltage dependent, especially in the $I \rightarrow C_1$ transition. This voltage dependence is directly observable in the voltage protocol to study the rate of recovery from inactivation (Figure 2.13e). We note that Scheme 3 can account for the inactivation observed during a depolarizing pulse (Figure 2.13d) even though there is no direct connection between the open and inactivated states. This is because the model permits the channel to transition back and forth between the opened and the pre-opened state. From the pre-opened state the channels can enter the inactivated state, which ultimately acts as a sink. Thus, according to the model, inactivation observed during a depolarizing pulse represents channels transiting from O to pre-opened \bullet to I . These data do not demonstrate the absence of a direct connection between O and I . They simply indicate that given the currently available data it is not necessary to invoke such a connection.

A subtle feature of the voltage-dependence of inactivation is also compatible with the absence of a direct connection between O and I . Figure 2.13g presents in greater detail data from series of depolarizing pulses, similar to Figure 2.12. The graph in the middle of Figure 2.13g shows the fraction of remaining current as a function of pulse number for a series of depolarizing pulses of different duration. The data are fit to exponential functions of pulse number. The graph on the right shows one minus the exponential base, which approximates the fraction of inactivation in successive pulses of the series as a function of pulse duration. Two curves are for pulse depolarization voltages of 20 mV (filled circles) and 100 mV (empty circles). For short duration pulses the 100 mV depolarization causes a larger fraction of channels to inactivate (Figure 2.13g, right panel inset). This is easy to understand in terms of Scheme 3 because at 100 mV the voltage sensors transit from C_0 to C_1 more rapidly, causing channels to achieve the pre-open state from which they can inactivate. As the pulse duration is lengthened, however, the curves cross over, meaning fewer channels inactivate at 100 mV compared to 20 mV. This observation seems to suggest that channels are relatively protected from inactivation when the open state is favored by strong depolarization.

Lipid dependence of gating

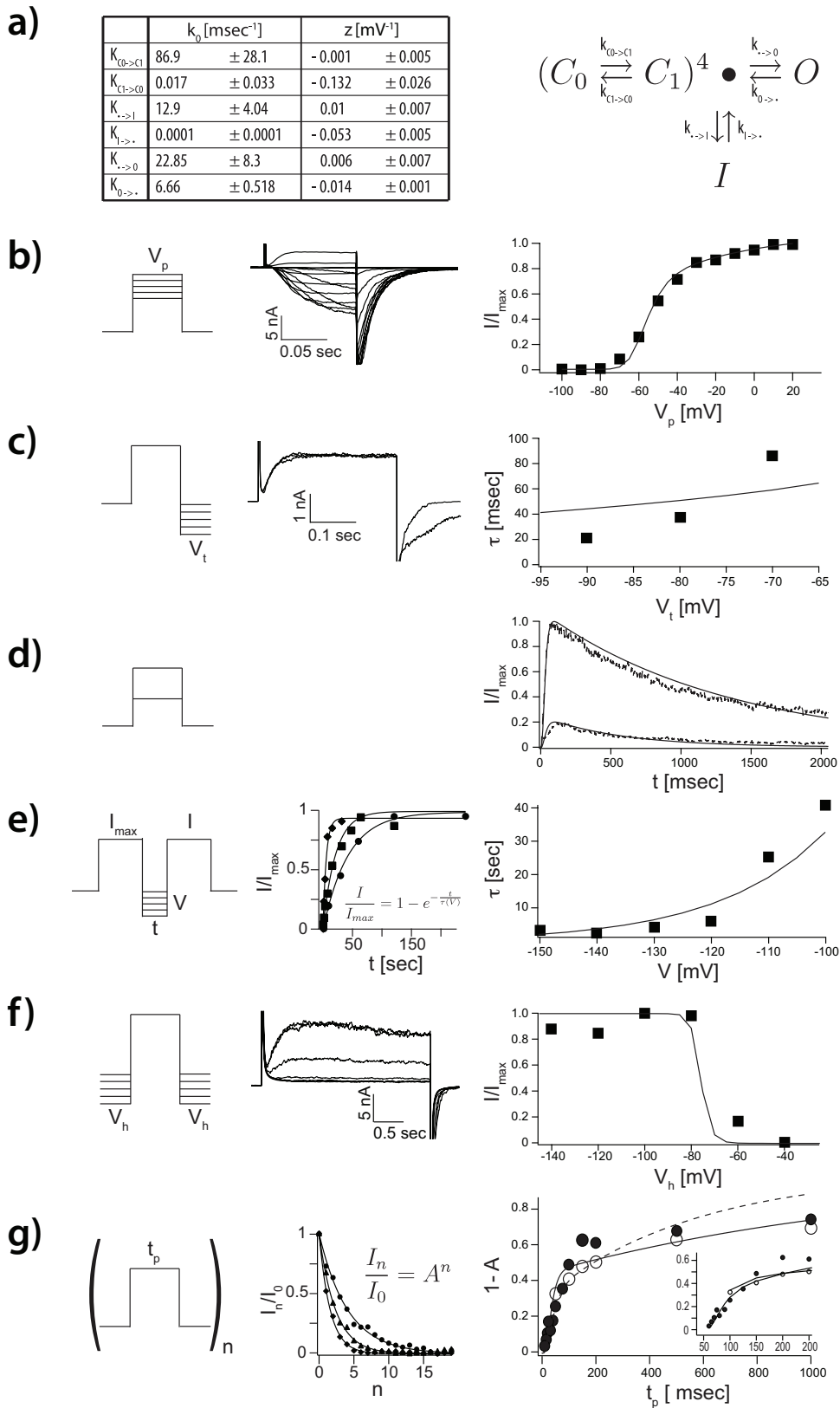
KvAP gating has been shown to depend on properties of the lipid membrane (Schmidt et al., 2006). The experiments described in this study so far were carried out using planar bilayers formed from Di-phytanoylphosphatidylcholine (DPhPC). Figure 2.14a-g shows the current response to the same voltage protocols described in Figure 2.13a-g but in membranes formed from Palmitoyl-Oleoyl-phosphatidylethanolamine (POPE) and Palmitoyl-Oleoyl-phosphatidylglycerol (POPG) at a ratio of 3 to 1. The currents in POPE:POPG membranes are qualitatively similar, but there are quantitative differences. For example, channels activate at more negative voltages and the shape of the activation curve is somewhat different (Figure 2.13b and Figure 2.14b). The inactivation observed during a depolarizing pulse occurs at a slower rate (Figure 2.13d and Figure 2.14d) and the curve describing the time constant for recovery from inactivation is shifted to more negative voltages in the POPE:POPG membranes (Figure 2.13e and Figure 2.14e). This latter effect is manifest in the tables of rate constants as a significantly smaller rate constant for exit out the inactivated state in POPE:POPG membranes (Figure 2.13a and Figure 2.14a). The practical consequence of this difference is that it is much easier to study KvAP channels in DPhPC

membranes: at a holding voltage of -100 mV recovery following a depolarizing pulse requires 10 seconds in DPhPC and 90 seconds in POPE:POPG.

States accessible to the voltage sensor toxin VSTx1

Voltage sensor toxins from tarantula venoms inhibit K_v channels by partitioning into the outer leaflet of the cell membrane and binding in a reversible manner to

Figure 2.14 (*following page*): **A detailed kinetic gating scheme for KvAP in POPE:POPG.** **a**, The rate constants and their voltage dependences (\pm estimated standard deviations, see Chapter 2.2.2) as derived from fitted data below for gating scheme 3 (see text). **b-g**, The solid lines in each right panel represent numerically modeled data using parameters from table in **(a)**. Unless otherwise noted datapoints represent mean values of at least three independent measurements. **b**, G/V data: A representative family of currents is shown (middle panel) for voltage pulses from a common holding voltage (-100 mV) to increasingly more positive depolarization voltages (final +20 mV, ΔV 10 mV). Corresponding tail currents (I/I_{max}) are plotted (right panel). **c**, Voltage dependence of deactivation: Currents were elicited by stepping from a common holding voltage to a common depolarization voltage. KvAP channels were closed (deactivated) by stepping back to increasingly negative hyperpolarization voltages (-60 mV to -160 mV, ΔV 10 mV). Two representative examples are shown (middle panel). Tail currents were fitted single exponential functions and the fitted values for τ plotted as a function hyperpolarization voltage (right panel, $n=1$). **d**, Fractional current response (I/I_{max} , dotted line) after prolonged depolarization to +20 mV and +100 mV respectively. **e**, Recovery from inactivation: Paired 200 ms depolarization pulses to +100 mV with increasing interpulse length were used to determine the fractional recovery of channel activity (I/I_{max}) at different holding voltage (-100 mV to -150 mV, ΔV 10 mV) during the interpulse. All channels were completely inactivated at the end of the first of the paired pulses. The fractional recovered currents are plotted as a function of interpulse length (representative examples, middle panel) a fitted to single exponential functions. The fitted values for τ are plotted as a function of interpulse holding voltage (right panel). **f**, Steady State inactivation: From increasingly more negative holding voltages (-40 mV to -140 mV, ΔV 20 mV), currents were elicited by stepping to a common depolarization voltage of +100 mV. Representative recordings are shown (middle panel). Fractional elicited current (I/I_{max}) are plotted as a function of holding voltage (right panel). **g**, Repetitive pulse of varying length t_p from a holding potential of -100 mV to +20 mV or +100 mV. Exemplary data for the fractional decrease in peak current I/I_{max} during depolarization as function of number of pulses (n) is shown (middle panel) for pulses to +100 mV and three different pulse lengths (100, 150 and 200 ms). The solid line represents a fit to $I_n/I_0 = A^n$. The fraction of inactivated channel $1 - A$ is plotted (right panel) against pulse length t_p for depolarization pulse to +20 mV (closed circles) and +100 mV (open circles).



the voltage sensor paddle (Lee and Mackinnon, 2004; Milesco et al., 2007; Ruta and Mackinnon, 2004; Swartz and Mackinnon, 1997b,a). In binding to the voltage sensor paddle voltage sensor toxins modify K_v channel gating. One type of voltage sensor toxin called VSTx1 inhibits KvAP channels (Ruta and Mackinnon, 2004; Ruta et al., 2003). When VSTx1 is applied the K^+ currents are reduced as shown (Figure 2.15a-b).

The graph in Figure 2.15c plots the fraction of uninhibited KvAP channels as a function of the VSTx1 concentration. This appears to be a reasonably standard titration curve except that at high toxin concentrations the uninhibited fraction does not approach zero. The reason for incomplete inhibition at high VSTx1 concentrations is that a fraction of the channels become uninhibited during the interval between depolarizing pulses. Figure 2.15d shows this effect of recovery from inhibition in a graph of the ratio of currents (I/I_{max}) in a pair of depolarizing pulses as a function of the intervening time duration (Δt) at the holding voltage. Two curves correspond to the absence (squares) and presence (circles) of a constant concentration of VSTx1. When the two depolarizing pulses are closely spaced the second pulse has less current. As the pulses are spaced further apart the current in the second pulse approaches that in the first. This behavior is qualitatively similar to the inactivation observed in KvAP in the absence of VSTx1 (Figure 2.11a and Figure 2.12). Inactivation is not observed even at the shortest time interval in the absence of VSTx1 in Figure 2.15d because at -120 mV (the holding voltage in this experiment) in DPhPC the time constant for recovery from inactivation is very brief (Figure 2.13e).

Figure 2.16a shows that a high concentration of VSTx1 has almost no effect over a time period of 600 seconds as long as the channels are held closed by negative membrane voltage (i.e. the first depolarizing pulse after a 600 second exposure to VSTx1 has close to control levels of current). Following a single depolarizing pulse, however, nearly all channels are inhibited on subsequent depolarizing pulses. The inhibition is completely reversible: if after inhibition the membrane is held at a negative voltage for a sufficiently long period of time the channels recover completely (Figure 2.16b).

These effects of VSTx1 on KvAP channels are compatible with two possible interpretations. A first interpretation is that VSTx1 binds to the voltage sensors independent of whether they are hyperpolarized or depolarized, and by binding the toxin

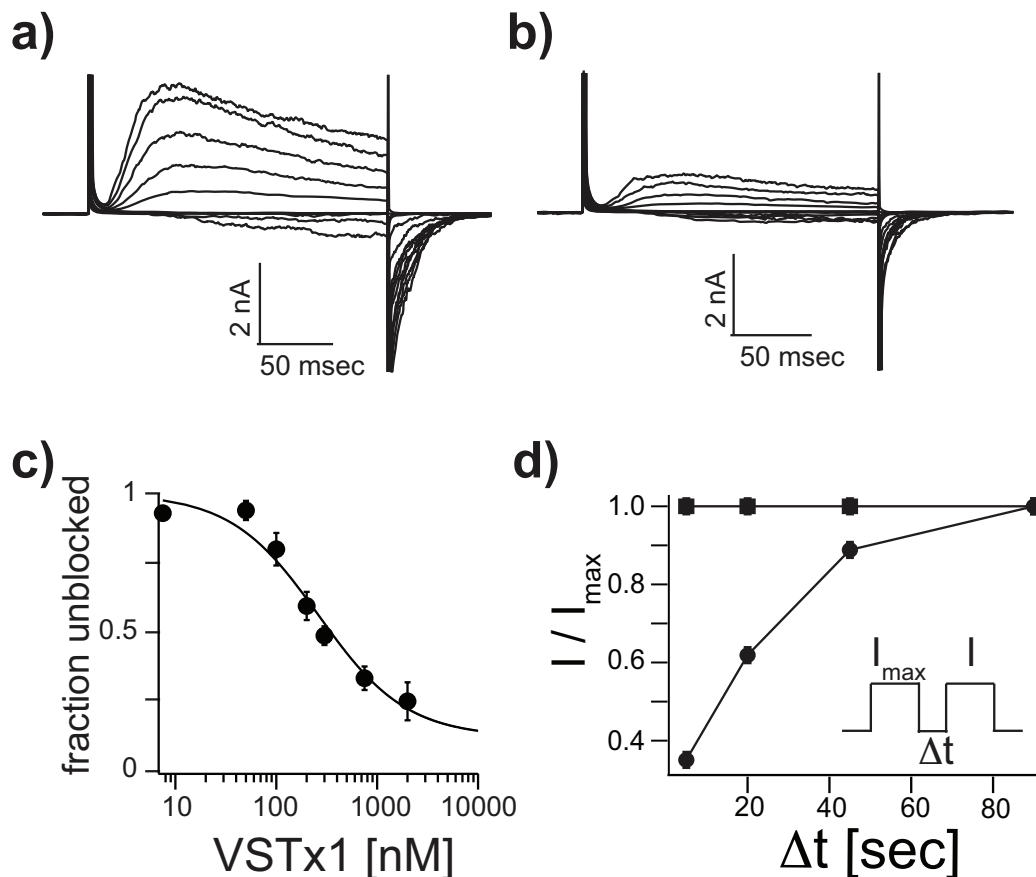


Figure 2.15: **Voltage sensor toxin VSTx1 and nature of the inactivated state.** All shown data was recorded with KvAP in the DPhPC decane bilayer system. Families of currents before (a) and after (b) the addition of 500 nM of VSTx1. Voltage pulses: -120 mV to +100 mV, ΔV 20 mV, interpulse length 20 seconds. c, VSTx1 affinity titration: Fraction of unblocked current I/I_{max} (mean \pm s.e.m, n=3) is graphed as a function of log(VSTx1 concentration). Voltage pulses: -120 mV to +100 mV, interpulse length 20 seconds. The solid line represents a fit to the titration data with $F_u = (1 + [VSTx1]/K_D)^{-1}$ with $K_D = 346 \pm 51$ nM. d, The fractional unblocked current I/I_{max} in a paired pulse experiment (mean \pm s.e.m, n=3) is plotted with (filled circles) and without (filled squares) 500 nM VSTx1 present as a function of interpulse length. As the interpulse length increases the fraction of unblocked current increase, indicating an apparently decreased toxin affinity.

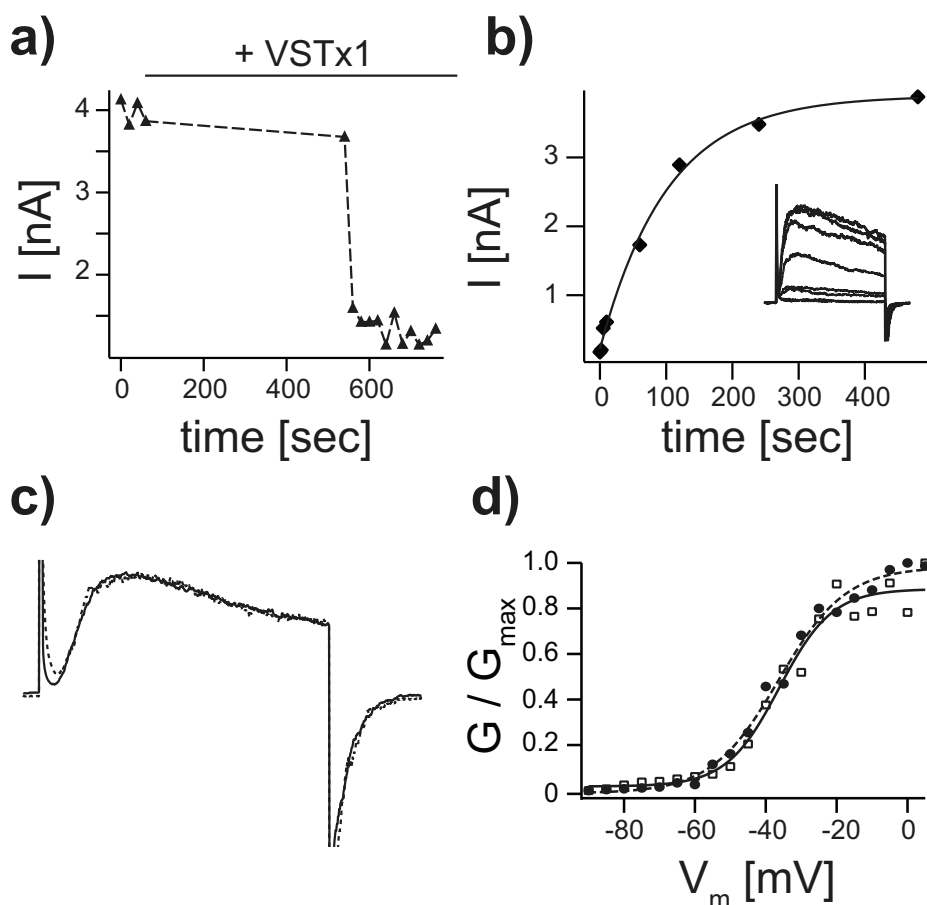


Figure 2.16: **Voltage sensor toxin VSTx1 and nature of the inactivated state.** **a**, VSTx1 is state dependent: Voltage pulse from -120 mV to $+100$ mV were elicited every 20 seconds. As the bilayer is held at -120 mV, $1 \mu\text{M}$ VSTx1 was added to the extracellular side of the channel. After a waiting period of 8 minutes without pulsing the above voltage protocols was resumed at an interpulse sequence of 20 seconds. During the hyperpolarized period no channel were blocked by VSTx1. Toxin block came on very rapidly after successive bilayer depolarizations. **b**, VSTx1 block can be overcome by prolonged hyperpolarization: Channels from (a) are blocked by addition of $1 \mu\text{M}$ VSTx1. Paired depolarization pulses with increasing interpulse length were used to determine the fractional recovery of channel activity by hyperpolarization in the presence of toxin. All channels were completely inactivated at the end of the first of the paired pulses by a set of 4 post train pulses. The fractional recovered currents are plotted as a function of interpulse length (representative example, inset) and fit to single exponential function (solid line). **c**, Normalized currents for pulses from -120 mV to $+100$ mV from families in (Figure 2.15a) and (Figure 2.15b) before (solid line) and after (dotted line) addition of 500 nM VSTx1. **d**, Boltzmann functions fit data from (Figure 2.15a) (filled circles) with $V_{0.5}$ (mV) and Z (mV^{-1}): -36.4 ± 1 , 9.5 ± 0.9 and data from (Figure 2.15b) (open squares): -36.2 ± 1.5 , 7.4 ± 1.35 .

stabilizes the inactivated state. For example, a KvAP channel with VSTx1 attached to its voltage sensors might have an increased rate into or a decreased rate out of the inactivated state. A second interpretation is that VSTx1 follows a simple rule: that it can bind to voltage sensors only when they are in a depolarized conformation. All of the properties described in Figure 2.15 and Figure 2.16 would follow naturally from this rule because amongst the states associated with depolarized voltage sensors the inactivated state is the most stable. Thus, by binding to the voltage sensor paddle VSTx1 would capture the voltage sensor depolarized, delay its return to the hyperpolarized conformation, and thereby prolong inactivation.

Figure 2.16c shows that when the residual uninhibited current in the presence of VSTx1 (or the current that has recovered from inhibition by holding the membrane voltage negative in the presence of VSTx1, as in Figure 2.16b) is superimposed on traces recorded prior to the addition of VSTx1 they are kinetically indistinguishable. The voltage-activation curves are also the same (Figure 2.16d). The simplest explanation here is that the uninhibited currents are due to channels that do not have VSTx1 attached to their voltage sensors, because it seems rather unlikely that toxin-bound channels would activate and deactivate with normal kinetics. On the basis of this reasoning I think the interpretation that VSTx1 binds only to the depolarized conformation of a voltage sensor is more likely. In other words the voltage sensor paddle becomes accessible to VSTx1 upon membrane depolarization, and can return to its hyperpolarized position only after VSTx1 dissociates.

2.2.3 Discussion

We have shown that upon membrane depolarization an approximately fixed fraction of KvAP channels inactivate instead of opening. This explains why in a series of depolarizing pulses separated by a short time interval the current level decreases as a function of pulse number. This gating behavior is unusual but not unique; it has been described in a number of K_v channels as well as Na_v channels (Aldrich et al., 1979; Aldrich, 1981; Klemic et al., 2001, 1998; Marom and Abbott, 1994; Marom and Levitan, 1994), and it accounts for a specific short-term memory effect in certain hippocampus neurons (Marom and Abbott, 1994).

The KvAP gating data are consistent with Scheme 3, which in overall connectivity is similar to models developed previously to describe gating of the Shaker K^+ channel (Hoshi et al., 1994; Schoppa and Sigworth, 1998b,c,a; Zagotta et al., 1994a,b).

The main difference between KvAP and Shaker is that for KvAP inactivation is connected to the pre-open state rather than the open state. Scheme 3 lends itself to a relatively simple structure-based physical interpretation. The $C_0 \rightleftharpoons C_1$ transition represents the conformational changes in a voltage sensor connecting hyperpolarized and depolarized conformations. During this transition the S4 gating charges cross the membrane voltage difference. This of course is the primary pulse in which the electric field within the membrane directly drives the protein conformation. The pre-open state would correspond to a channel with four depolarized voltage sensors just prior to pore opening. Assuming independent voltage sensors the pre-open probability is the probability of C_1 , given that the channel is not open or inactivated, to the fourth power. From the pre-open state the channel can either open or inactivate, the partition fraction being determined by the relative magnitudes of $k_{\bullet \rightarrow O}$ and $k_{\bullet \rightarrow I}$. During a sustained depolarizing pulse channels slowly inactivate through the sequence $O \rightleftharpoons \bullet \rightarrow I$. I is the lowest energy state given four depolarized voltage sensors and therefore channels eventually inactivate completely, or nearly so, with a sufficiently long depolarizing pulse.

This description of KvAP gating can explain the observed effects of VSTx1 if the toxin can bind only to the depolarized conformation of the voltage sensor, a conclusion that is strongly supported by the data in Figure 2.15 and Figure 2.16. Not only does it appear that the toxin cannot associate with a voltage sensor until the depolarized conformation is achieved, but the data also suggest that the voltage sensor cannot return to the hyperpolarized conformation until VSTx1 dissociates. This situation causes VSTx1 to effectively capture the voltage sensors in their depolarized conformation. This ultimately will favor inactivation because the inactivated state is the lowest energy conformation available to a channel with four depolarized voltage sensors. In terms of Scheme 3, VSTx1 inhibition of KvAP is most easily described as a reduction of the $k_{C_1 \rightarrow C_0}$ rate constant.

Studies show that the function of K_v channels is very sensitive to chemical and mechanical properties of lipid membranes (Schmidt and Mackinnon, 2008; Schmidt et al., 2006; Tabarean and Morris, 2002). My thesis research shows that membrane lipid composition influences several different transitions in KvAP gating. It will be interesting to understand mechanistically how different chemical components of lipid molecules, such as head group, glycerol backbone, ester and ether linkages, degree of saturation and structure (alkyl versus isoprenyl) of the tail, influence specific tran-

sitions in gating. Because of the extreme lipid sensitivity exhibited by K_v channels, any description of K_v channel function is only meaningful in the context of a defined membrane. The gating properties described here refer to KvAP in DPhPC-decane and POPE:POPG-decane lipid bilayers.

2.3 Gating Comparison of K_v Channels

2.3.1 Introduction

This part of my thesis research started with an experiment my thesis advisor Rod MacKinnon performed. He tested the sensitivity of the Paddle Chimæra, a $K_v1.2$ channel with a voltage sensor paddle from the $K_v2.1$ channel (Long et al., 2007; Tao and Mackinnon, 2008) in the planar bilayer system and found that Paddle Chimæra in this system was sensitive to the voltage sensor toxin VSTx1, even though according to previous studies it should not have been (Alabi et al., 2007). I set out to investigate whether this difference could be due to the different membrane environment that *Xenopus* oocytes provide when compared to planar lipid bilayers.

As described in Chapter 1.9, the function of certain membrane proteins depends upon properties of the cell membrane. In some cases protein activity can only be observed in the presence of specific lipid molecules (Robinson, 1982; Schmidt et al., 2006; Valiyaveetil et al., 2002). In other cases the membrane can have more subtle effects on the activity of a protein, as if the lipid environment exerts a regulatory effect on the membrane protein's function (Oliver et al., 2004; Perozo et al., 2002; Ramu et al., 2006).

Aside from creating a distinct chemical environment, the structure of the lipid bilayer gives it distinct material properties like fluidity, local curvature, thickness and tensile strength. How does this ensemble of both chemical and mechanical properties of the lipid membrane influence the function of a membrane protein? And could these differences be the reason why VSTx1 can block the Paddle Chimæra K_v channel in planar lipid bilayers?

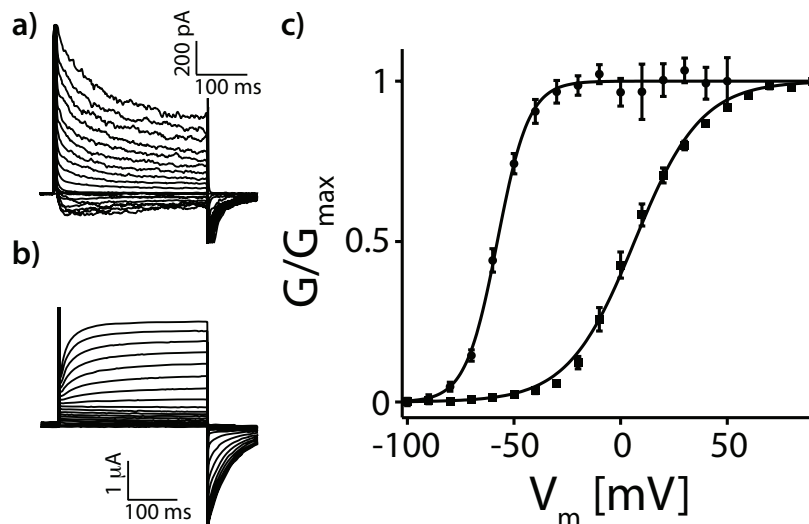


Figure 2.17: **The membrane regulates gating.** **a**, Paddle chimera in POPE:POPG vesicles was fused into POPE:POPG bilayers. Voltage pulses: holding potential (h.p.) -100 mV to 70 mV, $\Delta V = 10$ mV. **b**, Oocytes expressing paddle chimera from mRNA in two-electrode voltage clamp (TEVC). Voltage pulses: h.p. -100 mV to 70 mV, $\Delta V = 10$ mV. **c**, Boltzmann functions (solid lines) fit data (mean \pm s.e.m, $n = 13$) from **(a)** (filled circles) with $V_{0.5}$ (mV) and Z (mV^{-1}): -57.8 ± 0.4 , 3.4 ± 0.14 and data (mean \pm s.e.m, $n = 5$) from **(b)** (filled squares): 6.5 ± 0.5 , 1.6 ± 0.05 .

2.3.2 Results

The membrane regulates gating

Figure 2.17 shows several basic properties of two apparently different K_v channels. Upon membrane depolarization the channels in Figure 2.17a open (activate) very rapidly and then begin to undergo gradual closure while the membrane is still at the depolarized voltage (inactivation). Upon hyperpolarization channels return to their closed conformation (deactivate). The activation phase upon depolarization is so rapid that the capacitive current associated with charging the membrane to its new voltage obscures the K^+ current upstroke. In contrast to the fast activating channels, the K_v channels in Figure 2.17b activate much more slowly and no inactivation is evident during the duration of the depolarized pulse. Other properties further distinguish these channels. The midpoint voltage of the voltage-activation curve (voltage corresponding to half maximal activation) is -58 mV and 7 mV for fast- and slow-activating channels, respectively (Figure 2.17c). The fast-activating channels are also sensitive to the tarantula venom toxin VSTx1 (Figure 2.18a) whereas the slow-activating channels are insensitive (Figure 2.18b).

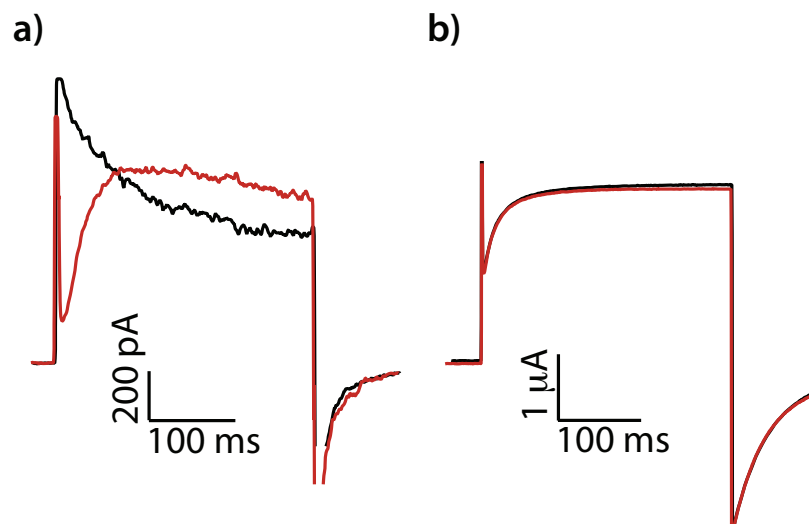


Figure 2.18: **The membrane regulates toxin sensitivity.** **a**, Paddle chimera in POPE:POPG bilayers, before (black) and after (red) addition of 500 nM VSTx1. Pulse from h.p. -100 mV to 70 mV. **b**, Paddle chimera in oocytes in TEVC, before (black) and after (red) addition of 1 μ M VSTx1. Pulse from h.p. -100 mV to 70 mV.

The distinct behavior of two apparently different K_v channels described in Figure 2.17 and Figure 2.18 actually represent the very same channels functioning in different membranes; the K_v channel is paddle chimæra. The properties of rapid activation, inactivation, a negative midpoint voltage and sensitivity to VSTx1 are observed when the channels are reconstituted into planar bilayers consisting of the lipids Palmitoyl-Oleoyl-phosphatidylethanolamine (POPE) and Palmitoyl-Oleoyl-phosphatidylglycerol (POPG) in a 3:1 ratio. The properties of slow activation, absence of inactivation, a midpoint voltage shifted by approximately 60 mV, and insensitivity to VSTx1 are observed when the channels are expressed in the membranes of *Xenopus* oocytes.

Channels studied in planar bilayers first have to be synthesized in yeast cells and then purified in detergent, reconstituted into lipid vesicles and fused with the planar bilayer (Tao and Mackinnon, 2008). Channels studied in oocyte membranes are synthesized by the oocytes after injection of RNA. In order to compare channels with the same history I fused yeast-synthesized channels directly into oocyte membranes by injecting vesicles into the oocyte (Figure 2.19a) (Morales et al., 1995). This maneuver enables a direct comparison of compositionally identical channels fused into cell membranes and planar bilayers. With respect to activation, inactivation, midpoint voltage and VSTx1 sensitivity currents measured in oocytes after RNA injection and

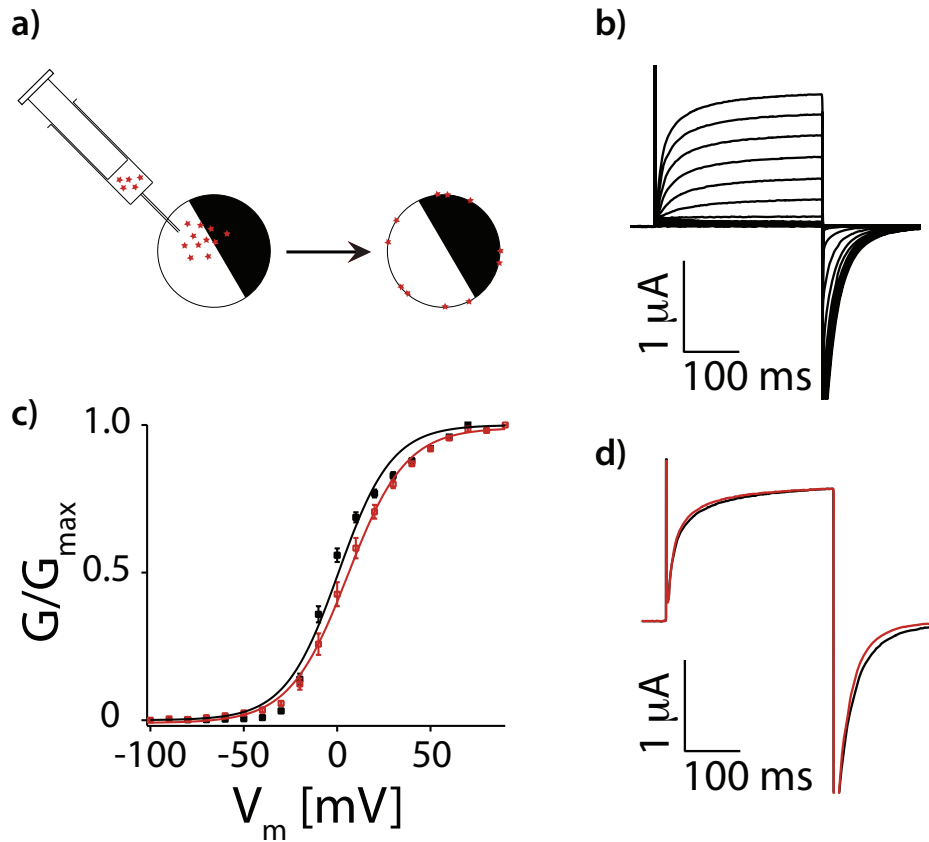


Figure 2.19: **The membrane regulates gating.** **a**, Cartoon depicting the injection of reconstituted paddle chimera protein (red stars) into *Xenopus* oocytes. **b**, Paddle Chimera vesicle injected oocytes in TEVC. Voltage pulses: h.p. -100 mV to 70 mV, $\Delta V=10$ mV. **c**, Boltzmann functions (solid lines) fit data (mean \pm s.e.m, n=5) from (Figure 2.17) (filled circles) with $V_{0.5}$ (mV) and Z (mV^{-1}): 6.5 ± 0.5 , 1.6 ± 0.05 and data (mean \pm s.e.m, n=7) from (b) (filled squares): 0.7 ± 1.2 , 1.7 ± 0.14 . **d**, Paddle chimera vesicle injected oocytes in TEVC, before (black) and after (red) addition of $1 \mu\text{M}$ VSTx1. Pulse from h.p. -100 mV to 70 mV.

after vesicle injection were indistinguishable (Figure 2.19b-d). Therefore, the distinct channel properties observed in oocyte membranes and planar bilayers must be due to environmental differences, either in the membrane or in the oocyte cytoplasm.

Effect of membrane lipid composition

To evaluate the effect of lipid composition on function, I produced planar bilayers from lipids that mimic the oocyte membrane (Hill et al., 2005). In the oocyte-like bilayers the K_v channels are more similar to channels in oocytes in that they do not inactivate (Figure 2.20b) and their voltage-activation curve is shifted to somewhat more positive voltages (Figure 2.20d). However, the midpoint of activation is still not near that observed in oocytes. Of course, I am not able to produce a genuine oocyte membrane mimic in the bilayer system for a number of reasons; oocyte membranes probably have different lipid components in their inner and outer leaflets (i.e. they are asymmetric), many minor components of the oocyte membrane are still unknown, and the planar bilayers contain decane (Miller, 1986). It might seem reasonable to think that if we could accurately replicate the composition of an oocyte membrane then I would observe oocyte-like K_v function in the bilayer system. However, previous studies (Gu et al., 2001; Laitko et al., 2006) and the experiments described below show that physical properties of the membrane other than lipid composition are also important to K_v channel function.

Effect of membrane mechanical state

Figure 2.21 compares K_v channels in planar bilayers of POPE and POPG to K_v channels in oocyte membranes using whole cell recording and isolated membrane patches with different configurations. The corresponding recording from SF9 insect cells are shown in Figure 2.22. The K_v channels in isolated membrane patches of both *Xenopus* oocytes and SF9 cells (Figure 2.21b-e and Figure 2.22a) exhibit properties that are intermediate between planar bilayers (Figure 2.21a) and oocytes recorded in the whole cell mode (Figure 2.21f and Figure 2.22b). Moreover, for *Xenopus* oocytes, there is a graded response depending on the patch configuration. On-cell patches in the absence of negative pipette pressure and outside-out patches cause channels to be more whole cell-like in their behavior, whereas on-cell patches after application of negative pipette pressure and inside-out patches cause channels to exhibit more bilayer-like behavior. The response can be quantified using the midpoint voltage (Figure 2.21g). In addition to the midpoint shift there is a noticeable change

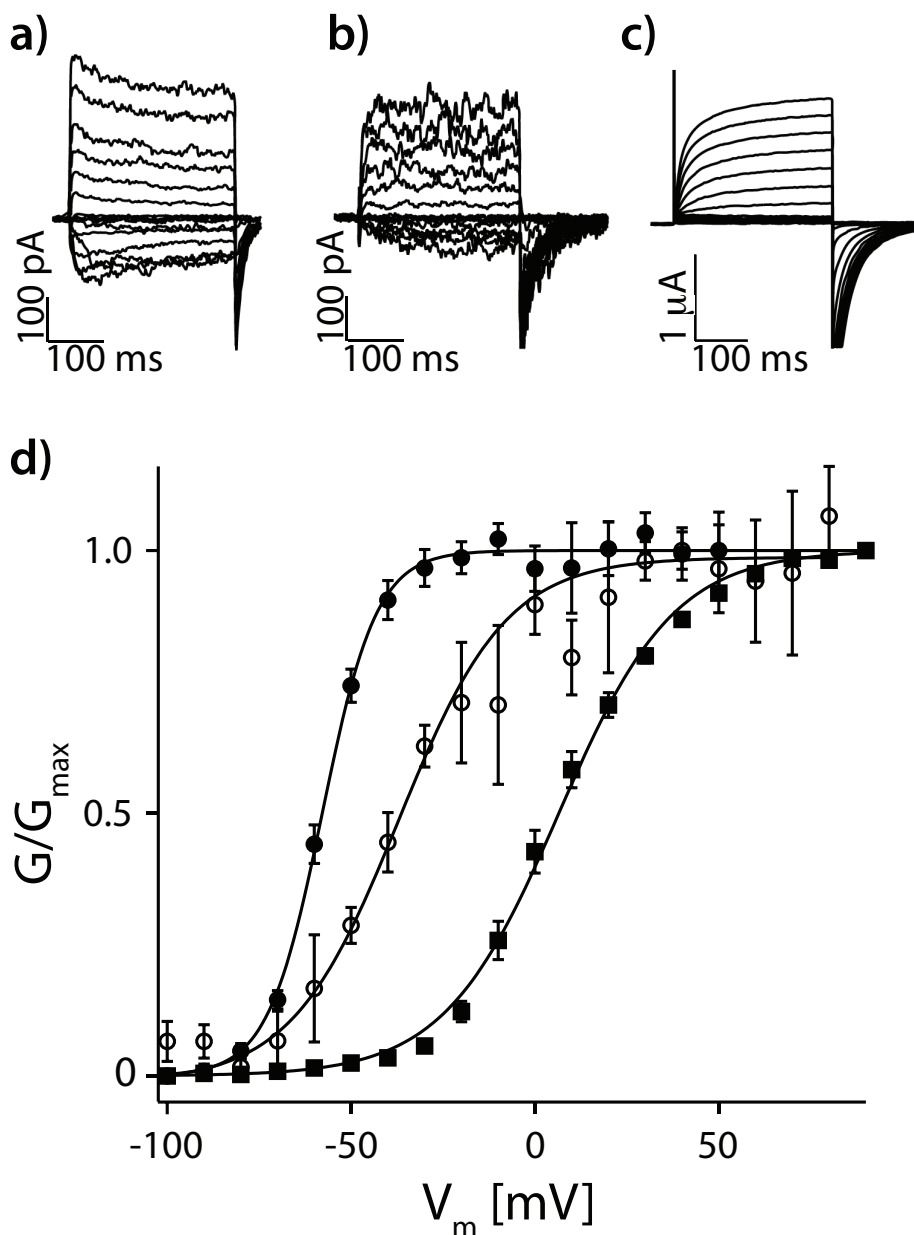


Figure 2.20: **The effect of lipid composition.** Paddle chimera in POPE:POPG vesicles was fused into bilayers of POPE:POPG (a) or 1,2-Dieicosenoyl-sn-Glycero-3-Phosphocholine : Brain Sphingomyelin : Cholesterol 2:1:1 (b). CTX was used for capacitance transient subtraction in (a) and (b). c, Oocytes expressing paddle chimera from mRNA in two-electrode voltage clamp (TEVC). Voltage pulses (a-c): h.p. -100 mV to 70 mV, $\Delta V = 10$ mV. d, Boltzmann functions (solid lines) fit data (mean \pm s.e.m, $n = 13$) from (a) (filled circles) with $V_{0.5}$ (mV) and Z (mV $^{-1}$): -57.8 ± 0.4 , 3.4 ± 0.14 , data (mean \pm s.e.m, $n = 3$) from (b) (open circles): -37.1 ± 1.9 , 1.7 ± 0.16 and data (mean \pm s.e.m, $n = 5$) from (c) (filled squares): 6.5 ± 0.5 , 1.6 ± 0.05 .

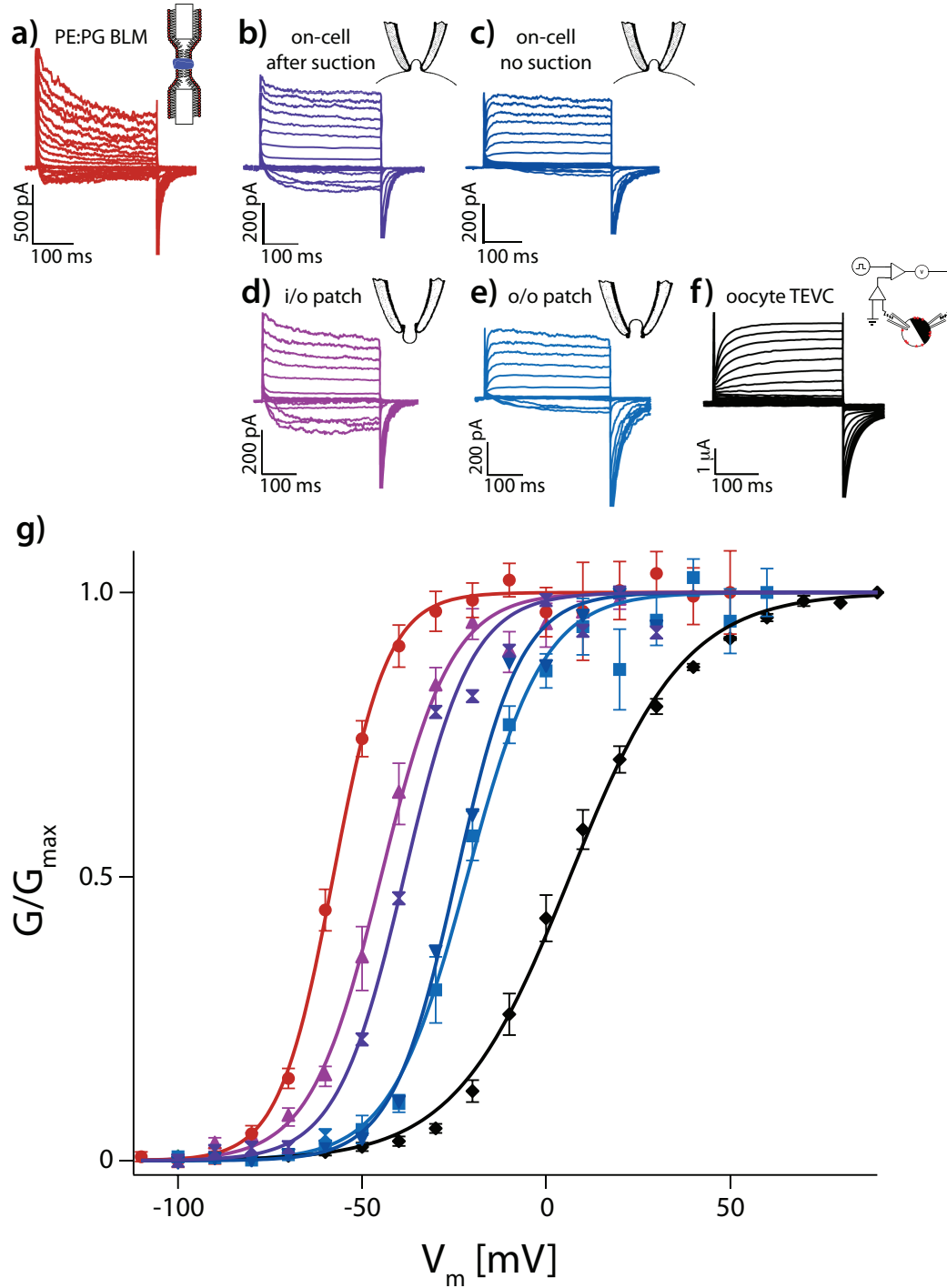


Figure 2.21: **The effect of membrane configuration.** **a-f**, Paddle chimera in various membrane configurations as denoted by the accompanying label. All voltage pulses h.p. -100 mV to 70 mV, $\Delta V = 10$ mV. **g**, Boltzmann functions (solid lines) fit data (mean \pm s.e.m, $n = 4-13$, except **(b,c)** from **(a)** (red) with $V_{0.5}$ (mV) and Z (mV^{-1}): -57.8 ± 0.4 , 3.4 ± 0.14 , **(b)** (lilac): -38.6 ± 1 , 2.7 ± 0.27 , **(c)** (purple): -24.4 ± 0.7 , 2.9 ± 0.2 , **(d)** (indigo): -44.8 ± 0.8 , 2.6 ± 0.19 , **(e)** (light blue): -21.5 ± 1 , 2.4 ± 0.21 , **(f)** (black): 6.5 ± 0.5 , 1.6 ± 0.05

in the slope of the activation curves: more negative midpoint voltages are associated with steeper activation curves.

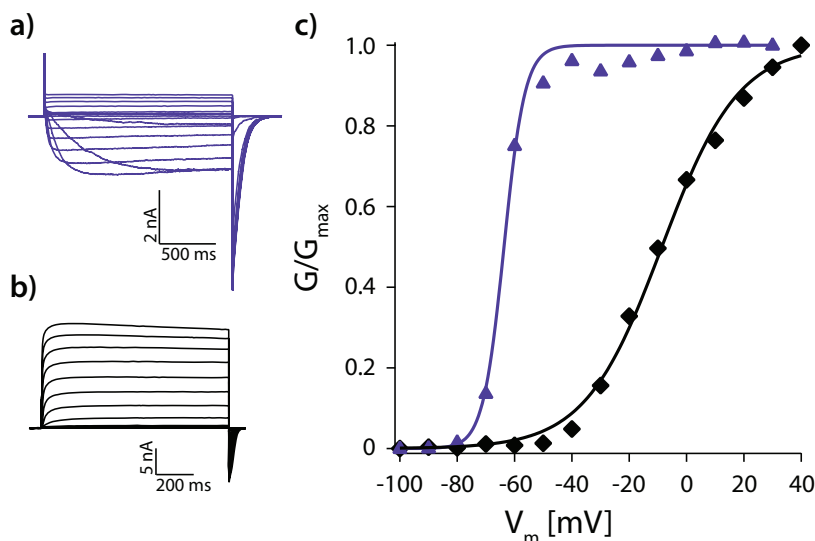


Figure 2.22: **The effect of membrane configuration.** **a**, Paddle Chimæra in on-cell patch **(a)** or whole-cell configuration **(b)** recorded from the same SF9 insect cell. **c**, Boltzmann functions (solid lines) fit data from **(a)** with $V_{0.5}$ (mV) and Z (mV^{-1}): -63.69 ± 0.53 , 3.65 ± 0.4 (on-cell patch), and from **(b)** -8.69 ± 0.65 , 13.4 ± 0.58 (whole cell).

Figure 2.23 shows that Paddle Chimæra channels in an outside-out patch can be converted from oocyte-like behavior to bilayer-like behavior by applying positive pressure inside the pipette. This effect is irreversible, meaning that once the positive pressure inside the pipette is returned to zero the behavior of the channels remains bilayer-like for the remainder of the experiment. Voltage-activation curves corresponding to three different stages during the conversion are shown (Figure 2.23a-c). As pressure is applied the curves change in three respects: the midpoint voltage shifts negative, the slope increases, and the maximum amplitude increases. The midpoint voltage shift and slope increase are similar to differences in the curves shown in Figure 2.21g. In Figure 2.21g data for each curve were obtained from a different patch, rendering a comparison of the amplitudes meaningless. For this reason the data in Figure 2.21g have been normalized to unity.

In Figure 2.23d the data were recorded from a single patch, thus the systematic increase in current amplitude is meaningful. The current could possibly increase by one or a combination of three possible occurrences: the single channel current (i)

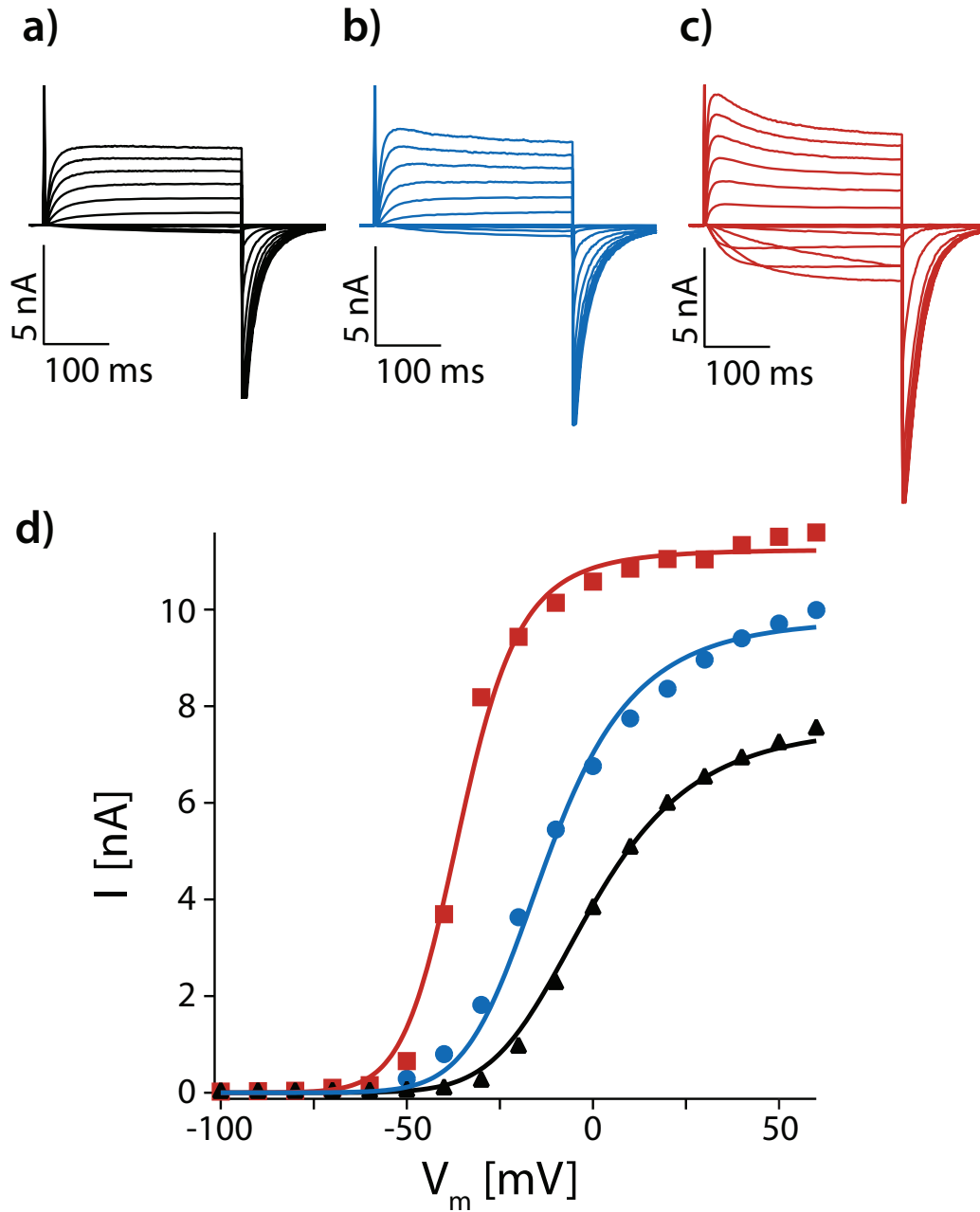


Figure 2.23: **The effect of membrane forces.** Paddle chimæra in the same outside-out patch with 0 mmHg (**a**, black), 5 mmHg (**b**, blue) and 15 mmHg (**c**, red) of transient pressure applied. Voltage pulses **a-c**: h.p. -100 mV to 70 mV, $\Delta V = 10$ mV. **d**, The solid curves are fit globally to the data from (**a-c**) with Equation 2.4 (see Chapter 2.3.2 using the relationship $\langle I \rangle = xP_O: L(0\text{mmHg}) = 1.98 \pm 0.11$, $L(5\text{mmHg}) = 5.9 \pm 0.42$, $L(15\text{mmHg}) = 79.3 \pm 10.6$, $V_m = -17.8 \pm 1$ mV, $z = 1.07 \pm 0.03$ q_e , $x = 8805 \pm 39$).

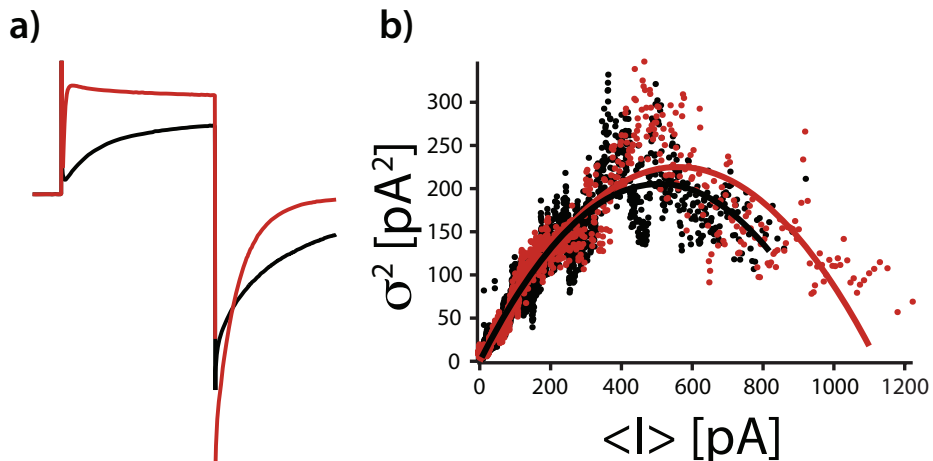


Figure 2.24: **The effect of membrane forces** **a**, Average traces (50 - 60 sweeps each) of paddle chimera in the same outside-out patch for pulses from h.p. -100 mV to 50 mV. Applied pressure is 0 mmHg (black) and 15 mmHg (red). **f**, Nonstationary Fluctuation analysis for patch data after 0 mmHg (black) and 15 mmHg (red) applied pressure. The solid curve is fit to the data with the relationship $\sigma^2 = I \cdot \langle I \rangle - \frac{\langle I \rangle^2}{N}$ (see Chapter 2.3.2), with $i = 0.812 \pm 0.002$ pA and $N = 1245 \pm 8$ channels for 0 mmHg (black) and $i = 0.802 \pm 0.003$ pA and $N = 1399 \pm 9$ channels for 15 mmHg (red).

could increase, the number of channels in the patch (N) could increase, or the open probability (P_o) could increase. By analyzing the relationship between mean current $\langle I \rangle$ and variance σ^2 for channels in a membrane patch before and after conversion from oocyte-like behavior to bilayer-like behavior it is possible to determine the origin of the current increase through the expressions (Sigworth, 1980):

$$\langle I \rangle = iNP_o \quad (2.2)$$

$$\sigma^2 = i \langle I \rangle - \frac{\langle I \rangle^2}{N} \quad (2.3)$$

This analysis shows that N and i remain approximately constant (the curves are nearly the same) while maximum P_o increases (data points extend to higher values of $\langle I \rangle$) (Figure 2.24a,b). In the example shown maximum P_o increased from 0.79 to 1.0. Analysis of multiple patches shows that maximum P_o increases from a range 0.6 to 0.8 initially to near 1.0 when channels convert from oocyte-like to bilayer-like gating behavior. In summary, three changes in the voltage-activation curve occur when the channels convert: the midpoint voltage shifts negative, opening becomes a steeper function of membrane voltage, and a higher maximum P_o is achieved. These gating effects are not unique to the paddle chimera channel. The Shaker K_v channel and

K_v2.1, for example, undergoes a similar conversion following patch excision from the oocyte surface (Figure 2.25 and Figure 2.26).

Membrane tension

The conversion of gating behavior in an excised oocyte membrane patch cannot be attributed to lipid composition of the membrane. The effect here is presumably related to the mechanical state of the membrane. What do planar bilayers and membrane patches on a glass pipette have in common that distinguishes their mechanical state from that of intact cell membranes? Past studies indicate that planar bilayers and membrane patches on glass pipettes are both under tension. Work by Haydon and colleagues estimated the tension of phosphatidylcholine bilayers with decane to be in the range of 3 to 5 dyn/cm (Cook et al., 1968; Requena et al., 1977). Webb and colleagues measured the line adhesion tension on cell membrane patches in glass pipettes and showed that its value is variable, ranging from 0.5 to 4 dyn/cm, depending on the specific patch (Opsahl and Webb, 1994). The source of membrane tension in these systems probably originates in the boundary. In a planar bilayer the boundary is formed by the torus of lipid and solvent and perhaps the solid support surrounding the bilayer. In a patch pipette the boundary is formed by lipid adhering to the glass at the patch perimeter.

The effect of lipid adhering to the patch pipette glass is demonstrated in the series of still-frames in Figures 2.27. Here giant unilamellar vesicles (GUVs) made of DOPC brought in contact with Borosilicate glass. Lipid adheres so strongly, that a lipid membrane without an underlying cytoskeleton will disintegrate within a matter of seconds. In contrast to membrane patches, large membrane vesicles unrestrained by boundaries can have very low tensions ($< 10^{-2}$ dyn/cm) (Kwok and Evans, 1981; Rawicz et al., 2000). Likewise, the tension of cell membranes under normal physiological conditions is near zero (Dai et al., 1998; Hochmuth et al., 1996; Wolfe and Steponkus, 1983). Cell membranes typically have excess membrane area in the form of folds and invaginations. This is particularly true of stage 6 *Xenopus* oocyte membranes, in which electrical capacitance measurements show that the actual membrane area is approximately ten times greater than the area calculated on the basis of the oocyte radius (Zhang and Hamill, 2000). We have not measured membrane tension in our experiments, however, the similar gating behavior in patch pipettes and planar bilayers (both high tension systems) compared to whole-cell oocyte membranes (a low

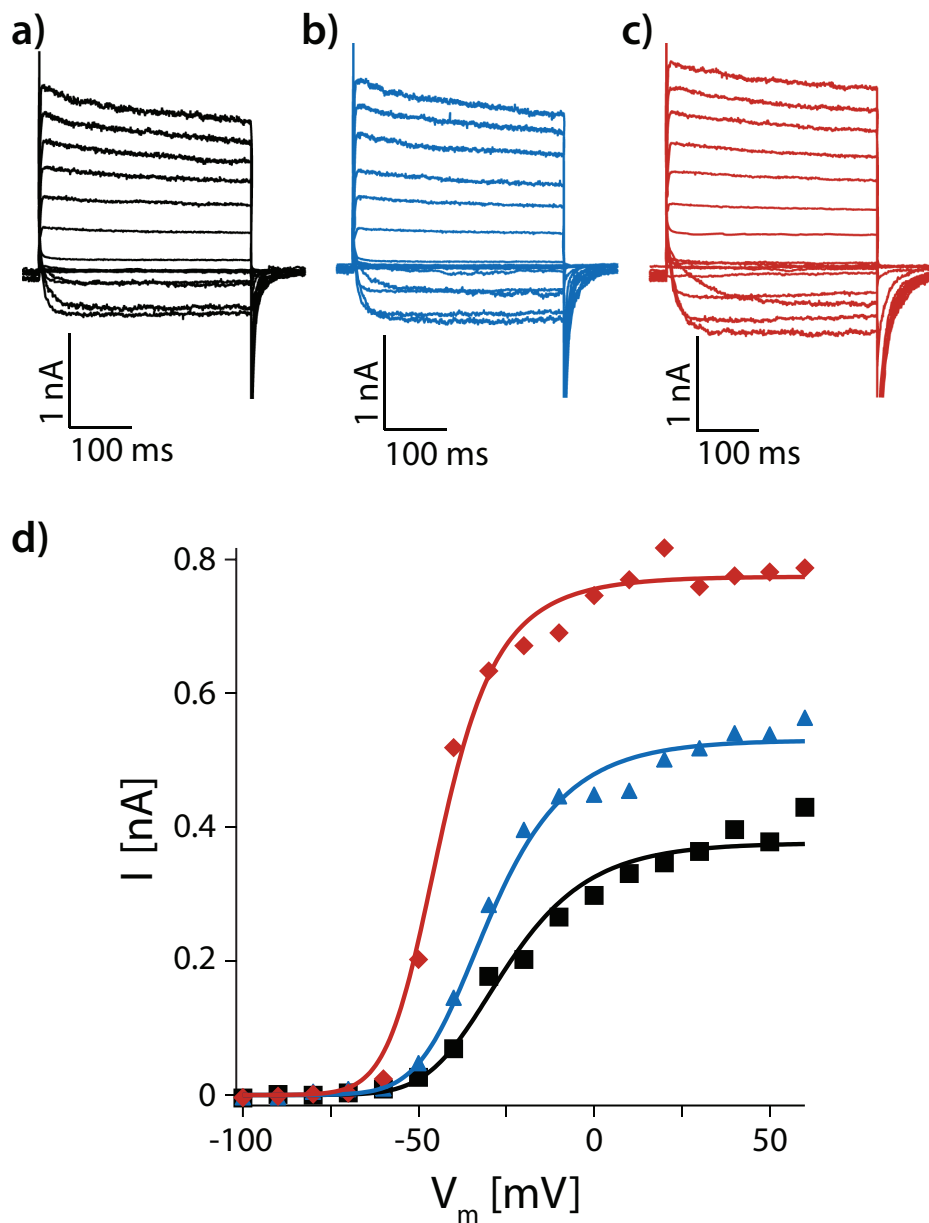


Figure 2.25: **Membrane forces alter gating in Shaker K_v .** Shaker K_v in the same outside-out patch at different time points after patch excision: 0 minutes (**a**, black), 4 minutes (**b**, blue) and 8 minutes (**c**, red). Voltage pulses **a-c**: h.p. -100 mV to 70 mV, $\Delta V = 10$ mV. **d**, The solid curves are fit globally to data from (**a-c**) with Equation 2.4 (see Chapter 2.3.2) using the relationship $\langle I \rangle = xP_O$: $L(t=0 \text{ minutes}) = 0.8 \pm 0.05$, $L(t=4 \text{ minutes}) = 1.7 \pm 0.15$, $L(t=8 \text{ minutes}) = 10.6 \pm 2.26$, $V_m = -45.6 \pm 1.3$ mV, $z = 1.5 \pm 0.08$ q_e , $x = 847 \pm 22$.

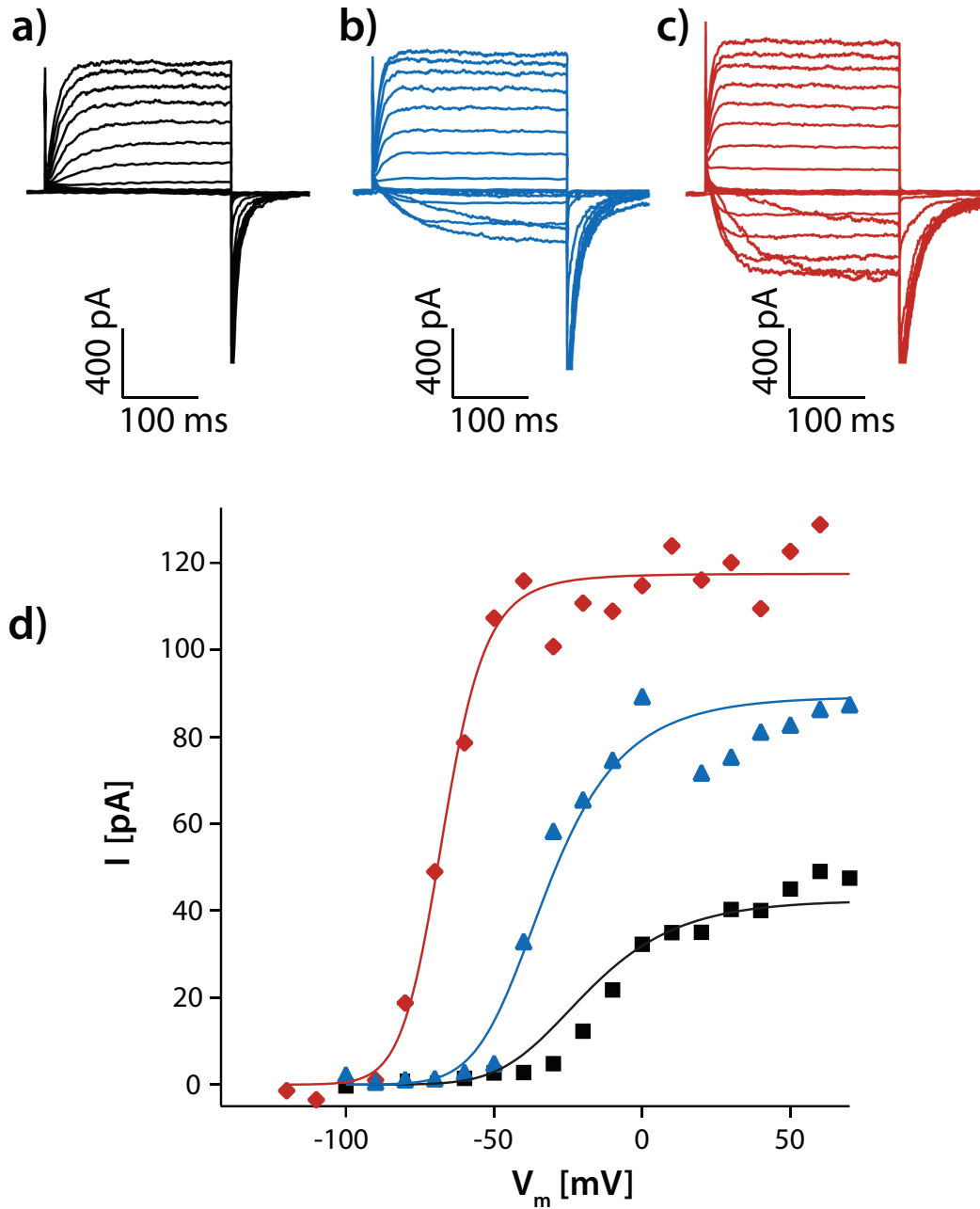


Figure 2.26: **Membrane forces alter gating in $K_v2.1$.** $K_v2.1$ channels in the same on-cell patch with 0 mmHg (a, black), 5 mmHg (b, blue) and 15 mmHg (c, red) of transient suction applied. Voltage pulses a-b: h.p. -100 mV to 70 mV, $\Delta V = 10$ mV, c: h.p. -120 mV to 70 mV, $\Delta V = 10$ mV. d, The solid curves are fit globally to data from (a-c) with Equation 2.4 (see Chapter 2.3.2) using the relationship $\langle I \rangle = xP_O$: $L(0 \text{ mmHg}) = 0.56 \pm 0.05$, $L(5 \text{ mmHg}) = 3.1 \pm 0.41$, $L(15 \text{ mmHg}) = 165 \pm 86.1$, $V_m = -46.8 \pm 2.7$ mV, $z = 1.2 \pm 0.1$ q_e , $x = 118 \pm 2.2$.

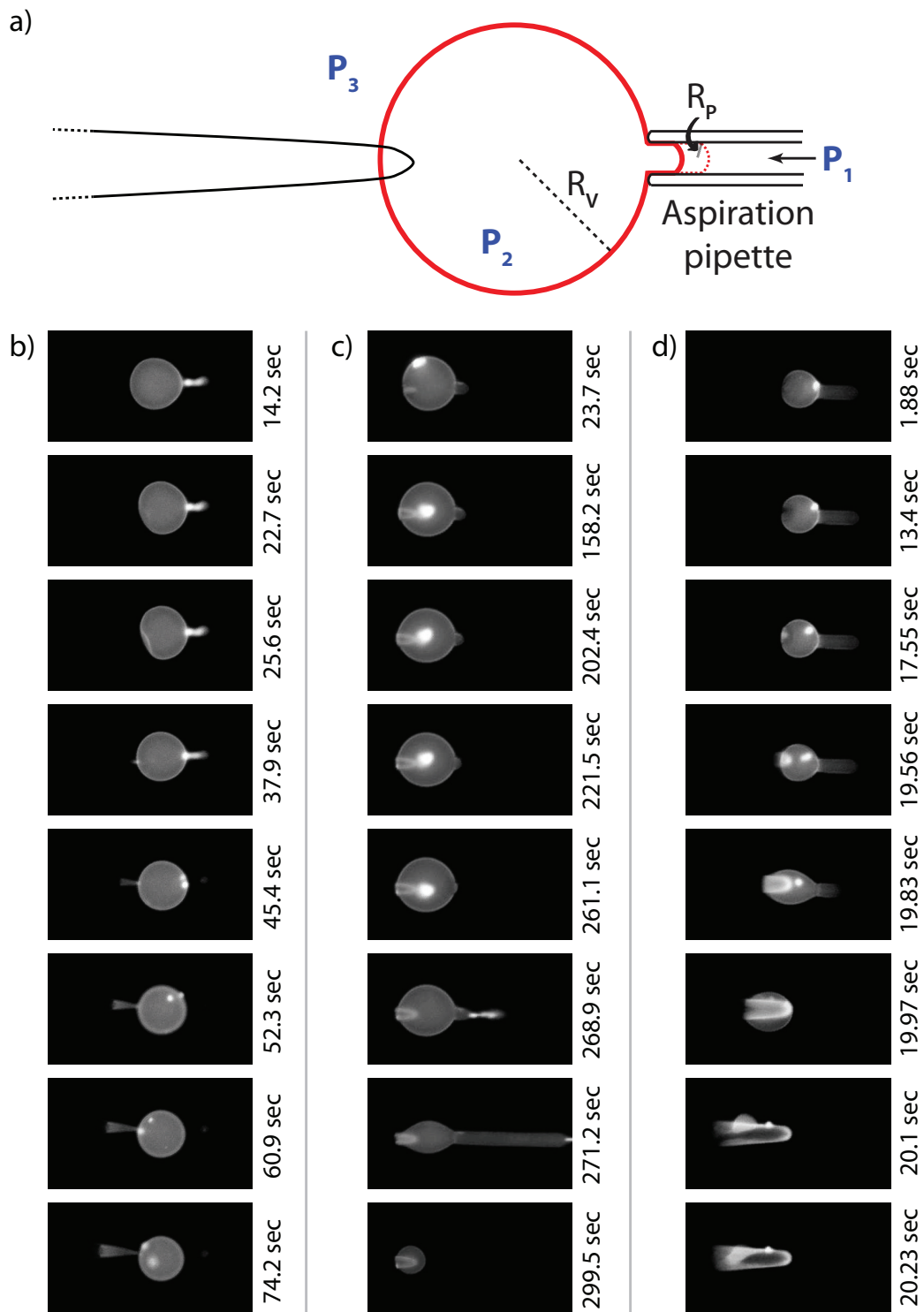


Figure 2.27: **Lipid adheres to glass.** **a**, Experimental Setup. **b-d**, Giant Unilamellar Vesicles (GUVs) formed with DOPC and Rhodamine-DOPE under different amounts of membrane tension [low (**a**), medium(**b**), high(**c**)] are brought in contact with a molten borosilicate glass rod. Invariably, the lipid/glass adhesion leads to destruction of the GUV. Timepoints are indicated in each frame.

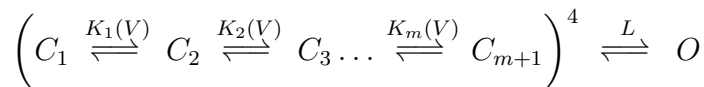
tension system) suggests that the mechanical property of the membrane influencing the channels in Figure 2.23, Figure 2.25 and Figure 2.26 might be membrane tension. The irreversibility, I suspect, stems from the fact that positive pressure in the pipette is having its effect by increasing the contact between the lipid membrane and the glass. Even when no pressure is applied to a patch the channels convert, albeit more slowly than when pressure is applied, to bilayer-like behavior, as if the system always moves toward an equilibrium state in which adhesion forces at the boundary eventually become balanced by membrane tension. The data in Figure 2.25 for the Shaker K_v channel provide an example of spontaneous conversion over time in the absence of applied pressure.

A structure-based hypothesis

Detailed kinetic studies of Shaker K_v channel gating show that upon membrane depolarization the channel undergoes multiple transitions during its sojourn from a closed state to the open state (Hoshi et al., 1994; Schoppa and Sigworth, 1998b,c,a; Zagotta et al., 1994a,b). Most of the voltage dependence occurs in the early kinetic transitions, prior to pore opening, and then eventually the pore opens in a concerted manner. Atomic structures of K_v channels are entirely consistent with this kinetic description (Long et al., 2005a, 2007). The structures reveal four voltage sensors disposed as nearly independent domains surrounding the pore, suggesting that conformational changes can occur within each voltage sensor independently. Each voltage sensor is connected to the pore through an S4-S5 linker helix (Figure 2.28a). Four S4-S5 linker helices are positioned as if to constrict the pore when the voltage sensors are in their closed *hyperpolarized* conformation. Presumably when the four voltage sensors achieve their *depolarized* conformation the S4-S5 linker helices move and thus influence the pore's equilibrium between its closed and opened conformations.

A simple state diagram captures this description (Yifrach and Mackinnon, 2002):

Scheme 4.



Here m transitions must occur within each of four independent voltage sensors before the pore can open. Voltage-dependent equilibrium constants $K_i(V)$ characterize conformational transitions within the voltage sensors, the equilibrium constant L characterizes the conformational transition of the pore from closed to open. If all voltage dependent steps are collapsed into a single transition, $K(V) = e^{zF(V-V_m)/RT}$, and

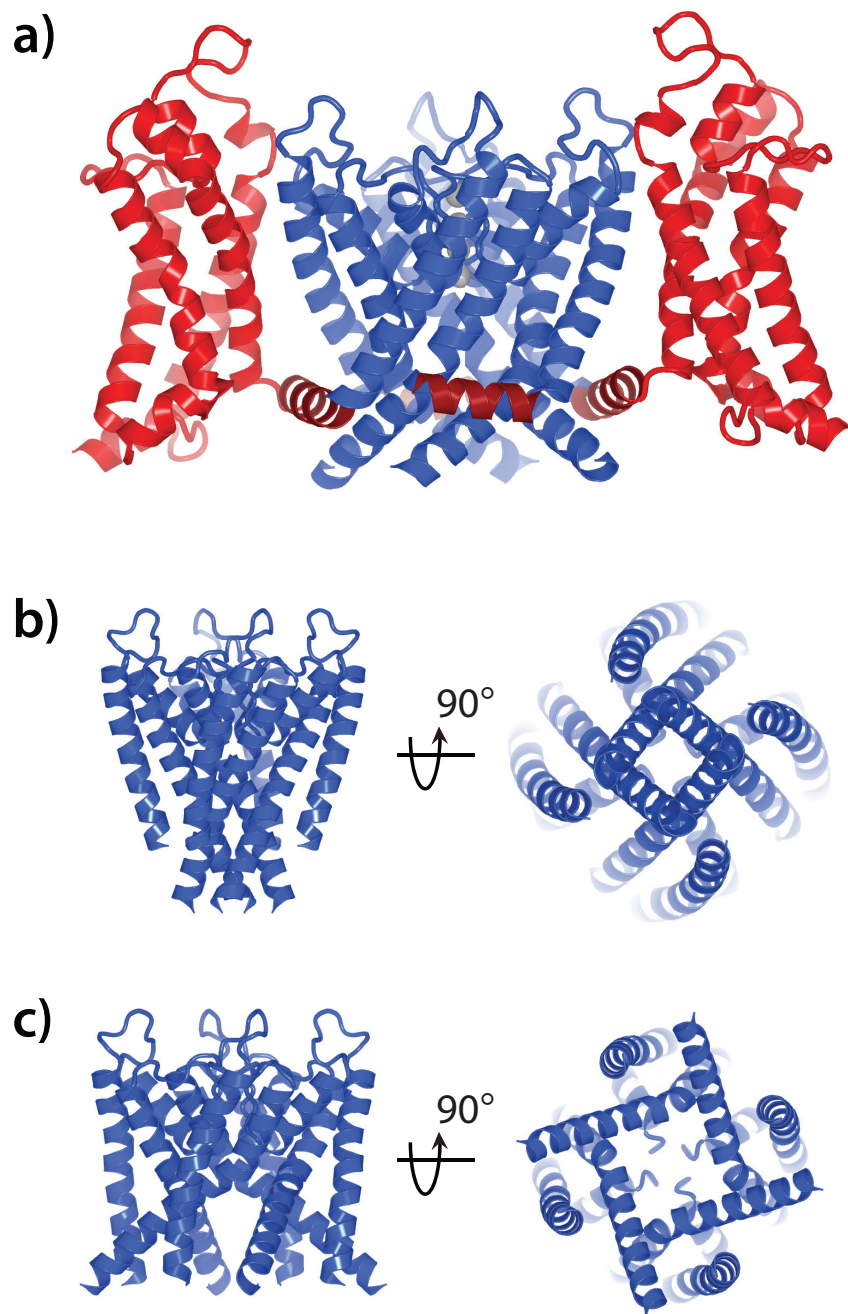


Figure 2.28: **A structural description.** **a**, Sideview of the transmembrane region of paddle chimera (PDB 2R9R). Pore domains are colored in blue, Voltage sensor domains are colored light-red. S4-S5 linkers are colored in dark-red. Only 2 voltage sensor domains are shown for simplicity. **b**, Pore domain of the KcsA structure (PDB code: 1K4C) in a closed conformation. **c**, Pore domain of the KcsA structure in an open conformation based on the MthK structure (PDB 1LNQ).

L is assumed to be voltage-independent, then the open probability P_o as a function of the equilibrium constants is given by (see Appendix 5.2 for derivation):

$$P_o = \frac{L \cdot \left(\frac{e^{zF(V-V_m)/RT}}{1 + e^{zF(V-V_m)/RT}} \right)^4}{1 + \left(\frac{e^{zF(V-V_m)/RT}}{1 + e^{zF(V-V_m)/RT}} \right)^4 \cdot L} \quad (2.4)$$

V_m is the membrane voltage at which the probability that all four voltage sensors are in the up position $P_{up} = 0.5$; z is the apparent valence of each voltage sensor. Using this simple realization of this model, I can account for the three curves in Figure 2.23 by adjusting a single parameter L . Recall that these curves differ in three quantitative aspects: midpoint voltage, steepness, and maximum P_o . All three aspects are satisfied simultaneously through the adjustment of L (but not $K_i(V)$). Similarly, data for the Shaker K_v channel and $K_v2.1$ can also be fit by this model with adjustment of L alone accounting for the gating conversion after patch excision (Figures 2.25 and 2.26, solid curves). The agreement between theory and data suggests that the mechanical effect of the membrane exerts its influence predominantly on the pore-opening step in K_v channel activation.

Atomic structures of closed and opened K^+ channels show that pore opening involves a substantial conformational change that expands the cross sectional area within the membrane's inner leaflet and changes the pore shape from that of wedge when closed, narrower near the cytoplasmic surface, to cylindrical when opened (Figure 2.28b,c) (Jiang et al., 2002). These conformational changes tie in nicely with the hypothesis that different membrane tensions underlie the curves in Figure 2.23d, Figure 2.25d and Figure 2.26d. In the theory of thin film mechanics, membrane proteins should be affected by the influence of tension on membrane thickness, curvature, and area dilation (Ursell et al., 2008). The shape change and area dilation associated with pore opening in K^+ channels suggests that this transition should be very sensitive to membrane tension.

If the effect of membrane tension on pore opening were mediated solely through area dilation of the pore ΔA , then a change in the free energy difference (between closed and opened conformations of the pore) brought about by a change in membrane tension $\Delta\gamma$, would relate to the ratio of equilibrium constants at low and high tension,

$\frac{L_1}{L_2}$, according to:

$$\Delta A \Delta \gamma = RT \ln \frac{L_2}{L_1} \quad (2.5)$$

In Figure 2.23d the theoretical curves correspond to $L_1 = 2$ in the presumed low-tension limit and $L_2 = 80$ in the presumed high-tension limit, which according to Equation (2.5) corresponds to a free energy change for the pore opening equilibrium of $3.7RT$ ($2.6RT$ for Shaker, and $5.1RT$ for $K_v2.1$ (Figure 2.25d and Figure 2.26d). The tension change in our experiments is unknown, but if I insert the maximum value of 4 dyn/cm ($1RT/\text{nm}^2$) reported by Opsahl and Webb (Opsahl and Webb, 1994) for membrane patches on glass electrodes the value ΔA comes out around 3 to 4 nm^2 , which would represent an approximate 20% expansion of the pore cross-sectional area. Without a direct measurement of tension and description of the contributions made by area expansion, curvature and thinning I do not take these absolute numbers seriously, but they serve as a check on the physical plausibility of the hypothesis.

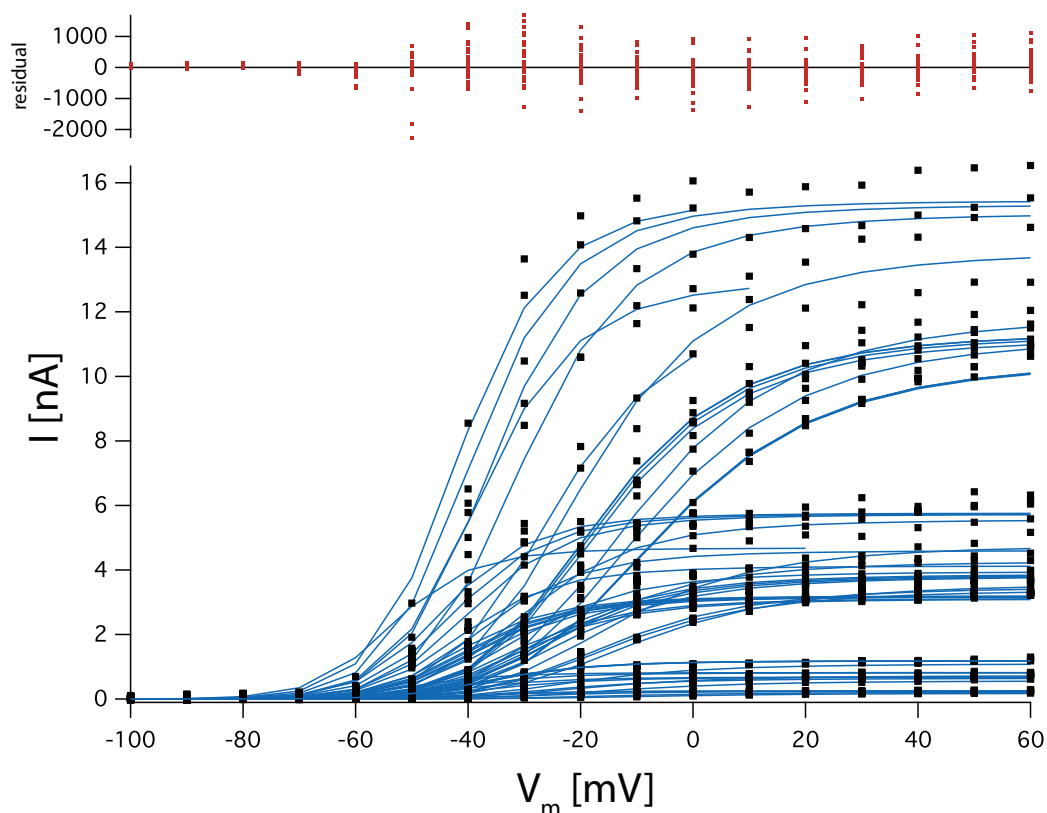


Figure 2.29: **Global Fit for tension scaling.** **a**, Global fit of 57 families of current extracted from 11 outside-out patches. Solid blue lines represent a fit of each family (black dots) to Equation 2.4 (see 2.3.2) with $\langle I \rangle = iNP_o$. Fitting residuals are graphed above (red dots). Fitting parameters are summarized in Table 2.1.

Tension Scaling

I have at this point no direct knowledge of the membrane tension that paddle chimæra channels are subjected to in oocytes or membrane patches. However, if I assume that the observed mechanosensitivity can be explained solely by footprint dilation deformation of the channel and I use the value of 4 dyn/cm ($1RT/\text{nm}^2$) as the maximal membrane tensions of a patch, I can assign each fitted value of L to a specific value of tension γ' .

The dataset used for this analysis contains 11 individual patches from which 57 families of current were extracted. Each family represents one value of membrane tension γ' that was altered either by spontaneous or pressure induced lipid/glass adhesion. Each G/V curve is fitted according to Equation (2.4) with $\langle I \rangle = xP_o$. The results of this global fit are shown in Figure 2.29 and the fitting parameters are summarized in Table 2.1. While the voltage dependence of the voltage-sensor movement, $K(V) = e^{zF(V-V_m)/RT}$, was constrained to be the same across all patches, the product of channel number and single channel conductance ($x = iN$) was constrained only within the families belonging to the same patch. These constraints express the hypothesis that the difference between the G/V curves can be explained solely by a membrane tension dependent change in the late-opening step equilibrium constant L . An unknown tension γ' can be found as (see Appendix 5.1 for derivation):

$$\gamma' = \gamma_{max} \cdot \frac{\ln\left(\frac{L_{\gamma'}}{L_{\gamma=0}}\right)}{\ln\left(\frac{L_{\gamma_{max}}}{L_{\gamma=0}}\right)} \quad (2.6)$$

$L_{\gamma=0}$ and $L_{\gamma_{max}}$ are the minimum and maximum fitted parameter L , respectively (see Table 2.1). Figure 2.30 shows plots of channel open probability as a function of scaled tension γ' at different depolarization voltages. The open probability P_o is calculated with for each family using the relationship $\langle I \rangle = iNP_o$ by dividing the patch current with the fitted parameter $x = iN$. The resulting plots recast data from whole-cell and patch recordings: At zero tension (i.e. whole-cell oocytes) the midpoint of activation ($P_o = 0.5$) can be found at +10 mV (Figure 2.30, middle row, right panel). At maximal tension $\gamma_{max} = 4$ dyn/cm ($1 RT/\text{nm}^2$) the midpoint is found at -50 mV (Figure 2.30, top row, second to left panel). Interestingly, a closer inspection of the data reveals that the channel open probability is most sensitive to modest changes in tension at membrane voltages around -20 mV. A change in membrane tension by 1.6 dyn/cm ($0.4 RT/\text{nm}^2$) will increase the open probability by 50% at -20mV, whereas

the same change of membrane tension at -40mV or $+20\text{mV}$ will increase it only by 5% or 20% respectively (see Figure 2.30, top row, second to right panel and Figure 2.30, bottom row, left panel).

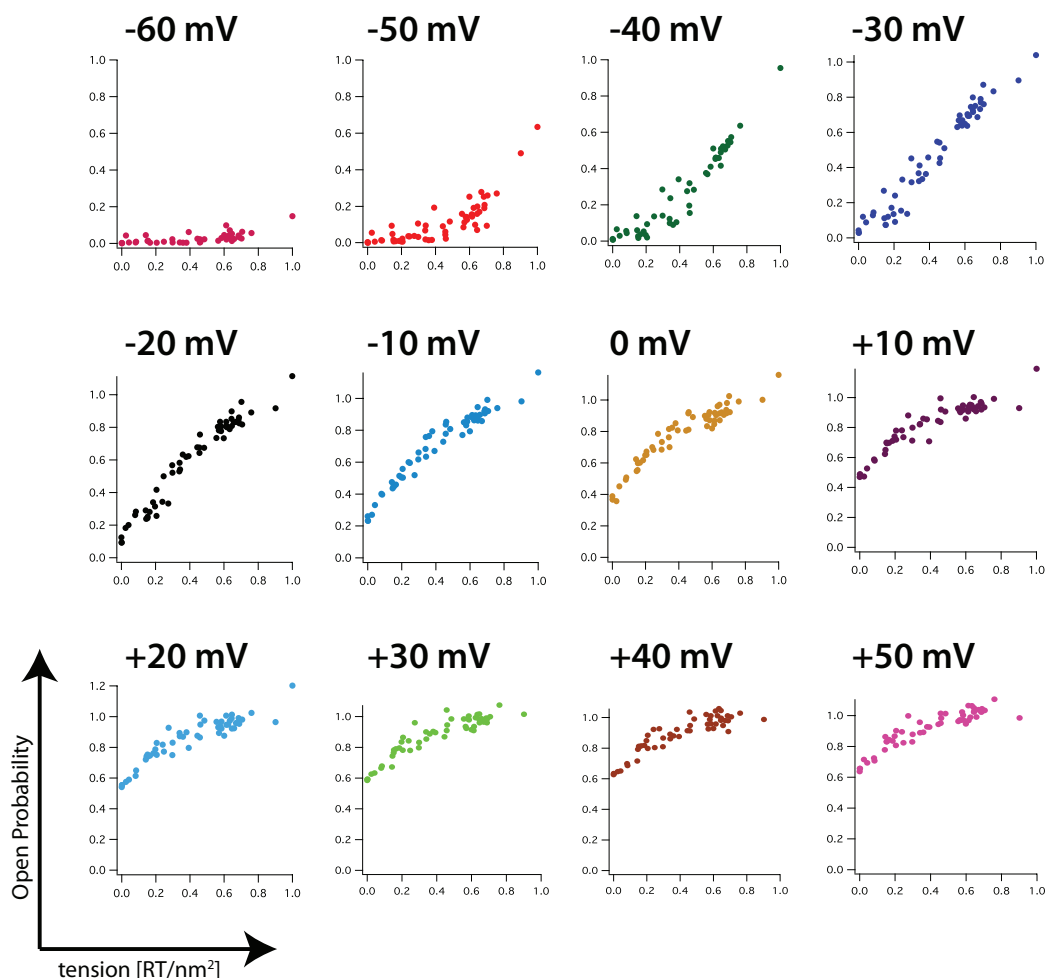


Figure 2.30: **Tension sensitivity at different membrane voltages.** a, Paddle Chimæra open probability as a function of calculated tension γ' at different membrane voltages.

Membrane mechanical state and voltage sensor toxins

The most puzzling initial observation in this study concerns the dependence of VSTx1 sensitivity on the membrane: channels are sensitive to this toxin in planar bilayers but insensitive in oocytes (Figure 2.18). VSTx1 and other voltage sensor toxins partition into the membrane in order to modify K_v channel gating (Lee and

Table 2.1: Global Fitting Parameters for Tension Scaling

Globals	V_m	-25	± 0.5	[mV]							
	z	1.12	± 0.02								
Locals	late-step equilibrium constant L										$x = iN$
Patch 1	1.97	1.97	1.95	2.4	3.02	7.4	23.4	41.9	64.7	88.4	15675
	± 0.1	± 0.1	± 0.1	± 0.1	± 0.1	± 0.4	± 1.8	± 3.5	± 5.7	± 8	± 87
Patch 2	4.5	13.74	12.4	15.3	23.7						4108
	± 0.6	± 2.5	± 2.3	± 2.9	± 4.9						± 90
Patch 3	3.1	9.8	50.5	445							4688
	± 0.4	± 1.5	± 9.8	± 99							± 86
Patch 4	6	5.7	5.3	6	12.6	55.2					13215
	± 0.4	± 0.4	± 0.4	± 0.4	± 1.1	± 5.8					± 155
Patch 5	7.1	82.4	261								821
	± 5.5	± 88	± 296								± 76
Patch 6	4.3	12.3	39.9	73.9							691
	± 3.5	± 12.7	± 49	± 94							± 81
Patch 7	4.8	9.86	80.39								4171
	± 0.7	± 1.8	± 19								± 103
Patch 8	4.5	21.7	65	90	121						5806
	± 0.4	± 3	± 10	± 14	± 20						± 63
Patch 9	8.7	43	46.6	44.9							1210
	± 4.7	± 30	± 32	± 31							± 73
Patch 10	23.3	27	46.4	57.8	64.4	54.7	69.4	81.7			3228
	± 5.5	± 6.5	± 12	± 15	± 17	± 14	± 19	± 22			± 47
Patch 11	2.2	4.2	16.5	60.7	54.2						254
	± 4.4	± 9	± 48	± 206	± 183						± 78

Mackinnon, 2004; Milesu et al., 2007). Moreover, the type of lipid in the membrane is known to influence the partition coefficient and therefore one might expect lipid compositional differences to be at the root of the differential VSTx1 sensitivity in the two membrane systems (Jung et al., 2005; Lee and Mackinnon, 2004). Against expectation, experiments show that VSTx1 sensitivity is in fact dependent upon the mechanical state of the membrane (Figure 2.31). When applied to channels in an outside-out patch from oocytes VSTx1 causes a slowing of activation (Figure 2.31a,b) similar to the effect observed in planar bilayers (Figure 2.18a). The kinetic changes are also associated with a shift in the midpoint voltage to more positive values (Figure 2.31c, open circles).

Insensitivity of the paddle chimera channel to VSTx1 applied to whole oocytes cannot be attributed to an inability of the toxin to reach the surface: VSTx1 does not affect paddle chimera channels recorded in whole cell mode in devitellinized oocytes (data not shown) and the pore-blocking toxin CTX, which is similar in size to VSTx1, inhibits the paddle chimera channel in whole oocytes and in planar lipid bilayers with similar affinities (Figure 2.32). Furthermore, Swartz and colleagues have shown that in whole oocytes VSTx1 inhibits a chimera $K_v2.1$ channel containing the KvAP voltage sensor paddle (Alabi et al., 2007). Therefore VSTx1 must be able to reach the oocyte surface.

The apparent affinity of VSTx1 for paddle chimera in excised membrane patches and in planar bilayers is high, as it exerts its effect in the 10 to 50 nM range (Figure 2.33a,b). Molecular specificity is also an essential component of the VSTx1-paddle chimera interaction: VSTx1 does not affect $K_v1.2$ in planar bilayers (Figure 2.33c,d). Paddle chimera and $K_v1.2$ differ only in the amino acid composition of the voltage sensor paddle, which has been shown to form the binding site for voltage sensor toxins (Swartz and Mackinnon, 1997b,a). Apparent high affinity and molecular specificity distinguish in a fundamental manner the VSTx1-paddle chimera interaction from the previously reported GsMTx4-stretch-activated channel interaction (Suchyna et al., 2004). GsMTx4 modifies stretch-activated channel gating with low affinity (500 nM range) and in the absence of traditional molecular specificity, as the *D*-enantiomeric form of the toxin was reported to be as effective as the *L*-enantiomer (Suchyna et al., 2004). Amphipathic, membrane active molecules such as capsaicin have been shown to alter gating of voltage-dependent Na^+ (Na_v) channels. These agents exert their effects in the 10 μ M range and can be mimicked by detergents (Lundbaek, 2008). In

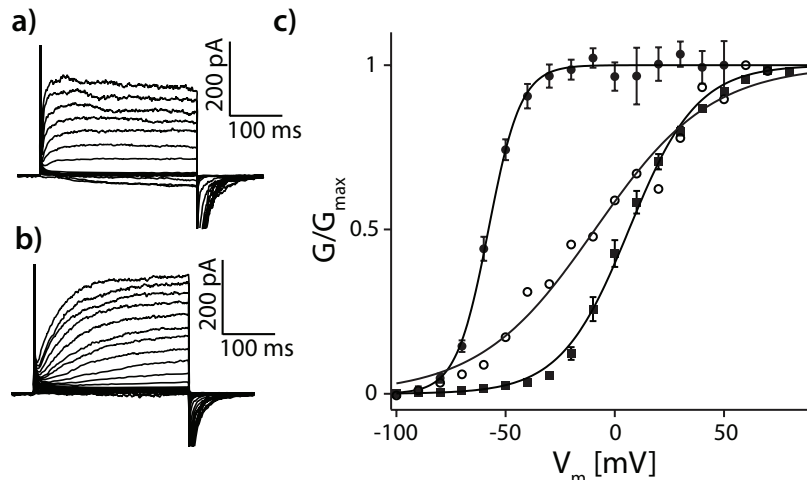


Figure 2.31: **Membrane mechanics and voltage sensor toxins.** All voltage pulses from h.p. -100 mV to 70 mV, $\Delta V = 10$ mV. **a-b**, Paddle chimera in an outside-out patch, before **(a)** and after **(b)** addition of 500 nM VSTx1. **c**, Boltzmann functions (solid lines) fit data (except data from **(b)** mean \pm s.e.m, $n = 5-13$) from Figure 2.17 (POPE:POPG bilayer, filled circles) with $V_{0.5}$ (mV) and Z (mV^{-1}): -57.8 ± 0.4 , 3.4 ± 0.14 , data from **(b)** (open circles) with $V_{0.5}$ (mV) and Z (mV^{-1}): -9.1 ± 2 , 0.9 ± 0.07 and data from Figure 2.17 (whole-cell oocyte, filled squares) with $V_{0.5}$ (mV) and Z (mV^{-1}): 6.5 ± 0.5 , 1.6 ± 0.05 .

contrast to low-affinity amphipathic agents acting on Na_v channel gating and GsMTx4 acting on stretch-activated channels, VSTX1 functions at low concentration, exhibits molecular specificity mediated by the protein surface of the voltage sensor paddle, and yet it is sensitive to the mechanical state of the membrane.

How can we understand voltage sensor toxin sensitivity being a function of the mechanical state of the membrane? Theoretical studies predict that under certain circumstances tension-dependent aggregation of membrane proteins can occur (Goulian et al., 1993). It is therefore possible that tension changes can influence toxin affinity. A more likely explanation, I think, is implied by a feature of the data: VSTx1-inhibited channels in planar bilayers and patches actually appear similar in behavior to channels recorded from whole oocytes (Figure 2.31a,b and Figure 2.33a). VSTx1 inhibited channels in planar bilayers, for example, exhibit slow activation, little inactivation, and the midpoint voltage is shifted to positive voltages (Figure 2.31c). These features are all qualitatively similar to paddle chimera channels in whole oocytes. Therefore voltage sensor toxins might actually modify gating by altering the mechanical forces acting between the channel and the membrane. In this

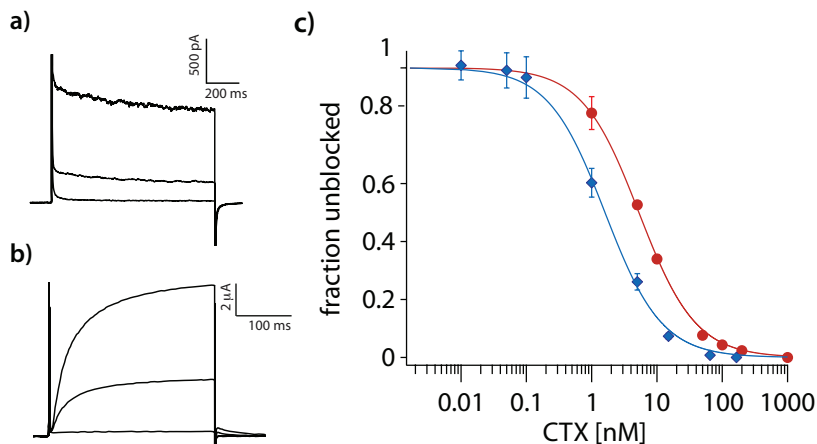


Figure 2.32: **Pore-blocking toxin CTX affinity.** **a**, Paddle chimera in POPE:POPG bilayers with 0 nM (top trace), 5 nM (middle trace) and 165 nM (bottom trace) Charybdotoxin (CTX) added. **b**, Paddle chimera in *Xenopus* oocytes with 0 nM (top trace), 10 nM (middle trace) and 1000 nM (bottom trace) CTX added. **c**, CTX affinity titration with Paddle chimera in POPE:POPG bilayers (blue squares) and *Xenopus* oocytes (red circles). Fraction of unblocked current I/I_{max} (mean \pm s.e.m, $n = 3-4$) is graphed as a function of $\log(\text{CTX concentration})$. The solid line represents a fit to the data with $I/I_{max} = (1 + [CTX]/K_D)^{-1}$ with $K_D(\text{bilayer}) = 1.6 \pm 0.09$ nM and $K_D(\text{oocyte}) = 5.3 \pm 0.14$ nM.

view I hypothesize that by binding through specific protein-protein interactions at the protein-lipid interface VSTx1 causes the paddle chimera channel to experience low-tension like forces even in a high-tension membrane.

These data have revealed a new aspect of voltage sensor toxins: not only do they partition into the membrane but their effect on a voltage-dependent channel appears to be somehow mediated through the mechanical state of the lipid membrane and its interaction with the channel.

2.3.3 Discussion

The functional characteristics of K_v channels can depend on both the lipid composition and the mechanical state of the membrane. The effects of composition on the paddle chimera channel are modest, being somewhat similar in magnitude to the effects of lipid head group modifying lipases on various K_v channels (Ramu et al., 2006). The effects of the mechanical state are large and appear to act predominantly through the pore-opening transition, which occurs after the voltage sensor conformational changes have occurred. Interpreting our results in the context of past studies

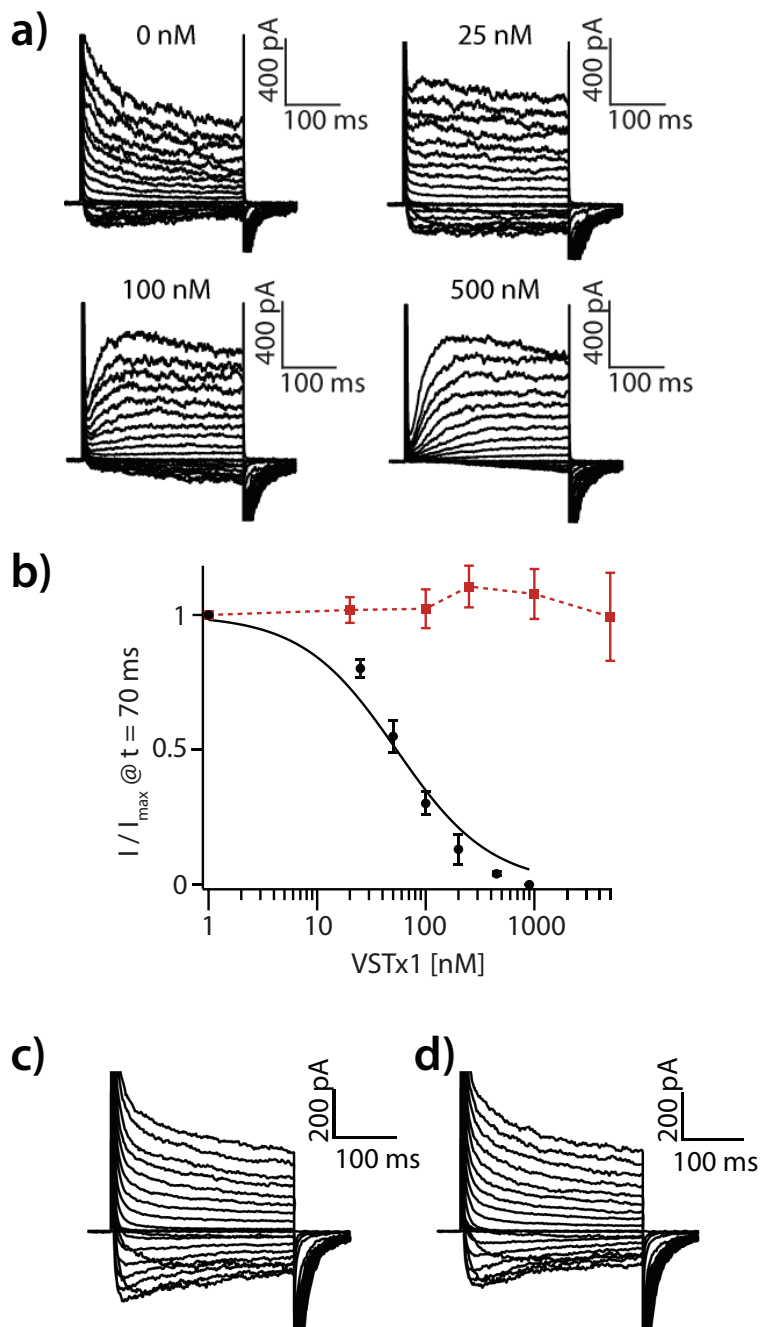


Figure 2.33: **Membrane mechanics and voltage sensor toxins.** **a**, Paddle chimera in POPE:POPG bilayers. VSTx1 was added to the indicated concentration. **b**, VSTx1 affinity titration with Paddle chimera (black circles) and $K_v1.2$ channels (red squares) in POPE:POPG bilayers. Fraction of residual current I/I_{max} (mean \pm s.e.m, $n = 3$) at $t = 70$ ms after depolarization is graphed as a function of $\log(\text{VSTx1 concentration})$. The solid line represents a fit the titration data with $I/I_{max} = (1 + [\text{VSTx1}]/K_D)^{-1}$ with $K_D = 54 \pm 8.8$ nM. **c-d**, $K_v1.2$ in POPE:POPG bilayers, before (**c**) and after (**d**) addition of 500 nM VSTx1.

of membrane tension in planar bilayers (Cook et al., 1968; Requena et al., 1977) and membrane patches on glass electrodes (Opsahl and Webb, 1994), I hypothesize that increased membrane tension in these systems favors the area-expanded open conformation of the pore. Numerous past studies have shown that Shaker K_v channel gating can be modified (10 mV shifts of midpoint voltage) by applying high pressures (30 to 60 mm Hg) to cell-attached patches (Laitko et al., 2006; Tabarean and Morris, 2002). The effects described here are different and correspond to mechanical effects associated with zero pressure membrane patches on glass electrodes and zero pressure planar lipid bilayers. Our findings imply that the conventional electrophysiological tools used to characterize channel function may, by affecting the mechanical state of the membrane, perturb significantly the behavior of some voltage-dependent channels.

Voltage sensor toxins were first understood as allosteric modifiers that bind to voltage sensors through protein-protein interactions that determine their molecular specificity (Swartz and Mackinnon, 1997b,a). That original view was then modified to include the concept that voltage sensor toxins partition into the membrane in order to gain access to their binding site on the voltage sensor paddle and increase their local concentration near the channel (Lee and Mackinnon, 2004; Milesco et al., 2007). The findings presented here suggest that the reason for membrane partitioning may be more than site access and local toxin concentration. I suspect that the fundamental mechanism of VSTx1 action is connected to its ability to modify membrane forces experienced by the ion channel.

Chapter 3

Conclusions and Outlook

In the preceding chapters I have presented my work that describes how both the chemical and mechanical properties of lipid membranes regulate K_v channel function and pharmacology. These results clearly demonstrate that the lipid membrane is not solely a passive solvent for membrane proteins. By putting my work into context with previous studies, I will expand on the impact of my thesis research on our understanding of protein-lipid interactions in general and membrane-dependent K_v channel function in particular.

3.1 The origin of cationic gating charges

Shortly before I started to work on a lipid-related project, the first crystal structure of a eukaryotic K_v channel had been solved, the rat $K_v1.2$ (Long et al., 2005a,b). This structure reinforced the concept first observed in the KvAP crystal structure (Jiang et al., 2003a,b), that the voltage sensors of K_v channels are arranged as independent domains at the perimeter of the protein facing the lipid membrane. Most importantly, some of the arginines that carry the gating charge are themselves exposed to the lipid environment. After the KvAP crystal structure was published, the most often repeated criticism involved how energetically unreasonable it is to place gating charge arginines within the hydrophobic core of the membrane; with the new $K_v1.2$ structure, history was bound to be repeated.

3.1.1 The lipid membrane stabilizes voltage sensor conformation during gating

The obvious question to ask at that time was, given the lipid exposure of gating charges, how does the lipid membrane stabilize the arginine residues and what is the true energetic penalty for their placement?

This question had previously been addressed in studies by von Heijne and colleagues. Using an *in vitro* translocation assay that measured the efficiency of membrane insertion of helical segments with different amino acid composition, they found that the energetic penalty of placing a charged arginine in the middle of the membrane could be offset by having hydrophobic residues flanking it (Hessa et al., 2005b,a). In fact, when they used a helical segment that reflected the S4 helix of KvAP, the probability for insertion into the membrane was 50%. They also found that the cost of placing the arginines within the hydrophobic membrane core depends on their position within the helical segment and is lowest when placed at the edges. Such placed arginines can participate in lipid-headgroup interactions or benefit from hydration. Molecular dynamic simulations lend strong plausibility to the existence of such interactions (Freites et al., 2005), experimental evidence, however, was missing.

Since a multidentate hydrogen bond between the positively charged guanidinium group of the arginines and the negatively charged phosphodiester of the lipids was the likeliest interaction pair, I designed an experimental system that allows the replacement of the phosphodiester with lipid species that provide different hydrogen bonding patterns (i.e. DOTAP or EDOPC). I found that K_v channel gating was absolutely dependent on the presence of a negatively charged phosphodiester. This presented the first experimental evidence that during specific gating steps the gating charge arginines are stabilized by interacting with the headgroups of phospholipid molecules, thus strongly reducing the energetic cost of placing them within the membrane.

3.1.2 Molecular Evolution of Voltage Sensors

These experiments also provide some insight as to why all known voltage sensors use positively charged amino acids to sense changes in voltage. Theoretically, negative charges could be utilized as well, if the electromechanical transduction connection to the pore was inverted. The answer to this conundrum has to be connected to the

evolution of voltage sensors themselves. Arguably cell membranes evolved before the first membrane proteins. Most theories on the emergence of the first cells suggest that the simplest bilayer forming molecules are long chain (>C9) fatty acids, carboxylic acids and monoglycerides such as those extracted with organic solvent from the Murchison meteorite. These lipids readily formed vesicles at intermediate pH, micelles at high pH and an oil phase at low pH (Deamer and Pashley, 1989; Deamer and Bramhall, 1986; Monnard et al., 2002). Dworking and colleagues suggest that more complex phospholipids emerged later (Deamer and Dworkin, 2005). As work on the evolution of the genetic code by Davis and others suggests, this may have coincided with the inclusion of the amino acids arginine and lysine in the genetic code. It has been proposed that primitive, self-sustaining biochemical pathways existed before a gene-based hereditary system (Davis, 1999, 2002). These included the reductive citrate cycle, the reductive pentose phosphate pathway and the so-called central trunk. They make up the central biochemical pathway (CBP). Davis proposes that the emergence of genetically encoded amino acids correlates with the number of *additional* chemical reactions (starting from the CBP) that are required to generate each amino acid. While amino acids such as glutamate that require only one additional reaction may have evolved early, hydrophobic amino acids such as leucine and isoleucine (4 reactions) emerged later. They emerged however, at the same time that primitive fatty acid synthesis was invented with the addition of acyl-CoA to the chemical make-up of primitive life. Interestingly, the amino acid arginine and lysine emerged together with phospholipids (10 steps). It is therefore entirely conceivable that this co-evolution signifies a deep biochemical and function connection of arginines, lysine and phospholipid from the earliest forms of life.

Voltage sensors are thought to have evolved independently from channel pores (Kumánovics et al., 2002) and pore-less voltage-sensor containing proteins are still found in modern organisms (Murata et al., 2005; Ramsey et al., 2006; Sasaki et al., 2006). The function of the primordial voltage sensor is unknown, but is probably moved or tumbled in response to changes in transmembrane potential caused by fluctuations in the ionic composition of the surrounding medium. The biological maxim that structure subserves function implies that the simplest voltage sensor relied on already existing structures for function. The omnipresent phosphodiester with an extremely low pKA of 1-2 (thus a permanent negative charge) is the obvious interaction partner. For this reason positive charges were chosen to sense voltage changes.

Other membrane proteins contain lipid-facing arginines that are important for their gating, for example the prokaryotic membrane protein, MscS, a mechanosensitive channel. They are located in a helical hairpin at the periphery of the membrane spanning region. Although a detailed molecular mechanism for MscS gating has not yet been described, this channel's modulation by voltage and membrane tension is attributed to a movement of these arginines in response to membrane depolarization (Bass et al., 2002).

3.1.3 Voltage sensors enrich phospholipids in the protein vicinity

I have mentioned the concepts of wetting and capillary condensation as means of protein organization in the introductory Chapter 1.3. Briefly, these concepts state that membrane proteins surround themselves with the lipid species that results in the lowest energy lipid-protein interaction profile. As a consequence, certain lipid species can be concentrated around a membrane protein as an annular lipid shell (Gil et al., 1997). It is very likely that KvAP embedded in mixed phospholipid/cationic lipid bilayers is an example of such system. The mol-fraction of DOTAP (or EDOPC) in the bilayer has to be greater than 50% to observe appreciable shifts in midpoint of activation (see Figure 2.4c and Figure 2.8d). This nonlinear response can be explained if the interaction of the gating charge arginines with the phosphodiester of POPE or POPG lowers the free energy of KvAP being embedded in the bilayer. KvAP thus will reside in a phospholipid enriched phase that buffers the addition of DOTAP or EDOPC to the bilayer. Once a certain mol-fraction of phospholipids has been replaced with cationic lipids, the wetting effect alone cannot concentrate a sufficient number of phospholipids around the channel. That these annular phospholipids seem to act in a cooperative fashion, is obvious from the steep increase of midpoint of activation after the 50% threshold in crossed (see Figure 2.4c and Figure 2.8d).

An unresolved question is the the actual conformation of the voltage sensor domain in lipid membrane containing high mol-fractions of DOTAP (or EDOPC). We do not know the answer for the planar bilayer system. A recent study in *Xenopus* oocytes shed light on this question. In oocytes, a subfraction of K_v channels associates with sphingomyelin and the gating of these channels can be altered by the action of Sphingomyelinase D (SMase D), an enzyme that cleaves the choline of sphingomyelin, thus leaving behind ceramide-1-phosphate. Another enzyme, SMase C,

cleaves choline-1-phosphate, leaving behind ceramide, a lipid molecule without a negatively charged phosphodiester. SMase C treatment of oocytes altered the gating of Shaker K_v , $K_v1.3$ or $K_v2.1$ as well as Kir1.1. While the modification of K^+ currents carried by the voltage-sensor-less Kir1.1 indicates that an electrostatic component of the gating is altered, both ionic and gating currents of the K_v channels decreased. This observation suggests that the absence of phosphodiesters on the external membrane leaflet creates an insuperable energy barrier to the gating charge movement, essentially trapping the voltage sensor at the internal membrane leaflet (Xu et al., 2008).

3.2 Voltage Sensor Toxins

Small protein toxins that bind the voltage sensor from the extracellular side of the membrane and alter gating of the channel were first isolated from tarantula venom. The best studied member of this family is Hanatoxin, which inhibits the $K_v2.1$ channel with nanomolar affinity (10-100 nM). The binding site of Hanatoxin has been identified through alanine-scanning mutagenesis and mapped to parts of the S3b of the voltage sensor domain (Swartz and Mackinnon, 1997b,a). Early studies indicated that Hanatoxin can bind to the closed channel and alter energetics of channel activation (Lee et al., 2003). This together with the apparent slow binding kinetics was construed as evidence that voltage sensor toxins remain bound during channel gating. Later another voltage sensor toxin, VSTx1, was purified from the same spider which inhibits KvAP with nano-molar affinity (25nM) (Ruta and Mackinnon, 2004; Ruta et al., 2003). Lee and colleagues have shown that VSTx1 exhibits a very low affinity for KvAP suspended in detergent micelles (Lee and Mackinnon, 2004). However, the amphiphilic nature of VSTx1 allows it to partition into the lipid bilayer, thereby increasing its effective concentration and apparent affinity for KvAP. They suggested that VSTx1 binds and dissociates rapidly from the KvAP channel, invalidating the assumption made to conclude that the toxin stays bound with the voltage sensor paddle during gating. Later studies concluded that membrane partitioning is a concept often times used by small molecule toxins (Posokhov et al., 2007).

Data I presented indicates that VSTx1 can only bind to the depolarized conformation of the voltage sensor. What conformation of KvAP does the inactivated state represent? I cannot answer this question for KvAP, or in fact with certainty for any K_v channel undergoing what has been termed C-type inactivation (Hoshi et al.,

1991). C-type inactivation might represent different physical processes in different K_v channels. In the Shaker channel, the C-type inactivated state is associated with a change in the reactivity of cysteine residues substituted at certain locations near the selectivity filter (Yellen et al., 1994). This observation has led to the proposal that a conformational change of the selectivity filter underlies C-type inactivation (Baukrowitz and Yellen, 1995). Studies of gating in $K_v2.1$ and $K_v3.1$ show that these channels can inactivate from the pre-open state and the open state by a mechanism that is thought to be distinct from C-type inactivation in Shaker (Klemic et al., 1998, 2001). It is likely that inactivation occurs through different physical mechanisms in different K_v channels. In KvAP channels, given the extreme degree to which inactivation occurs prior to pore opening, it is natural to wonder whether inactivation in KvAP could be related to the efficiency with which the voltage sensors open the pore. For example, when the voltage sensors go from hyperpolarized to depolarized the S4-S5 linkers presumably relieve their constriction on the S6 helices, which form the gate at the intracellular pore entryway, and perhaps even lift the S6 helices so they open. If the linker helices can disengage with some probability (related to the fraction of channels that successfully open) one could imagine that the gate would close even though the voltage sensors remain in a depolarized conformation. This kind of slippage mechanism would be mechanistically akin to desensitization in glutamate receptor channels in which activated ligand binding domains cause pore opening and then dislodge while still bound to ligand, allowing the pore to close again (Armstrong et al., 2006). Further studies will be required to support or refute such a mechanism.

What I have also shown is that VSTx1 activity can depend on the mechanical state of the membrane. This represents a new step in the understanding of the function of these toxins. It seems possible that they are not classical allosteric inhibitors as previously thought, but rather exhibit their effects through an alteration of the way ion channels sense the material properties of the bilayer. An important unanswered question is whether VSTx1 does not have an effect on K_v channel gating in *Xenopus* oocytes because it binds but does not show efficacy or because it does not bind in the first place. Does the alteration of membrane tension induce the binding of the toxin? Molecular dynamics simulations have suggested that VSTx1 partitioning can locally deform the bilayer; such deformation would result in local changes of surface tension and fluidity (Wee et al., 2008). The presence of molecular specificity argues that VSTx1 has to interact with the channel at some level. This interaction could be a direct protein-protein interaction, or it could be mediated by specific lipid molecules

to form a ternary interaction complex. In the latter case, the molecular specificity of VSTx1 would be a consequence of specific lipid molecules associating with the K_v channel that mediate the contact with the toxin. Lu and colleagues found that, in the presence of Hanatoxin, the lipase SMase C had a decreased effect on K_v channel gating, which itself depends on the presence of intact sphingomyelin molecules (Xu et al., 2008). This suggests that either Hanatoxin binding involves the formation of a ternary complex between toxin, lipid and channel that is sufficiently stable to protect the participating lipid from cleavage by the lipase or that hanatoxin binding creates a sufficiently large exclusion volume that protects sphingomyelin molecules located nearby.

Recently, Schwartz and coworkers have used the modification of GxTx1 affinity to $K_v2.1$ by SMase D to investigate exactly this question (Milescu et al., 2009). They come to the conclusion that one way to explain the effect of lipid modification on toxin affinity would be to postulate that Tarantula toxin binds the paddle motif with higher affinity when sphingomyelin is bound ($K_D^{+SM} < K_D^{-SM}$); in effect they propose that the presence of sphingomyelin is required for high-affinity toxin binding, akin to a ternary toxin-lipid-channel complex; mutations on the channel would weaken toxin binding by disrupting paddle-lipid interactions, rather than altering the protein-protein interaction between toxin and channel.

However, postulating that tarantula toxins bind with higher affinity when sphingomyelin is bound may not warranted by their data: wildtype $K_v2.1$ binds GxTx1 with an affinity of 203 nM; after the sphingomyelin cleavage with Smase C, this affinity is increased to 52 nM. An alternative explanation for their results is that the choline headgroup of sphingomyelin is interfering with high affinity toxin binding. Because the choline headgroup is cleaved, wildtype Shaker binds GxTx1 with higher affinity after treatment with SMase D. In the case of the E277A mutant of the $K_v2.1$ channel in Schwartz's and colleagues' study, it is possible that the mutation causes the sphingomyelin headgroup binding pocket to be reordered in a way that is strongly interfering with toxin binding. Therefore the affinity drops sharply to 30,000 nM. After treatment with SMase D the disordered choline headgroup is cut out of the way and toxin binding is rescued ($K_D = 3570$ nM). The case of V282A can be interpreted the same way. The difference in magnitude of rescue can be explained if electrostatic interactions between toxin and channel residue E277 are involved; it is possible that E277 is one of the major contributors to toxin binding. Treatment with SMase D will

not restore the glutamate, which is why affinity levels are not recovering to wildtype levels, as they are in the case of V282A. In the context of protein-protein interactions, a valine to alanine substitution is arguably less disruptive. However, the fact that there is some recovery in the case of E277A could be explained if the creation of a negatively charged ceramide-1-phosphate increased the local negative charge in this region of the voltage sensor.

This possible alternative explanation for the results of Swartz and colleagues aside, their study clearly demonstrates that the voltage sensor toxin affinity can be modulated by adjacent lipid molecules. It is therefore not surprising that a mechanical alteration of the lipid bilayer can lead to qualitatively similar effects. The mechanical alteration itself can be the causative agent that increases the apparent toxin affinity. Alternatively, the increase in membrane tension can lead to the dissolution of lipid microdomains in patched membranes. In low tension membranes, specific lipid species in these microdomains could interact tightly with the voltage sensor, obscuring toxin binding sites. If these microdomains dissolve under the influence of higher membrane tension, the toxin binding sites could become accessible and toxin affinity might increase. This scenario is entirely conceivable when considering the alternative interpretation of the study by Swartz and colleagues. I propose investigating the affinity of the paddle chimæra K_v channel in other cell systems such as HEK or SF9 cells to investigate whether the oocyte membranes possibly provide a specific and tightly binding lipid species that obscure the VSTx1 activity. Alternatively, the effect of Smase C and Smase D treatment of oocytes on VSTx1 affinity and activity will be illuminating as well.

3.3 Intrinsic Mechanosensitivity

Based on the membrane system dependent gating properties of the eukaryotic Paddle Chimæra K_v channel, I proposed that voltage-dependent K^+ channels possess an intrinsic mechanosensitivity (see Chapter 2.3.2). I interpreted this finding in the context of past studies regarding membrane tension in different membrane systems. I hypothesized that the mechanical state of the membrane acts predominantly through the concerted late opening step of the pore, independently of voltage sensor conformational changes that occur in preceding steps.

I would like to start this chapter with a short review of the existing literature on mechanosensitivity in eukaryotic ion channels. This background shall serve as a point of reference for a discussion of the broader implications of hypothetical K_v channel mechanosensitivity.

3.3.1 Precedent for mechanosensitivity in eukaryotic ion channels

Skm Na_v channel

Morris and colleagues (Tabarean et al., 1999) have reported on the effect of membrane stretch on the human Skm1 Na_v channel expressed in *Xenopus* oocytes. In their initial characterization using cell-attached patches, they noticed that when the Skm1 α subunit was expressed alone without the β subunit, Na^+ currents showed an unpredictable mix of slow and fast components. After observing that the mode of gigaohm seal formation which subjects the membrane to a variable amount of membrane tension, was predictive of the resultant slow/fast component mix, they suggested that the mechanical history of the patch was responsible for this variability. In cell-attached patches that were obtained without applying negative pressure there was much less of the fast component. Application of suction for several minutes to such patches could completely switch the Na^+ current from slow to fast gating mode. Channels remained in the fast gating mode after the release of suction; the conversion was therefore irreversible. The G/V curve of the fast component activated at more negative potentials, identical to when both Skm1 α and β subunit are coexpressed in the oocyte. These observations are qualitatively congruent with those I made for various K_v channels (Shaker, $K_v1.2$, $K_v2.1$ and Paddle Chimæra, see Chapter 2.3.2). However, in the study of Skm1 the peak Na^+ current sometimes increased by 25% and other times decreased by the same amount. This is different from my observation of K_v channels; a pressure-induced conversion of gating mode in cell-attached patches is always accompanied by an increase in peak K^+ current.

Brehm and colleagues reported similar findings when they compared the Skm1 Na_v channel in cut-open oocytes and macropatch recordings (Shcherbatko et al., 1999). Specifically, recording the Na_v in macropatches both in the absence and presence of β subunit led to a left-shifted voltage dependence of inactivation and activation. Patch excision and treatment with cytoskeleton disrupting drugs led to an acceleration of this conversion. They also found that application of suction can induce a shift

to fast inactivation and through video imaging they revealed that this pressure induced shift coincides with the detachment of the lipid membrane from the underlying cytoskeleton.

Morris speculates that membrane stretch could directly affect the folding state of the Na_v channel, by “lowering a large energy barrier, thereby allowing some domain to assume a previously inaccessible low energy secondary or tertiary conformation.” Both reports suggest that the loss of an intact cytoskeleton is the causative agent for the observed conversion. They both reference well established reports of specific interaction between cytoskeleton-binding proteins and the Skm1 α subunit through a C-terminal PDZ-binding domain (Gee et al., 1998; Wood and Slater, 1998). The fact that coexpression of the β subunit resembles a suction-induced fast gating mode is compatible with such cytoskeletal interactions if the β subunit interferes with the normal binding of the components to the α subunit. Based on this observation, Brehm and colleagues speculate that coexpression the β subunit decreases the cytoskeleton-conferred mechanoprotection that the Na_v channel would usually experience.

The uni-axial stretching of cells on an extensible substrate beyond the elastic response of the cytoskeleton should in theory mimic the pathological conditions of patch recording. In a recent study Morris and colleagues subjected HEK cells stably transfected with $\alpha\text{Na}_v1.6$ to pathological stretches of 50% or more (Wang et al., 2009). Using Na^+ sensitive dyes they find that cytoplasmic Na^+ levels rapidly (within 2 minutes) increase after stretching. This is consistent with the activation curve of this channel shifting to more hyperpolarized voltages, an effect they observed with conventional electrophysiology in patched membranes. The Na^+ levels remain high after the release of cell stretch. Unlike for Skm1, the coexpression of a $\beta1$ subunit did not change the response of $\alpha\text{Na}_v1.6$ to abrupt membrane stretch. The authors liken HEK cell stretching experiments to pathological trauma of myelinated axons and speculate that abrupt stretching is causing an irreversible disruption of the cytoskeleton, thus removing the cell’s protection against transient and maintained membrane stress. They suggest that the membrane stretch induced conversion of Na_v activation to more hyperpolarized voltages leads to a Na^+ leak in stretch-traumatized axons, explaining the neuroprotective effect of Na_v blockers in head trauma models.

BK channel with STREX exon

Sokabe and colleagues (Naruse et al., 2009) identified a stress hormone-induced splicing variant of the BK channel in chicken cardiomyocytes that includes a C-terminal cysteine-rich sequence (STREX domain). The STREX domains confer sensitivity to whole cell shear stress. Overexpression of the STREX domain *in trans* leads to a loss of BK channel mechanosensitivity, implicating that binding to an unknown membrane-associated component confers said mechanosensitivity in the first place. Another study showed that the STREX exon contains a palmitoylation site, indicating that this segment is membrane anchored *in vivo* (Tian et al., 2004).

NMDA receptor

Ascher and colleagues (Casado and Ascher, 1998; Paoletti and Ascher, 1994) report that in excised outside-out patches, NMDA receptor responses are depressed similarly by suction and addition of lysophospholipid, whereas they are potentiated by applying positive pressure and arachidonic acid. They propose that NMDA receptor activity is modulated by amphiphatic compounds that cause pressure changes in the lipid bilayer: amphiphatic compounds of different shape partition asymmetrically into the bilayer and thus alter the spontaneous local curvature. Compounds with a large hydrophilic head (lysophospholipid) mimic the effects of suction on an outside-out patch, which they interpret as negative areal strain; compounds with a small hydrophilic head (arachidonic acid) mimic the effects of positive pressure (i.e. increased areal strain). Citing earlier studies that demonstrate a cytoskeletal connection of the NMDA receptor (Kornau et al., 1997), they consider the possibility that such connection to cytoskeletal elements could be a candidate for force transmission; they reject this idea, however, pointing out that mechanosensitivity is preserved in excised patches in which the cytoskeletal connection of the NMDA receptor are probably severed (Paoletti and Ascher, 1994).

Cardiac Muscarinic Potassium Channel GIRK1/4

Weiss and colleagues (Ji et al., 1998) study the effect of hypotonic swelling on *Xenopus* oocytes that express Kir3.1/Kir3.4 heterotetramers together with excess $G\beta\gamma$. They find a 25% reduction in K^+ current carried by these channels upon oocyte swelling; Kir1.1 and Kir2.1 do not show this effect. In an attempt to measure the unitary conductance of Kir3.4 channels, they note a rapid rundown of K^+ current in cell-attached patches of 1-3 μm diameter. When they use giant patches (20-30

μm) the rundown is slowed significantly. Patch excision always led to an immediate disappearance of channel activity. While they interpret their results in the context of mechanical forces acting on Kir3.4 channel, the possibility remains that patch formation and subsequently increased membrane tension can lead to the dissolution of lipid rafts that concentrate $G\beta\gamma$ (see Chapter 1.7)(Khan et al., 2003; Moffett et al., 2000; Schroeder et al., 1997). The observed reduction in K^+ current could therefore be an expression of loss of $G\beta\gamma$ mediated activation.

N-type Ca^{2+} channels

Morris and colleagues (Calabrese et al., 2002) report that N-type Ca_v channels recombinantly expressed in HEK cells can reversibly elicit 1.5-fold increased peak Ba^{2+} currents when the cell is inflated under hydrostatic pressure in whole-cell clamp. A T-type Ca_v channel did not show the same peak current increase. In this study, Morris and coworkers had to battle the cytoskeleton of the HEK cell; it was necessary to apply positive pressures in excess of 40 mmHg for more than 10 seconds before the cell was visibly inflated. The increase in peak Ba^{2+} current coincided with the cell inflation and not with the application of positive pressure. While the steady-state inactivation of the Ca_v channel shifted to more hyperpolarizing voltages by -18 mV, the activation G/V curve remained unaltered.

In an effort to explain the origin of the increased peak currents, the researchers use cell-attached recordings to measure the single channel conductance. When they apply suction to these patches (equivalent to applying pressure in whole cells), they report that the single channel conductance remains unaltered and a slight increase in channel open probability. I want to point out, however, that the cell-attached recordings are flawed because the prepulse holding voltage (-70mV) is not sufficient to fully recover the channel from steady-state inactivation they reported in the same paper. While not explicitly mentioned, the presented data would argue that the open probability in pressurized and unpressurized cell-attached patches is not significantly different. In fact, it is the same within the error reported. I propose that by moving from whole cell to cell-attached recordings the open probability has already increased, similar to my observations for K_v channels (see Chapter 2.3.2).

L-type Ca^{2+} channel

Farrugia and colleagues (Lyford et al., 2002) report that exposure of $\text{Ca}_v1.2$ expressing HEK or CHO cells to shear stress increases whole-cell peak Ba^{2+} and Ca^{2+} conductances by 20%. The activation G/V curve was not shifted for either Ba^{2+} or Ca^{2+} currents. The inhibition of intracellular kinase signaling with kinase inhibitor and deletion of the C-terminal proline-rich domain did not disrupt this response. They have expressed $\text{K}_v2.1$ as a control and subjected the cells to the same shear stresses but did not see a similar response as observed for $\text{Ca}_v1.2$. Additional experiments are needed to reconcile the latter observation with my data of $\text{K}_v2.1$ mechanosensitivity when expressed in oocytes.

TREK-1 and TRAAK

Barhanin and coworkers identified a family (K2P) of weakly inward-rectifying K^+ channels that is characterized by four transmembrane and two-pore forming domains. The first family member was TWIK-1 (Lesage et al., 1996) and subsequently two other members, TREK-1 and TRAAK were identified to be mechanosensitive channels (Patel et al., 1998; Maingret et al., 1999). Osmotic swelling and shrinking of cells increases and decreases, respectively, whole cell TREK-1 currents. The amphiphatic crenators trinitrophenol (anionic) and lysophosphocholine (neutral) mimic the effect of high micro-molar concentrations of arachidonic acid or -50 mmHg suction applied to on-cell patches, suggesting that TREK-1 and TRAAK respond to the local spontaneous curvature of the bilayer. Conversely, the cationic cupformers chlorpromazine and tetracaine inhibited activity. It seems therefore that the expansion of the outer bilayer leaflet is responsible for TREK-1 and TRAAK gating. This leaflet expansion sensitivity is dependent on the presence of the C-terminal region of TREK-1 that contains a RKKEE charge cluster, which is likely interacting electrostatically with the inner leaflet of the membrane.

MECs in *C.elegans*

The first members of the Mec (mechanosensory abnormal) family were identified in mutant screen for touch-insensitive *C.elegans* (Chalfie, 1993; Chalfie and Au, 1989; Driscoll and Chalfie, 1991). Mec-4 was shown to be homologous to deg-1, a gene product that mediates the swelling induced degeneration of certain neurons (Tavernarakis and Driscoll, 1997). Together with mec-10, unc-8, unc-105, flr-1, mec-4 and deg-1 were proposed to belong to the superfamily of degenerins (Bianchi, 2007). When

mec-4 and *mec-10* are coexpressed in *Xenopus* oocytes they carry amiloride-sensitive Na^+ currents (Bianchi et al., 2004). In 2005 Goodman and colleagues (O'Hagan et al., 2005) presented direct electrophysiological evidence from touch receptors in *C.elegans* that changing external force but not sustained force evoke mechanoreceptor current that again were carried by Na^+ and were sensitive to amiloride. They showed that null mutations in *mec-4*, *mec-2* and *mec-6* eliminated these responses and suggest that *mec-4/mec-10* oligomers form Na^+ channels that are mechanically coupled to external forces by the accessory proteins *mec-2* and *mec-6*.

Based on sequence similarity, an epithelial Na^+ channel (EnaC) has been classified as a DEG family member. Interestingly, when reconstituted into planar lipid bilayers the open probability of EnaC increase from 0.5 to 0.95 after the application of 0.25 mmHg of hydrostatic pressure (Awayda et al., 1995). This mechanosensitivity is not evident when EnaC is expressed in whole cells in which the underlying cytoskeleton is compensating for membrane tension changes (Awayda and Subramanyam, 1998; Palmer and Frindt, 1996).

nompC and TRP channels

Studies of mechanoreceptive-defective *Drosophila* mutants that also showed the absence of mechanoreceptor potentials recorded from external sensory bristles led to the identification of *nompC* (Kernan et al., 1994; Walker et al., 2000). *NompC* contains 29 N-terminal ankyrin repeats and the C-terminus of *NompC* shares approximately 20% sequence identity with the transient receptor potential (TRP) class of ion channels (Colbert et al., 1997; Harteneck et al., 2000). The zebrafish and mouse orthologs of *nompC*, called *TRPN1* and *TRPA1*, respectively, were shown to be critical for sensory hair cell mechanotransduction (Corey et al., 2004; Sidi et al., 2003). The removal of *nompC* function leads to larval deafness and imbalance, functional consequences of the eliminated electrical responses on zebrafish and mouse hair cells. Howard and Bechstedt later hypothesised that the N-terminal ankyrin repeats of *TRPN1* or *TRPA1* form a helical structure that acts as a gating spring coupling the channel part to the microtubule structures of the cell (Howard and Bechstedt, 2004).

3.3.2 Artifacts from lipid glass interaction - increased membrane tension

The preceding section summarizes examples of eukaryotic mechanosensitive channels; this collection is by no means complete. It is important to realize that even within this small sample of mechanosensitive processes, experimental procedures, assumptions and observations vary widely. Aside from studies on Na_v channels, the observed mechanosensitivity was always reversible. Some studies compared whole cell recordings to patch recordings. The intrinsically higher resting tension of membrane patches was not specifically taken into account in any of these studies. Virtually every study had a different mode of altering membrane tension.

Mechanosensitivity as an artifact

If I postulate that patch recordings alter the mechanical state of the membrane, how do I see the supposed mechanosensitivity? As something artifactual or as something of biological relevance? Early on after the first mechanosensitive channels had been described, the possibility was raised that membrane changes induced by the tight seal formation give rise to an artifactual mechanosensitivity in specific channels. There are reports that question the reality of mechanosensitive channels as biological transducers and propose that such channel activity is an artifact of patch-clamp recording (Gustin, 1991; Milton and Caldwell, 1990; Morris and Horn, 1991a). The “artifact” idea originally arose from a discrepancy observed between membrane patch and whole cell mechanosensitivity in snail neurons (Morris and Horn, 1991b). This study reported that although single mechanosensitive K^+ channels could be activated in membrane patches, macroscopic currents could not be elicited in mechanically activated whole cells. While there have been subsequent reports demonstrating that the above observation cannot be generalized to all cell types (Cui et al., 1995; Davis et al., 1992), they all downplayed the obvious concern that recordings from patches can lead to an overestimation of the intrinsic mechanosensitivity of certain proteins. Sakmann and Neher raised concerns three decades ago as to whether the mechanical perturbation associated with tight seal formation would result in changes in the physiological properties of the patch (Sakmann and Neher, 1984). However, at that time, the *general* agreement between data recorded from whole cell and patch clamp appeased these concerns. Looking more closely however, there is a long history of patch and whole cell characterization of ion channels not adding up. In several cases time-dependent irreversible shifts in gating properties have been observed. Zhou et.

al (1991) and Moorman et al. (1990) observed that in both cell-attached and outside-out patches, Na^+ channels tended to switch to fast gating by the end of the recording (>12 minutes) (Moorman et al., 1990; Zhou et al., 1991). Jonas and colleagues introduce a “fudge” factor to explain difference in outside-out patches and whole cell recordings (Engel and Jonas, 2005). After recording Na^+ currents from patches they can only make their gating model work when they assume a 12mV shift “as a result of Donnan potentials” resulting from patch formation.

Patch physiology

Imaging of patched membranes indicated that even in the absence of applied pressure or suction, the patch membrane is pulled flat and perpendicular to the wall of the patch pipette (Opsahl and Webb, 1994; Sokabe and Sachs, 1990; Zhang and Hamill, 2000). Opsahl and Webb were the first to measure the intrinsic membrane tension that is generated at the lipid/glass interface (Opsahl and Webb, 1994). Electrical membrane capacitance measurement indicate that the patch’s area is consistent with that of a flat membrane disk (Zhang and Hamill, 2000), quite different to the plasma membrane of *Xenopus* oocytes and animal cells before patch formation (see Chapter 1.10.1). The likeliest scenario by which tight-seal formation alters the membrane structure is that the lipid/glass adhesion is smoothing out surface folds and microvilli. Even though part of the cytoskeleton is initially drawn into the nascent membrane patch (Hamill and McBride, 1992; Ruknudin et al., 1991; Sokabe and Sachs, 1990) there is good evidence that in the process the underlying cytoskeleton becomes decoupled from the lipid bilayer (Hamill and McBride, 1992, 1997; Zhang et al., 2000). Cytoskeleton-bilayer interactions can be expected to depend on various factors, most importantly cell preparation and mechanical history of the patch. The degree of preservation of the cytoskeleton in patch recordings is therefore completely uncontrollable and represents a continuum from fully intact to completely decoupled. Morphological and functional changes of the patched membrane will manifest themselves in a time-dependent manner even in the absence of mechanical stimulation. For example, polymerized F-actin is in equilibrium with the free G-actin monomer form. Patch excision is equivalent to infinitely diluting the free G-actin; as a consequence F-actin will depolymerize. Mechanical stimulation in particular will specifically induce these changes.

In their initial study of membrane patch morphology, Sakmann and Neher (Sakmann and Neher, 1995) observed that tight seals obtained with applied suction had a

characteristic omega-shape, while in tight seals that formed spontaneously (i.e. without suction) no membrane was drawn into the pipette and no membrane deformation was evident. When Sachs and colleagues imaged the patch formed on chicken skeletal muscle, they observed that with repetitive suction and pressure steps, the membrane could be separated from the underlying cytoskeleton; a clear space developed between the two (Sokabe and Sachs, 1990). The same has been shown for patches made on *Xenopus* oocytes (Hamill and McBride, 1992). Analogous to this membrane detachment in patches, cell ghosts can be produced by applying positive pressure during whole cell recordings. The required initial pressure to inflate a HEK cell, for example, is quite high (>50mmHg), however after cytoskeleton detachment, much smaller pressure (<5mmHg) can inflate the cell (Calabrese et al., 2002). The absolute difference in these pressure values is a testament to the mechanoprotective role of the cellular cytoskeletal network.

3.3.3 Mechanoprotective role of the cytoskeleton

There is no question that a membrane reservoir exists to protect the bilayer from excessive mechanical loads. The earliest report providing evidence that Na_v and K_v channels rely on the cytoskeleton for such mechanoprotection came from Terakawa *et al.* (Terakawa and Nakayama, 1985). Using electron microscopy and electrophysiology, they demonstrated that the cytoskeleton in squid axons is destroyed when they are perfused with KCl or KBr, but not KF. Inflating KF-perfused axons had little effect as evident in action potentials and voltage-clamped currents, whereas KCl- or KBr-perfused axons reversibly depolarized and showed altered gating properties of K_v and Na_v channels. Similarly, TREK and NMDA channels become more mechanosensitive after the cortical cytoskeleton is disrupted (Paoletti and Ascher, 1994; Wan et al., 1999).

As pointed out earlier for Na_v channels, there are numerous examples for ion channel interactions with the cytoskeleton, for example through G-ankyrin with β -spectrin elements or through PDZ-binding domains to the dystrophin-actin membrane skeleton (Gee et al., 1998; Wood and Slater, 1998). Similar interactions are reported for Ca^{2+} channels (Sadeghi et al., 2002). From a viewpoint of cellular organization these interactions localize such ion channels in proper density at specific junctional, peri- and extra-junctional regions.

It is entirely conceivable that the apparent mechanosensitivity of K_v and other channels is secondary to the disruption of the cytoskeleton that underlies the lipid membrane. The important point, however, is that such a scheme is compatible with an altered membrane tension as the principal stimulus for the induced functional conversion. It is a well established fact that the cytoskeleton underlying the plasma membrane stabilizes membrane invagination (see Chapter 1.10.1). Membrane invaginations of this kind are areas of excess membrane that can buffer changes in membrane tension and are likely to be the reason for the low resting tension in cells (Dai et al., 1998; Raucher and Sheetz, 1999; Sens and Turner, 2006, 2004). If the membrane associated cytoskeleton is disrupted, either physically by transiently applied excess tension on a patch or by spontaneous depolymerization of F-actin upon patch excision, then the membrane tension buffering system could be rendered nonfunctional.

An example of how this could work comes from a study conducted in Salamander retinal ganglion (Schubert and Akopian, 2004). It reports that K_v and Ca_v channels are modulated by the actin cytoskeleton. Disruption of F-actin with either Lactrunculin B or Cytochalasin B resulted in inhibition of sustained outward K^+ currents and high-voltage activated Ca^{2+} currents. This state is accompanied by a left-shift in the G/V curve for I_K but not I_{Ca} .

Still, the question remains: What is the operating element that is altered after disruption of the cytoskeleton? Does the disruption of the cytoskeleton expose ion channels to excessive membrane tension, thus acting directly? Or does it act indirectly, through a scheme like has been suggested for the regulation of pressure sensing in kidney cells by the polycystin TRPP1 (a cell-matrix interaction membrane protein) and TRPP2 (a TRP family 6TM channel) (Sharif-Naeini et al., 2009)? Filamin A was identified as an interaction partner for TRPP2 in a proteomic screen. Filamin A stiffens the cytoskeleton and organizes the plasma membrane into microvillo with a small radius of curvature ($R_c \approx 0.1 \mu\text{m}$) by crosslinking actin filaments and increasing their polymerization. According to the Laplace-Young-Relation ($\tau = \frac{\Delta P \cdot R_c}{2}$), the small radius of curvature would reduce the membrane tension that develops for a given osmotic or hydrostatic pressure, thus mechanosensitive channels localized in the vicinity of TRPP2 would reside in a relatively mechano-protected zone unless, of course, the underlying cytoskeleton is destroyed.

3.3.4 The biological relevance of tension regimes

We have to consider the possibility that mechanosensitivity is just another aspect of protein regulation, and that there is no such thing as a truly specialized mechanosensitive protein with no other function but to be a force transducer. The clonal nature of the majority of mechanosensitive proteins is unknown, most likely because every ion channel is mechanosensitive to some extent, making the identification of one specific component impossible when using natural cell preparations.

I think the discussion on whether mechanosensitivity is an artifact is besides the point: there is no question that membrane proteins are intrinsically mechanosensitive, as discussed in the introduction (see Chapter 1.10.1). I am convinced, however, that conceptually the idea of intrinsic mechanosensitivity of ion channels is correct. We are not looking at an experimental artifact, because the patch induced conversion has also been described for several K_v channels (Shaker, $K_v1.2$, $K_v2.1$ and Paddle Chimæra) and a member of the Na_v family (Skm). It would not be too far a stretch to propose that this intrinsic mechanosensitivity could be a property of all 6 transmembrane domain containing channels. To this family belong: voltage-dependent sodium, potassium and calcium channels and also transient receptor potential channels. Mechanosensitivity may be an unavoidable property of any membrane protein if at least one of its conformations has a different shape than the others. Restricting a membrane protein to shape-neutral conformation changes would significantly restrict the possible molecular motions and is thus highly unlikely.

We as researchers have to be aware of the limitations of experimental systems for studying mechanical forces in the lipid bilayer. The biggest limitation is that we do not have good models that describe the response of living tissue to mechanical deformation on any scale. Whole cells necessarily have a cytoskeleton that helps the bilayer resist deformation; in effect the deformation of a bilayer with an underlying cytoskeleton is plastic or viscoelastic at best (Ingber, 2008; Ji et al., 2008). Conversely, due to lipid/glass adhesion, membrane patches are necessary under a tension that exceeds the resting tension of cells by three orders of magnitude. The cytoskeleton in patches is most likely destroyed and thus the bilayer in patches will follow deformation elastically. Any protein that responds to biologically relevant force cues is mechanically saturated in patches. This implies that studying membrane proteins

in patches will produce results that are irrelevant to the actual biological nature of mechanosensation.

K_v channels are superior mechanosensitive channels

We have as of now no direct way to study the open probability of K_v channels in a system that allows the control of membrane tension. Other groups, however, have tried to use the Laplace-Young-Relation ($\tau = \frac{\Delta P \cdot R_c}{2}$) to relate the radius of curvature of a pressurized patch to membrane tension (Moe and Blount, 2005; Sukharev et al., 1999). These measurements have resulted in graphs plotting quantities such as open probability against membrane tension. The implicit assumption in these studies is, that in the absence of applied pressure, the membrane tension is zero. We know from various studies that this is not true. The residual tension of unpressurized patches is between 0.5-4 dyn/cm (Opsahl and Webb, 1994). The actual tension of the pressurized patches is therefore larger by this amount. Since the gating of channels such as MscL and MscS occurs at large values of membrane tension, in the context of MscL the introduced error would be maximally 10% of the presumed gating tension. It is however instructive to compare the mechanosensitivity of MscL to that of K_v channels. Based on the tentative scaling of membrane tension in various patch recordings (Chapter 2.3.2), I found that paddle chimæra's open probability can be raised by 50% at physiological membrane voltages of -20mV by increasing the membrane tension by 1.6 dyn/cm (0.4 RT/nm²). This value is 1/10th that of MscL gating (Moe and Blount, 2005; Sukharev et al., 1999). I would therefore argue that K_v channels are superior to MscL as reporters of lower bilayer tension regimes. This supreme sensitivity could hint at a biological role of K_v channel mechanosensitivity that needs further exploring. Together with the fact that various single amino acid mutations can render MscL sensitive to much lower tension values (Blount et al., 1996), it is very likely that the relative gating properties of K_v channels and mechanosensitive channels of MscL's nature are matched with their physiological roles: K_v channels modulate cell excitability, while MscL channels open when the cell is exposed to dramatic osmotic conditions under near lytic tensions, to avoid catastrophic loss of cell integrity.

Chapter 4

Material and Methods

4.1 Protein purification and reconstitution

4.1.1 KvAP

KvAP channel protein (M14-K295) inserted in the pQE60 vector (Qiagen) with a C-terminal hexahistidine tag, was expressed using *E.coli* XL1-Blue cell culture grown in LB medium supplemented with 10 mM BaCl₂. Protein production was induced with 0.4 mM isopropyl- β -D-thiogalactopyranoside (IPTG). Cells were harvested and lysed in lysis buffer containing 50 mM Tris-HCl pH 8.0, 100 mM KCl, and protease inhibitors Leupeptin, Pepstatin, Aprotinin and Phenyl-methyl-sulphonyl fluoride (PMSF). Protein was extracted with 40 mM decylmaltoside (DM) for 3 hours at room temperature in lysis buffer and purified with Co²⁺ IMAC resin using resin buffer containing 5 mM DM, 20 mM Tris-HCl pH 8.0 and 100 mM KCl. After one wash with resin buffer plus 15 mM imidazole, the protein was eluted with resin buffer containing 400 mM imidazole. Immediately after elution, 1 unit thrombin per 3mg of protein was used to cleave the hexahistidine tag overnight at room temperature. Thereafter, the protein was concentrated to 10 mg/ml and run on a Superdex-200 (10/30) column in resin buffer.

Following gel filtration the eluted channel was concentrated to 5-10 mg/ml before reconstitution. Depending on the lipid species two different methods were used for reconstitution. In the first method, which is a modification of a published procedure (Ruta et al., 2003), lipids in chloroform were transferred with a glass syringe into a glass test tube, dried with an argon stream, washed with pentane, and then placed under room vacuum for 30 minutes. Dried lipids were then hydrated with dialysis buffer containing 450 mM KCl and 10 mM Hepes-KOH pH 7.4 at a lipid concentra-

tion of 10 mg/ml. The lipid suspension was vortexed briefly and sonicated 5-10 times (30 second each) to produce small unilamellar vesicles. Decylmaltoside (DM) was added into the vesicle suspension to a final concentration of 10 mM. The mixture was rotated for 30 minutes at room temperature and then KvAP protein was added to the lipid/detergent mixture to a protein-to-lipid ratio (w/w) ranging from 0.1 to 1.0. Detergent concentration was then raised to 17.5 mM. The mixture was incubated for two hours at room temperature and then dialyzed against the dialysis buffer. The buffer was changed every 12 hours. After three days the vesicles were collected, flash-frozen with liquid nitrogen, and stored at -80°C .

In a second method for reconstitution of KvAP into DOPA, DOG and DOGS vesicles, the lipids were prepared as described above. A mixture of 50 mM DM and 50 mM β -octyl-glucoside (β -OG) was used to dissolve the lipids completely. Concentrated KvAP protein was added to the lipid-detergent micelles and then incubated and dialysed as described above.

4.1.2 MthK

MthK (M107I) channel protein inserted into the pQE70 vector (Qiagen) with a thrombin cleavage site between the C-terminal hexahistidine tag and the channel was expressed using *E.coli* XL1-Blue cell culture grown in LB. Protein production was induced with 0.4 mM isopropyl- β -D-thiogalactopyranoside (IPTG). Cells were harvested and lysed in lysis buffer containing 50 mM Tris pH8.0, 100 mM KCl, and protease inhibitors Leupeptin, Pepstatin, Aprotinin and Phenyl-methyl-sulphonyl fluoride (PMSF). Protein was extracted with 40 mM decylmaltoside (DM) for 3 hours at room temperature in lysis buffer and purified on a Co^{2+} IMAC resin using resin buffer containing 5 mM DM, 20 mM Tris-HCl pH 8.0 and 100 mM KCl. After one wash with resin buffer plus 25 mM imidazole, the protein was eluted with resin buffer containing 300 mM imidazole. Immediately after elution, 1 unit thrombin per 3mg of protein was used to cleave the hexahistidine tag. After 3 hours at room temperature cleavage was halted by addition of 4-Amidino-phenyl-methyl-sulphonyl fluoride (APMSF). Protein was concentrated to 10 mg/ml and run on a Superdex-200 (10/30) column in buffer containing 5 mM DM, 20 mM Hepes-KOH pH 7.0 and 100 mM KCl. Following gel filtration the eluted channel was concentrated to 5-10 mg/ml before reconstitution. The reconstitution method followed the same protocols as for KvAP (see above).

4.1.3 $K_v1.2$ and Paddle Chimæra

$K_v1.2$ and Paddle Chimæra channels were cloned as an N-terminal hexahistidine tagged construct with a thrombin cleavage site into the pICZ-C vector (Invitrogen) together with rat the $\beta 2$ gene. Both channel contain two amino acid substitutions (L15H, N207Q, C31S, C32S, C435S and C482S). Transformation of *Pichia pastoris* and expression were performed as previously described (Long et al., 2005a); fermented cell were frozen at -80°C . Cell were lysed by in a bead mill (Retsch) under cryogenic conditions and extraction for 3 hours at room temperature with 60 mM DM in buffer containing 50 mM Tris-HCl pH 7.5, 150 mM KCl, 10 mM β -Mercaptoethanol, 20 mM TCEP and protease inhibitors Leupeptin, Benzamidine, Soy Trypsin Inhibitor, Pepstatin, Aprotinin and PMSF. Channel protein was purified using Co^{2+} IMAC resin and maintained in lysis buffer without protease inhibitor but with 0.1 mg/ml lipids (POPE:POPC:POPG 1:1:1 w/w) (resin buffer). The resin is washed with resin buffer containing 30 mM imidazole and 6 mM DDM and eluted with resin buffer containing 300 mM imidazole and 6mM DM.

After elution from the IMAC resin the protein was concentrated to 20 mg/ml and further purified on a Superdex-200 (10/30) column. The gel filtration buffer contained 20 mM Tris-HCl pH 7.5, 100 mM KCl, 2 mM DTT, 2 mM TCEP, 6 mM DM and 0.1 mg/ml lipids.

The eluted channels were reconstituted using the reconstitution method described for KvAP (see above) with minor modifications: 4% Octyl-*D*-maltopyranoside (OM) was used for lipid solubilization and the dialysis buffer contained 2 mM DTT. Dialysis was performed at 4°C for 4-6 days.

4.2 Electrophysiology

4.2.1 Bilayer Recordings

The bilayer experiments followed published procedures (Heginbotham et al., 1998; Ruta et al., 2003). Lipids of desired compositions were prepared by dissolving dried lipids at 20 mg/ml in decane. Lipid dissolved in decane was painted over a $300\ \mu\text{m}$ hole in a polystyrene partition that separated two aqueous chambers (Miller, 1986). Once formation and thinning of a planar lipid membrane was detected through monitoring of the electrical capacitance, lipid vesicles were delivered to the membrane surface with a pipette. Vesicle fusion was facilitated by the presence of a salt gradient across the membrane: 15 mM KCl on the side opposite vesicle addition (*trans* side) and 150

mM KCl on the side of vesicle addition (*cis* side). Both sides were buffered with 10 mM Hepes-KOH at pH 7.4. After vesicle fusion, the salt concentration on the *trans* side was raised to 150 mM.

For channel activation experiments described in Figure 2.3 KvAP in DOTAP vesicles were fused into the DOTAP bilayer. Membrane voltage was pulsed as described in the figure legend. After $\tilde{15}$ minutes, empty (void of channel) POPE:POPG vesicles were fused with the bilayer during the interval between two pulses.

For channel recordings of MthK in DOTAP or EDOPC membranes, channel-containing vesicles were fused with the membrane, KCl was added to the *trans* side to abolish the salt gradient, and then CaCl_2 was added to the *trans* side (corresponding to the intracellular side of the channel) to a concentration of 5-10 mM. Charybdotoxin was added to the *cis* side (corresponding to the extracellular side of the channel).

Voltage-clamp measurements in whole-cell mode were made using an Axopatch 200B amplifier (Axon Instruments) that was interfaced to a PC via a DigiData 1440A AD/DA converter (Axon Instruments). Clampex software (Axon Instruments) was used to control the hardware. The membrane current was filtered at 1.0 - 2.0 kHz and sampled at least 5.0 kHz. All voltages are reported according to electrophysiological convention, with the extracellular side of the channel taken as ground.

4.2.2 Whole Oocyte Recordings

mRNA encoding the Shaker K_v , $K_v1.2$, $K_v2.1$ or Paddle Chimæra protein α subunit was prepared by T7 polymerase transcription and injected into *Xenopus laevis* oocytes. Reconstituted paddle chimæra protein in POPE:POPG 3:1 (w/w) vesicles was dialyzed against 100 mM KCl, 10 mM Hepes-KOH pH 7.4 for 2 hours and injected into *Xenopus laevis* oocytes. K^+ currents were recorded under two-electrode voltage clamp (OC725C, Warner Instrument Corp.) 1-2 days after mRNA injection or 12-24 hours after vesicle injection. Electrodes were drawn from borosilicate glass capillaries (VWR) and filled with 3 M KCl. Oocyte bath solution contained (mM): 98 KCl, 0.3 CaCl_2 , 1 MgCl_2 , 5 Hepes-KOH pH 7.4. Analog data from the amplifier were filtered (1kHz) using the built-in 4-pole Bessel filter, digitized at 10kHz (Digidata 1440A, Molecular Devices) and stored on a computer hard-disk.

4.2.3 Patch Clamp Recordings

K^+ currents from Shaker K_v , $K_v2.1$ and Paddle Chimæra were recorded in on-cell, inside-out and outside-out configuration from oocytes 5-6 days after mRNA

injection or in on-cell or whole cell configuration 4 days after viral infection of SF9 cells (Paddle Chimæra only). Electrodes were drawn from borosilicate patch glass (VWR) and polished (MF-83, Narishige Co.) to a resistance of 0.8 - 1.2 M Ω . For all oocyte patch configurations the extracellular solution contained (mM): 100 KCl, 2 MgCl₂, 5 Hepes-KOH pH 7.4 and the intracellular solution contained (mM): 100 KCl, 1 EGTA, 5 Hepes-KOH pH 7.4. For SF9 cell patch configurations the extracellular solution contained (mM): 135 NaCl, 10 KCl, 4 CaCl₂, 5 MgCl₂ and MES-KOH pH 6.4 and the intracellular solution contained (mM): 85 KCl, 60 KF, 1 MgCl₂, 5 EGTA and 10 Hepes-KOH pH 7.2. The analog signals were filtered (1kHz) using the built-in 4-pole Bessel filter of an Axopatch 200B patch clamp amplifier (Molecular Devices) in patch-mode, digitized at 10 kHz (Digidata 1440A, Molecular Devices) and stored on a computer hard-disk, except for the nonstationary fluctuation analysis experiments, for which the analog signals were filtered at 5kHz and digitized at 20kHz. Patch pressure was generated using water-filled U-shaped tubing connected to atmospheric pressure and applied via the patch pipette sideport. The pressure was monitored using an in-line manometer (Sper Scientific Ltd.).

4.3 Kinetic Modeling

Numerical modeling was performed using the Runge-Kutta integration method and the composite data were fitted for rate constants by χ^2 minimization using the Levenberg-Marquardt algorithm in Igor Pro (Wavemetrics Inc.) via custom-written procedures. For G/V , steady-state inactivation and inactivation data the residuals were derived from the linear deviation between measured and modeled data. For recovery from inactivation and deactivation data the residuals were derived from the expression $[0.5 \cdot \ln \frac{\text{Calculated values}}{\text{Observed values}}]$. All rate constants were fitted for exponential voltage dependence according to $k(V) = k_0 \cdot e^{(z \cdot V)}$. The fitting errors (Figure 2.13 and Figure 2.14) are estimated standard deviations of the fitting coefficients. They are based on the coefficient values one would get if the same fit was performed an infinite number of times on the same underlying data (but with different noise each time) as implement in Igor Pro.

Chapter 5

Appendices

5.1 Tension Scaling

abbreviations

γ , membrane tension

L , late opening step equilibrium constant

Tension scaling

$$\text{Case 1.} \quad \text{for } \gamma = 0 \quad C \rightleftharpoons O \quad 0 = \Delta G = \Delta G^0 + RT \ln L_{\gamma=0}$$

$$\text{Case 2.} \quad \text{for } \gamma = \gamma_{max} \quad C \rightleftharpoons O \quad 0 = \Delta G = \Delta G^0 + RT \ln L_{max} - \gamma_{max} \Delta A$$

$$\begin{aligned} \therefore \quad \Delta G^0 &= -RT \ln L_{max} + \gamma_{max} \Delta A \\ -RT \ln L_{max} &= \Delta G^0 - \gamma_{max} \Delta A \\ L_{max} &= e^{\frac{-\Delta G^0 + \gamma_{max} \Delta A}{RT}} \end{aligned}$$

Difference between Case 1 and Case 2:

$$0 = RT \ln L_{\gamma=0} - RT \ln L_{\gamma_{max}} = \gamma_{max} \Delta A \quad (5.1)$$

$$\Delta A = \frac{1}{\gamma_{max}} \left[RT \ln \frac{L_{\gamma_{max}}}{L_{\gamma=0}} \right] \quad (5.2)$$

For an intermediate (unknown) tension γ' we have

$$0 = RT \ln L_{\gamma=0} - RT \ln L_{\gamma'} + \gamma' \Delta A \quad (5.3)$$

$$= RT \ln L_{\gamma=0} - RT \ln L_{\gamma'} + \gamma' \left[\frac{1}{\gamma_{max}} RT \ln \frac{L_{\gamma_{max}}}{L_{\gamma=0}} \right] \quad (5.4)$$

$$= RT \ln \frac{L_{\gamma=0}}{L_{\gamma'}} + \frac{\gamma'}{\gamma_{max}} \cdot RT \ln \frac{L_{\gamma_{max}}}{L_{\gamma=0}} \quad (5.5)$$

$$= -RT \ln \frac{L_{\gamma'}}{L_{\gamma=0}} + \frac{\gamma'}{\gamma_{max}} \cdot RT \ln \frac{L_{\gamma_{max}}}{L_{\gamma=0}} \quad (5.6)$$

$$\therefore L_{\gamma'} = L_{\gamma=0} \cdot e^{\left[\frac{1}{RT} \left(\frac{\gamma'}{\gamma_{max}} \cdot RT \ln \frac{L_{\gamma_{max}}}{L_{\gamma=0}} \right) \right]} \quad (5.7)$$

$$\text{or} \quad \frac{\gamma'}{\gamma_{max}} \cdot RT \ln \frac{L_{\gamma_{max}}}{L_{\gamma=0}} = RT \ln \frac{L_{\gamma'}}{L_{\gamma=0}} \quad (5.8)$$

We can solve for the unknown tension γ' :

$$\gamma' = \gamma_{max} \cdot \frac{\ln \left(\frac{L_{\gamma'}}{L_{\gamma=0}} \right)}{\ln \left(\frac{L_{\gamma_{max}}}{L_{\gamma=0}} \right)} \quad (5.9)$$

5.2 K_V channel open probability derivation

abbreviations

P, probability

V, membrane voltage

Probability of voltage sensor (VS) being 'up'

$$P(\text{VS up}) = P_u$$

$$P(\text{Pore open}) = P_o$$

given 4 independent voltage sensors

$$P(n \text{ up}) = \binom{4}{n} P_u^n \cdot (1 - P_u)^{4-n} \quad (5.10)$$

$$= \frac{4!}{n! \cdot (n-4)!} P_u^n \cdot (1 - P_u)^{4-n} \quad (5.11)$$

$$\frac{P_u}{1 - P_u} = e^{\frac{zFV}{RT}} \quad (5.12)$$

$$P_u = e^{\frac{zFV}{RT}} \cdot (1 - P_u) \quad (5.13)$$

$$P_u + P_u e^{\frac{zFV}{RT}} = e^{\frac{zFV}{RT}} \quad (5.14)$$

$$P_u = \frac{e^{\frac{zFV}{RT}}}{1 + e^{\frac{zFV}{RT}}} \quad (5.15)$$

opening is controlled by

$$P(4 \text{ up}) \underset{l_c}{\overset{l_o}{\rightleftharpoons}} O$$

$$P\left(\frac{4 \text{ up}}{\text{not } O}\right) \cdot P(\text{not } O) \cdot l_o = P_o \cdot l_c \quad (5.16)$$

$$P\left(\frac{4 \text{ up}}{\text{not } O}\right) = \binom{4}{4} P_u^4 (1 - P_u)^0 = P_u^4 = \left[\frac{e^{\frac{zFV}{RT}}}{1 + e^{\frac{zFV}{RT}}} \right]^4 \quad (5.17)$$

$$P_u^4 (1 - P_o) l_o = P_o l_c \quad (5.18)$$

$$P_u^4 (1 - P_o) L = P_o \quad \text{with} \quad \frac{l_o}{l_c} = L \quad (5.19)$$

$$X(1 - P_o) = P_o \quad \text{with} \quad X = P_u^4 \cdot L \quad (5.20)$$

$$X - XP_o = P_o \quad (5.21)$$

$$X = P_o + XP_o = P_o(1 + X) \quad (5.22)$$

$$P_o = \frac{X}{1 + X} = \frac{P_u^4 \cdot L}{1 + P_u^4 \cdot L} \quad (5.23)$$

$$P_o = \frac{\left[\frac{e^{\frac{zFV}{RT}}}{1 + e^{\frac{zFV}{RT}}} \right]^4 \cdot L}{1 + L \cdot \left[\frac{e^{\frac{zFV}{RT}}}{1 + e^{\frac{zFV}{RT}}} \right]^4} \quad (5.24)$$

Because $P_u \neq 0.5$ at $V = 0$ we actually have to introduce one more unknown into equation(5.24): let $V = V - V_m$ such that at $V = V_M \rightsquigarrow P_u = 0.5$

$$\therefore P_o = \frac{\left[\frac{e^{\frac{zF(V-V_m)}{RT}}}{1 + e^{\frac{zF(V-V_m)}{RT}}} \right]^4 \cdot L}{1 + L \cdot \left[\frac{e^{\frac{zF(V-V_m)}{RT}}}{1 + e^{\frac{zF(V-V_m)}{RT}}} \right]^4} \quad (5.25)$$

References

- Aggarwal, S. K. and MacKinnon, R. (1996). Contribution of the S4 segment to gating charge in the Shaker K⁺ channel. *Neuron*, 16(6):1169–77.
- Alabi, A. A., Bahamonde, M. I., Jung, H. J., Kim, J. I., and Swartz, K. J. (2007). Portability of paddle motif function and pharmacology in voltage sensors. *Nature*, 450(7168):370–5.
- Aldrich, R. W. (1981). Inactivation of voltage-gated delayed potassium current in molluscan neurons. A kinetic model. *Biophysical Journal*, 36(3):519–32.
- Aldrich, R. W., Getting, P. A., and Thompson, S. H. (1979). Inactivation of delayed outward current in molluscan neurone somata. *J Physiol (Lond)*, 291:507–30.
- Anderson, R. G. (1998). The caveolae membrane system. *Annu Rev Biochem*, 67:199–225.
- Anderson, R. G. W. and Jacobson, K. (2002). A role for lipid shells in targeting proteins to caveolae, rafts, and other lipid domains. *Science*, 296(5574):1821–5.
- Armstrong, N., Jasti, J., Beich-Frandsen, M., and Gouaux, E. (2006). Measurement of conformational changes accompanying desensitization in an ionotropic glutamate receptor. *Cell*, 127(1):85–97.
- Awayda, M. S., Ismailov, I. I., Berdiev, B. K., and Benos, D. J. (1995). A cloned renal epithelial Na⁺ channel protein displays stretch activation in planar lipid bilayers. *Am J Physiol*, 268(6 Pt 1):C1450–9.
- Awayda, M. S. and Subramanyam, M. (1998). Regulation of the epithelial Na⁺ channel by membrane tension. *J Gen Physiol*, 112(2):97–111.
- Barrantes, F. J. (2002). Lipid matters: nicotinic acetylcholine receptor-lipid interactions. *Mol Membr Biol*, 19(4):277–84.

- Başaran, N., Doebler, R. W., Goldston, H., and Holloway, P. W. (1999). Effect of lipid unsaturation on the binding of native and a mutant form of cytochrome b5 to membranes. *Biochemistry*, 38(46):15245–52.
- Bass, R. B., Strop, P., Barclay, M., and Rees, D. C. (2002). Crystal structure of *Escherichia coli* MscS, a voltage-modulated and mechanosensitive channel. *Science*, 298(5598):1582–7.
- Baukrowitz, T. and Yellen, G. (1995). Modulation of K⁺ current by frequency and external [K⁺]: a tale of two inactivation mechanisms. *Neuron*, 15(4):951–60.
- Bell, R. M. and Burns, D. J. (1991). Lipid activation of protein kinase C. *J Biol Chem*, 266(8):4661–4.
- Benachir, T. and Lafleur, M. (1995). Study of vesicle leakage induced by melittin. *Biochim Biophys Acta*, 1235(2):452–60.
- Bianchi, L. (2007). Mechanotransduction: touch and feel at the molecular level as modeled in *Caenorhabditis elegans*. *Mol Neurobiol*, 36(3):254–71.
- Bianchi, L., Gerstbrein, B., Frøkjær-Jensen, C., Royal, D. C., Mukherjee, G., Royal, M. A., Xue, J., Schafer, W. R., and Driscoll, M. (2004). The neurotoxic MEC-4(d) DEG/ENaC sodium channel conducts calcium: implications for necrosis initiation. *Nat Neurosci*, 7(12):1337–44.
- Blount, P., Sukharev, S. I., Schroeder, M. J., Nagle, S. K., and Kung, C. (1996). Single residue substitutions that change the gating properties of a mechanosensitive channel in *Escherichia coli*. *Proc Natl Acad Sci U S A*, 93(21):11652–7.
- Botelho, A. V., Huber, T., Sakmar, T. P., and Brown, M. F. (2006). Curvature and hydrophobic forces drive oligomerization and modulate activity of rhodopsin in membranes. *Biophysical Journal*, 91(12):4464–77.
- Boulais, N. and Misery, L. (2008). The epidermis: a sensory tissue. *Eur J Dermatol*, 18(2):119–27.
- Brady, J. D., Rich, T. C., Le, X., Stafford, K., Fowler, C. J., Lynch, L., Karpen, J. W., Brown, R. L., and Martens, J. R. (2004). Functional role of lipid raft microdomains in cyclic nucleotide-gated channel activation. *Molecular Pharmacology*, 65(3):503–11.

- Brotherus, J. R., Griffith, O. H., Brotherus, M. O., Jost, P. C., Silvius, J. R., and Hokin, L. E. (1981). Lipid-protein multiple binding equilibria in membranes. *Biochemistry*, 20(18):5261–7.
- Brown, D. A. and London, E. (2000). Structure and function of sphingolipid- and cholesterol-rich membrane rafts. *J Biol Chem*, 275(23):17221–4.
- Brusés, J. L., Chauvet, N., and Rutishauser, U. (2001). Membrane lipid rafts are necessary for the maintenance of the (alpha)7 nicotinic acetylcholine receptor in somatic spines of ciliary neurons. *J Neurosci*, 21(2):504–12.
- Burnstock, G. (1999). Release of vasoactive substances from endothelial cells by shear stress and purinergic mechanosensory transduction. *J Anat*, 194 (Pt 3):335–42.
- Burnstock, G. and Wood, J. N. (1996). Purinergic receptors: their role in nociception and primary afferent neurotransmission. *Current Opinion in Neurobiology*, 6(4):526–32.
- Calabrese, B., Tabarean, I. V., Juranka, P., and Morris, C. E. (2002). Mechanosensitivity of N-type calcium channel currents. *Biophysical Journal*, 83(5):2560–74.
- Campbell, R. B., Balasubramanian, S. V., and Straubinger, R. M. (2001). Phospholipid-cationic lipid interactions: influences on membrane and vesicle properties. *Biochim Biophys Acta*, 1512(1):27–39.
- Caroni, P. (2001). New EMBO members’ review: actin cytoskeleton regulation through modulation of PI(4,5)P(2) rafts. *EMBO J*, 20(16):4332–6.
- Cartailler, J.-P. and Luecke, H. (2003). X-ray crystallographic analysis of lipid-protein interactions in the bacteriorhodopsin purple membrane. *Annu Rev Biophys Biomol Struct*, 32:285–310.
- Casado, M. and Ascher, P. (1998). Opposite modulation of NMDA receptors by lysophospholipids and arachidonic acid: common features with mechanosensitivity. *J Physiol (Lond)*, 513 (Pt 2):317–30.
- Chalfie, M. (1993). Touch receptor development and function in *Caenorhabditis elegans*. *J Neurobiol*, 24(10):1433–41.
- Chalfie, M. and Au, M. (1989). Genetic control of differentiation of the *Caenorhabditis elegans* touch receptor neurons. *Science*, 243(4894 Pt 1):1027–33.

- Colbert, H. A., Smith, T. L., and Bargmann, C. I. (1997). OSM-9, a novel protein with structural similarity to channels, is required for olfaction, mechanosensation, and olfactory adaptation in *Caenorhabditis elegans*. *J Neurosci*, 17(21):8259–69.
- Cook, G., Redwood, W., Taylor, A., and Haydon, D. A. (1968). The molecular composition of black hydrocarbon films in aqueous solutions. *Colloid & Polymer Science*, 227(1):28–37.
- Corey, D. P., García-Añoveros, J., Holt, J. R., Kwan, K. Y., Lin, S.-Y., Vollrath, M. A., Amalfitano, A., Cheung, E. L.-M., Derfler, B. H., Duggan, A., Géléoc, G. S. G., Gray, P. A., Hoffman, M. P., Rehm, H. L., Tamasauskas, D., and Zhang, D.-S. (2004). TRPA1 is a candidate for the mechanosensitive transduction channel of vertebrate hair cells. *Nature*, 432(7018):723–30.
- Cui, C., Smith, D. O., and Adler, J. (1995). Characterization of mechanosensitive channels in *Escherichia coli* cytoplasmic membrane by whole-cell patch clamp recording. *J Membr Biol*, 144(1):31–42.
- Dai, J., Sheetz, M. P., Wan, X., and Morris, C. E. (1998). Membrane tension in swelling and shrinking molluscan neurons. *J Neurosci*, 18(17):6681–92.
- Damjanovich, S., Bene, L., Matkó, J., Alileche, A., Goldman, C. K., Sharrow, S., and Waldmann, T. A. (1997). Preassembly of interleukin 2 (IL-2) receptor subunits on resting Kit 225 K6 t-cells and their modulation by IL-2, IL-7, and IL-15: a fluorescence resonance energy transfer study. *Proc Natl Acad Sci USA*, 94(24):13134–9.
- Dan, N. and Safran, S. A. (1998). Effect of lipid characteristics on the structure of transmembrane proteins. *Biophysical Journal*, 75(3):1410–4.
- Darby, P. J., Kwan, C. Y., and Daniel, E. E. (2000). Caveolae from canine airway smooth muscle contain the necessary components for a role in Ca(2+) handling. *Am J Physiol Lung Cell Mol Physiol*, 279(6):L1226–35.
- Davis, B. K. (1999). Evolution of the genetic code. *Prog Biophys Mol Biol*, 72(2):157–243.
- Davis, B. K. (2002). Molecular evolution before the origin of species. *Prog Biophys Mol Biol*, 79(1-3):77–133.
- Davis, M. J., Donovitz, J. A., and Hood, J. D. (1992). Stretch-activated single-channel and whole cell currents in vascular smooth muscle cells. *Am J Physiol*, 262(4 Pt 1):C1083–8.

- Davis, M. J. and Hill, M. A. (1999). Signaling mechanisms underlying the vascular myogenic response. *Physiol Rev*, 79(2):387–423.
- de Foresta, B., le Maire, M., Orłowski, S., Champeil, P., Lund, S., Møller, J. V., Michelangeli, F., and Lee, A. G. (1989). Membrane solubilization by detergent: use of brominated phospholipids to evaluate the detergent-induced changes in Ca²⁺ - ATPase/lipid interaction. *Biochemistry*, 28(6):2558–67.
- Deamer, D. and Dworkin, J. (2005). Chemistry and physics of primitive membranes. *Topics in Current Chemistry*, 259:1.
- Deamer, D. W. and Bramhall, J. (1986). Permeability of lipid bilayers to water and ionic solutes. *Chemistry and Physics of Lipids*, 40(2-4):167–88.
- Deamer, D. W. and Pashley, R. M. (1989). Amphiphilic components of the Murchison carbonaceous chondrite: surface properties and membrane formation. *Origins of life and evolution of the biosphere : the journal of the International Society for the Study of the Origin of Life*, 19(1):21–38.
- Delling, M., Wischmeyer, E., Dityatev, A., Sytnyk, V., Veh, R. W., Karschin, A., and Schachner, M. (2002). The neural cell adhesion molecule regulates cell-surface delivery of G-protein-activated inwardly rectifying potassium channels via lipid rafts. *J Neurosci*, 22(16):7154–64.
- Dowhan, W. (1997). Molecular basis for membrane phospholipid diversity: why are there so many lipids? *Annu Rev Biochem*, 66:199–232.
- Dowhan, W. and Bogdanov, M. (2002). *Biochemistry of Lipids, Lipoproteins and Membranes*, volume 36. Elsevier, 4th edition.
- Driscoll, M. and Chalfie, M. (1991). The *mec-4* gene is a member of a family of *Caenorhabditis elegans* genes that can mutate to induce neuronal degeneration. *Nature*, 349(6310):588–93.
- Duggan, A., García-Añoveros, J., and Corey, D. P. (2000). Insect mechanoreception: what a long, strange TRP it's been. *Curr Biol*, 10(10):R384–7.
- Dulhunty, A. F. and Franzini-Armstrong, C. (1975). The relative contributions of the folds and caveolae to the surface membrane of frog skeletal muscle fibres at different sarcomere lengths. *J Physiol (Lond)*, 250(3):513–39.

- Dumas, F., Sperotto, M. M., Lebrun, M. C., Tocanne, J. F., and Mouritsen, O. G. (1997). Molecular sorting of lipids by bacteriorhodopsin in dilauroylphosphatidylcholine/distearoylphosphatidylcholine lipid bilayers. *Biophysical Journal*, 73(4):1940–53.
- East, J. M. and Lee, A. G. (1982). Lipid selectivity of the calcium and magnesium ion dependent adenosinetriphosphatase, studied with fluorescence quenching by a brominated phospholipid. *Biochemistry*, 21(17):4144–51.
- Eddidin, M. (2003). The state of lipid rafts: from model membranes to cells. *Annual review of biophysics and biomolecular structure*, 32:257–83.
- Engel, D. and Jonas, P. (2005). Presynaptic action potential amplification by voltage-gated Na⁺ channels in hippocampal mossy fiber boutons. *Neuron*, 45(3):405–17.
- Evans, E. and Hochmuth, R. (1978). *Mechanochemical properties of membranes*. Academic Press, Inc.
- Field, K. A., Holowka, D., and Baird, B. (1997). Compartmentalized activation of the high affinity immunoglobulin E receptor within membrane domains. *J Biol Chem*, 272(7):4276–80.
- Freites, J. A., Tobias, D. J., von Heijne, G., and White, S. H. (2005). Interface connections of a transmembrane voltage sensor. *Proc Natl Acad Sci USA*, 102(42):15059–64.
- Froud, R. J., East, J. M., Rooney, E. K., and Lee, A. G. (1986). Binding of long-chain alkyl derivatives to lipid bilayers and to (Ca²⁺ - Mg²⁺)-ATPase. *Biochemistry*, 25(23):7535–44.
- Gee, S. H., Madhavan, R., Levinson, S. R., Caldwell, J. H., Sealock, R., and Froehner, S. C. (1998). Interaction of muscle and brain sodium channels with multiple members of the syntrophin family of dystrophin-associated proteins. *J Neurosci*, 18(1):128–37.
- Gil, T., Ipsen, J. H., Mouritsen, O. G., Sabra, M. C., Sperotto, M. M., and Zuckermann, M. J. (1998). Theoretical analysis of protein organization in lipid membranes. *Biochim Biophys Acta*, 1376(3):245–66.
- Gil, T., Sabra, M. C., Ipsen, J. H., and Mouritsen, O. G. (1997). Wetting and capillary condensation as means of protein organization in membranes. *Biophys J*, 73(4):1728–41.

- Gillespie, P. G. and Walker, R. G. (2001). Molecular basis of mechanosensory transduction. *Nature*, 413(6852):194–202.
- Giorgione, J. R., Kraayenhof, R., and Epanand, R. M. (1998). Interfacial membrane properties modulate protein kinase c activation: role of the position of acyl chain unsaturation. *Biochemistry*, 37(31):10956–60.
- Goulian, M., Bruinsma, R., and PINCUS, P. (1993). Long-range forces in heterogeneous fluid membranes. *Europhys Lett*, 22(2):145–150.
- Gu, C. X., Juranka, P. F., and Morris, C. E. (2001). Stretch-activation and stretch-inactivation of Shaker-IR, a voltage-gated K⁺ channel. *Biophysical Journal*, 80(6):2678–93.
- Guskov, A., Kern, J., Gabdulkhakov, A., Broser, M., Zouni, A., and Saenger, W. (2009). Cyanobacterial photosystem ii at 2.9 Å resolution and the role of quinones, lipids, channels and chloride. *Nat Struct Mol Biol*, 16(3):334–42.
- Gustin, M. (1991). Single-Channel Mechanosensitive Currents. *Science*, 253(5021):800.
- Hackney, C. M. and Furness, D. N. (1995). Mechanotransduction in vertebrate hair cells: structure and function of the stereociliary bundle. *Am J Physiol*, 268(1 Pt 1):C1–13.
- Hajdú, P., Varga, Z., Pieri, C., Panyi, G., and Gáspár, Jr, R. (2003). Cholesterol modifies the gating of Kv1.3 in human T lymphocytes. *Pflugers Arch*, 445(6):674–82.
- Hamill, O. and McBride, D. W. (1997). Induced membrane hypo/hyper-mechanosensitivity: a limitation of patch-clamp recording. *Annu Rev Physiol*, 59:621–31.
- Hamill, O. P. and McBride, D. W. (1992). Rapid adaptation of single mechanosensitive channels in *Xenopus* oocytes. *Proceedings of the National Academy of Sciences of the United States of America*, 89(16):7462–6.
- Harteneck, C., Plant, T. D., and Schultz, G. (2000). From worm to man: three subfamilies of TRP channels. *Trends Neurosci*, 23(4):159–66.
- Heginbotham, L., Kolmakova-Partensky, L., and Miller, C. (1998). Functional reconstitution of a prokaryotic K⁺ channel. *J Gen Physiol*, 111(6):741–9.

- Heimpel, S., Basset, G., Odoj, S., and Klingenberg, M. (2001). Expression of the mitochondrial ADP/ATP carrier in *Escherichia coli*. Renaturation, reconstitution, and the effect of mutations on 10 positive residues. *J Biol Chem*, 276(15):11499–506.
- Helfrich, W. (1973). Elastic properties of lipid bilayers: theory and possible experiments. *Zeitschrift für Naturforschung Teil C: Biochemie, Biophysik, Biologie, Virologie*, 28(11):693–703.
- Hessa, T., Kim, H., Bihlmaier, K., Lundin, C., Boekel, J., Andersson, H., Nilsson, I., White, S. H., and von Heijne, G. (2005a). Recognition of transmembrane helices by the endoplasmic reticulum translocon. *Nature*, 433(7024):377–81.
- Hessa, T., White, S. H., and von Heijne, G. (2005b). Membrane insertion of a potassium-channel voltage sensor. *Science*, 307(5714):1427.
- Hill, W. G., Southern, N. M., MacIver, B., Potter, E., Apodaca, G., Smith, C. P., and Zeidel, M. L. (2005). Isolation and characterization of the *Xenopus* oocyte plasma membrane: a new method for studying activity of water and solute transporters. *AJP - Renal Physiology*, 289(1):F217–24.
- Hille, B. (2001). *Ion Channels of Excitable Membranes*. Sinauer Associates, Inc.
- Hochmuth, F. M., Shao, J. Y., Dai, J., and Sheetz, M. P. (1996). Deformation and flow of membrane into tethers extracted from neuronal growth cones. *Biophysical Journal*, 70(1):358–69.
- Hodgkin, A. L. and Huxley, A. F. (1945). Resting and action potentials in single nerve fibres. *J Physiol (Lond)*, 104(2):176–95.
- Hodgkin, A. L. and Huxley, A. F. (1952). A quantitative description of membrane current and its application to conduction and excitation in nerve. *J Physiol (Lond)*, 117(4):500–44.
- Hooper, N. M. (1999). Detergent-insoluble glycosphingolipid/cholesterol-rich membrane domains, lipid rafts and caveolae. *Mol Membr Biol*, 16(2):145–56.
- Hoshi, T., Zagotta, W., and Aldrich, R. W. (1990). Biophysical and molecular mechanisms of Shaker potassium channel inactivation. *Science (New York, N. Y.)*, 250:533–538.

- Hoshi, T., Zagotta, W. N., and Aldrich, R. W. (1991). Two types of inactivation in Shaker K⁺ channels: effects of alterations in the carboxy-terminal region. *Neuron*, 7(4):547–56.
- Hoshi, T., Zagotta, W. N., and Aldrich, R. W. (1994). Shaker potassium channel gating. i: Transitions near the open state. *J Gen Physiol*, 103(2):249–78.
- Howard, J. and Bechstetdt, S. (2004). Hypothesis: a helix of ankyrin repeats of the NOMPC-TRP ion channel is the gating spring of mechanoreceptors. *Curr Biol*, 14(6):R224–6.
- Howard, J., Roberts, W. M., and Hudspeth, A. J. (1988). Mechanoelectrical transduction by hair cells. *Annual review of biophysics and biophysical chemistry*, 17:99–124.
- Huang, C. L., Feng, S., and Hilgemann, D. W. (1998). Direct activation of inward rectifier potassium channels by PIP₂ and its stabilization by G betagamma. *Nature*, 391(6669):803–6.
- Ikonen, E. (2001). Roles of lipid rafts in membrane transport. *Curr Opin Cell Biol*, 13(4):470–7.
- Ingber, D. E. (1993). Cellular tensegrity: defining new rules of biological design that govern the cytoskeleton. *J Cell Sci*, 104 (Pt 3):613–27.
- Ingber, D. E. (1997). Tensegrity: the architectural basis of cellular mechanotransduction. *Annu Rev Physiol*, 59:575–99.
- Ingber, D. E. (2008). Tensegrity-based mechanosensing from macro to micro. *Prog Biophys Mol Biol*, 97(2-3):163–79.
- Ji, L., Lim, J., and Danuser, G. (2008). Fluctuations of intracellular forces during cell protrusion. *Nat Cell Biol*, 10(12):1393–400.
- Ji, S., John, S. A., Lu, Y., and Weiss, J. N. (1998). Mechanosensitivity of the cardiac muscarinic potassium channel. A novel property conferred by Kir3.4 subunit. *J Biol Chem*, 273(3):1324–8.
- Jiang, F., Ryan, M. T., Schlame, M., Zhao, M., Gu, Z., Klingenberg, M., Pfanner, N., and Greenberg, M. L. (2000). Absence of cardiolipin in the *crd1* null mutant results in decreased mitochondrial membrane potential and reduced mitochondrial function. *J Biol Chem*, 275(29):22387–94.

- Jiang, Q.-X., Wang, D.-N., and MacKinnon, R. (2004). Electron microscopic analysis of KvAP voltage-dependent K⁺ channels in an open conformation. *Nature*, 430(7001):806–10.
- Jiang, Y., Lee, A., Chen, J., Cadene, M., Chait, B. T., and Mackinnon, R. (2002). Crystal structure and mechanism of a calcium-gated potassium channel. *Nature*, 417(6888):515–22.
- Jiang, Y., Lee, A., Chen, J., Ruta, V., Cadene, M., Chait, B. T., and Mackinnon, R. (2003a). X-ray structure of a voltage-dependent K⁺ channel. *Nature*, 423(6935):33–41.
- Jiang, Y., Ruta, V., Chen, J., Lee, A., and Mackinnon, R. (2003b). The principle of gating charge movement in a voltage-dependent K⁺ channel. *Nature*, 423(6935):42–8.
- Jones, O. T. and McNamee, M. G. (1988). Annular and nonannular binding sites for cholesterol associated with the nicotinic acetylcholine receptor. *Biochemistry*, 27(7):2364–74.
- Jordan, P., Fromme, P., Witt, H. T., Klukas, O., Saenger, W., and Krauss, N. (2001). Three-dimensional structure of cyanobacterial photosystem i at 2.5 Å resolution. *Nature*, 411(6840):909–17.
- Jost, P. C. and Griffith, O. H. (1978). The spin-labeling technique. *Meth Enzymol*, 49:369–418.
- Jung, H. J., Lee, J. Y., Kim, S. H., Eu, Y.-J., Shin, S. Y., Milesco, M., Swartz, K. J., and Kim, J. I. (2005). Solution structure and lipid membrane partitioning of VSTx1, an inhibitor of the KvAP potassium channel. *Biochemistry*, 44(16):6015–23.
- Kernan, M., Cowan, D., and Zuker, C. (1994). Genetic dissection of mechanosensory transduction: mechanoreception-defective mutations of *Drosophila*. *Neuron*, 12(6):1195–206.
- Khan, T. K., Yang, B., Thompson, N. L., Maekawa, S., Epand, R. M., and Jacobson, K. (2003). Binding of NAP-22, a calmodulin-binding neuronal protein, to raft-like domains in model membranes. *Biochemistry*, 42(17):4780–6.

- Klemic, K. G., Kirsch, G. E., and Jones, S. W. (2001). U-type inactivation of Kv3.1 and Shaker potassium channels. *Biophysical Journal*, 81(2):814–26.
- Klemic, K. G., Shieh, C. C., Kirsch, G. E., and Jones, S. W. (1998). Inactivation of Kv2.1 potassium channels. *Biophysical Journal*, 74(4):1779–89.
- Kornau, H. C., Seeburg, P. H., and Kennedy, M. B. (1997). Interaction of ion channels and receptors with PDZ domain proteins. *Curr Opin Neurobiol*, 7(3):368–73.
- Kumánovics, A., Levin, G., and Blount, P. (2002). Family ties of gated pores: evolution of the sensor module. *FASEB J*, 16(12):1623–9.
- Kurzchalia, T. V. and Parton, R. G. (1999). Membrane microdomains and caveolae. *Curr Opin Cell Biol*, 11(4):424–31.
- Kwok, R. and Evans, E. A. (1981). Thermoelasticity of large lecithin bilayer vesicles. *Biophysical Journal*, 35(3):637–52.
- Laitko, U., Juranka, P. F., and Morris, C. E. (2006). Membrane stretch slows the concerted step prior to opening in a Kv channel. *J Gen Physiol*, 127(6):687–701.
- Lammerding, J., Kamm, R. D., and Lee, R. T. (2004). Mechanotransduction in cardiac myocytes. *Annals of the New York Academy of Sciences*, 1015:53–70.
- Laux, T., Fukami, K., Thelen, M., Golub, T., Frey, D., and Caroni, P. (2000). GAP43, MARCKS, and CAP23 modulate PI(4,5)P(2) at plasmalemmal rafts, and regulate cell cortex actin dynamics through a common mechanism. *J Cell Biol*, 149(7):1455–72.
- Lee, A. G. (1998). How lipids interact with an intrinsic membrane protein: the case of the calcium pump. *Biochim Biophys Acta*, 1376(3):381–90.
- Lee, H. C., Wang, J. M., and Swartz, K. J. (2003). Interaction between extracellular Hanatoxin and the resting conformation of the voltage-sensor paddle in Kv channels. *Neuron*, 40(3):527–36.
- Lee, S.-Y., Lee, A., Chen, J., and MacKinnon, R. (2005). Structure of the KvAP voltage-dependent K⁺ channel and its dependence on the lipid membrane. *Proceedings of the National Academy of Sciences of the United States of America*, 102(43):15441–6.

- Lee, S.-Y. and Mackinnon, R. (2004). A membrane-access mechanism of ion channel inhibition by voltage sensor toxins from spider venom. *Nature*, 430(6996):232–5.
- Lehtonen, J. Y. and Kinnunen, P. K. (1997). Evidence for phospholipid microdomain formation in liquid crystalline liposomes reconstituted with *Escherichia coli* lactose permease. *Biophysical Journal*, 72(3):1247–57.
- Lesage, F., Guillemare, E., Fink, M., Duprat, F., Lazdunski, M., Romey, G., and Barhanin, J. (1996). TWIK-1, a ubiquitous human weakly inward rectifying K⁺ channel with a novel structure. *EMBO J*, 15(5):1004–11.
- Lewis, R. N., Zhang, Y. P., Hodges, R. S., Subczynski, W. K., Kusumi, A., Flach, C. R., Mendelsohn, R., and McElhaney, R. N. (2001). A polyalanine-based peptide cannot form a stable transmembrane alpha-helix in fully hydrated phospholipid bilayers. *Biochemistry*, 40(40):12103–11.
- Lockwich, T. P., Liu, X., Singh, B. B., Jadlovec, J., Weiland, S., and Ambudkar, I. S. (2000). Assembly of Trp1 in a signaling complex associated with caveolin-scaffolding lipid raft domains. *J Biol Chem*, 275(16):11934–42.
- London, E. and Feigenson, G. W. (1981a). Fluorescence quenching in model membranes. 1. Characterization of quenching caused by a spin-labeled phospholipid. *Biochemistry*, 20(7):1932–8.
- London, E. and Feigenson, G. W. (1981b). Fluorescence quenching in model membranes. 2. Determination of local lipid environment of the calcium adenosinetriphosphatase from sarcoplasmic reticulum. *Biochemistry*, 20(7):1939–48.
- Long, S. B., Campbell, E. B., and Mackinnon, R. (2005a). Crystal structure of a mammalian voltage-dependent Shaker family K⁺ channel. *Science*, 309(5736):897–903.
- Long, S. B., Campbell, E. B., and Mackinnon, R. (2005b). Voltage sensor of Kv1.2: structural basis of electromechanical coupling. *Science*, 309(5736):903–8.
- Long, S. B., Tao, X., Campbell, E. B., and Mackinnon, R. (2007). Atomic structure of a voltage-dependent K⁺ channel in a lipid membrane-like environment. *Nature*, 450(7168):376–82.
- Luecke, H., Richter, H. T., and Lanyi, J. K. (1998). Proton transfer pathways in bacteriorhodopsin at 2.3 angstrom resolution. *Science*, 280(5371):1934–7.

- Lundbaek, J. (2008). Lipid Bilayer-mediated Regulation of Ion Channel Function by Amphiphilic Drugs. *J Gen Physiol*, 131(5):421.
- Lyford, G. L., Strege, P. R., Shepard, A., Ou, Y., Ermilov, L., Miller, S. M., Gibbons, S. J., Rae, J. L., Szurszewski, J. H., and Farrugia, G. (2002). $\alpha(1C)$ (Ca(V)1.2) L-type calcium channel mediates mechanosensitive calcium regulation. *Am J Physiol, Cell Physiol*, 283(3):C1001–8.
- MacDonald, R. C., Ashley, G., Shida, M., Rakhmanova, V., Tarahovsky, Y. S., Pantazatos, D., Kennedy, M., Pozharski, E., Baker, K., Jones, R., Rosenzweig, H., Choi, K., Qiu, R., and McIntosh, T. J. (1999). Physical and biological properties of cationic triesters of phosphatidylcholine. *Biophys J*, 77(5):2612–29.
- Maingret, F., Fosset, M., Lesage, F., Lazdunski, M., and Honoré, E. (1999). TRAAK is a mammalian neuronal mechano-gated K⁺ channel. *J Biol Chem*, 274(3):1381–7.
- Marom, S. and Abbott, L. F. (1994). Modeling state-dependent inactivation of membrane currents. *Biophysical Journal*, 67(2):515–20.
- Marom, S. and Levitan, I. B. (1994). State-dependent inactivation of the Kv3 potassium channel. *Biophysical Journal*, 67(2):579–89.
- Marsh, D. (2007). Lateral pressure profile, spontaneous curvature frustration, and the incorporation and conformation of proteins in membranes. *Biophys J*, 93(11):3884–99.
- Marsh, D. and Horváth, L. I. (1998). Structure, dynamics and composition of the lipid-protein interface. Perspectives from spin-labelling. *Biochim Biophys Acta*, 1376(3):267–96.
- Marsh, D., Watts, A., Pates, R. D., Uhl, R., Knowles, P. F., and Esmann, M. (1982). ESR spin-label studies of lipid-protein interactions in membranes. *Biophysical Journal*, 37(1):265–74.
- Martens, J. R., Navarro-Polanco, R., Coppock, E. A., Nishiyama, A., Parshley, L., Grobaski, T. D., and Tamkun, M. M. (2000). Differential targeting of Shaker-like potassium channels to lipid rafts. *J Biol Chem*, 275(11):7443–6.
- Martens, J. R., O’Connell, K., and Tamkun, M. (2004). Targeting of ion channels to membrane microdomains: localization of Kv channels to lipid rafts. *Trends Pharmacol Sci*, 25(1):16–21.

- Martens, J. R., Sakamoto, N., Sullivan, S. A., Grobaski, T. D., and Tamkun, M. M. (2001). Isoform-specific localization of voltage-gated K⁺ channels to distinct lipid raft populations. Targeting of Kv1.5 to caveolae. *J Biol Chem*, 276(11):8409–14.
- Meyer zu Heringdorf, D. and Jakobs, K. H. (2007). Lysophospholipid receptors: signalling, pharmacology and regulation by lysophospholipid metabolism. *Biochim Biophys Acta*, 1768(4):923–40.
- Milescu, M., Bosmans, F., Lee, S., Alabi, A., Kim, J., and Swartz, K. (2009). Interactions between lipids and voltage sensor paddles detected with tarantula toxins. *Nat Struct Mol Biol*.
- Milescu, M., Vobecky, J., Roh, S. H., Kim, S. H., Jung, H. J., Kim, J. I., and Swartz, K. J. (2007). Tarantula toxins interact with voltage sensors within lipid membranes. *J Gen Physiol*, 130(5):497–511.
- Miller, C. (1986). *Ion channel reconstitution*. Plenum Press.
- Milton, R. L. and Caldwell, J. H. (1990). How do patch clamp seals form? a lipid bleb model. *Pflugers Arch*, 416(6):758–62.
- Moe, P. and Blount, P. (2005). Assessment of potential stimuli for mechano-dependent gating of MscL: effects of pressure, tension, and lipid headgroups. *Biochemistry*, 44(36):12239–44.
- Moffett, S., Brown, D. A., and Linder, M. E. (2000). Lipid-dependent targeting of G proteins into rafts. *J Biol Chem*, 275(3):2191–8.
- Monnard, P.-A., Apel, C. L., Kanavarioti, A., and Deamer, D. W. (2002). Influence of ionic inorganic solutes on self-assembly and polymerization processes related to early forms of life: implications for a prebiotic aqueous medium. *Astrobiology*, 2(2):139–52.
- Moorman, J. R., Kirsch, G. E., VanDongen, A. M., Joho, R. H., and Brown, A. M. (1990). Fast and slow gating of sodium channels encoded by a single mRNA. *Neuron*, 4(2):243–52.
- Morales, A., Aleu, J., Ivorra, I., Ferragut, J. A., Gonzalez-Ros, J. M., and Miledi, R. (1995). Incorporation of reconstituted acetylcholine receptors from Torpedo into the Xenopus oocyte membrane. *Proceedings of the National Academy of Sciences of the United States of America*, 92(18):8468–72.

- Morris, C. and Horn, R. (1991a). Response. *Science*, 253(5021):801.
- Morris, C. E. and Horn, R. (1991b). Failure to elicit neuronal macroscopic mechanosensitive currents anticipated by single-channel studies. *Science*, 251(4998):1246–9.
- Munro, S. (2002). Organelle identity and the targeting of peripheral membrane proteins. *Curr Opin Cell Biol*, 14(4):506–14.
- Murata, Y., Iwasaki, H., Sasaki, M., Inaba, K., and Okamura, Y. (2005). Phosphoinositide phosphatase activity coupled to an intrinsic voltage sensor. *Nature*, 435(7046):1239–43.
- Nagy, P., Mátyus, L., Jenei, A., Panyi, G., Varga, S., Matkó, J., Szöllosi, J., Gáspár, R., Jovin, T. M., and Damjanovich, S. (2001). Cell fusion experiments reveal distinctly different association characteristics of cell-surface receptors. *J Cell Sci*, 114(Pt 22):4063–71.
- Nakamura, F. and Strittmatter, S. M. (1996). P2Y1 purinergic receptors in sensory neurons: contribution to touch-induced impulse generation. *Proceedings of the National Academy of Sciences of the United States of America*, 93(19):10465–70.
- Naruse, K., Tang, Q., and Sokabe, M. (2009). Stress-Axis Regulated Exon (STREX) in the C terminus of BK(Ca) channels is responsible for the stretch sensitivity. *Biochem Biophys Res Commun*.
- Nielsen, C., Goulian, M., and Andersen, O. S. (1998). Energetics of inclusion-induced bilayer deformations. *Biophysical Journal*, 74(4):1966–83.
- Nilius, B., Eggermont, J., Voets, T., Buyse, G., Manolopoulos, V., and Droogmans, G. (1997). Properties of volume-regulated anion channels in mammalian cells. *Prog Biophys Mol Biol*, 68(1):69–119.
- O’Hagan, R., Chalfie, M., and Goodman, M. B. (2005). The MEC-4 DEG/EnaC channel of *Caenorhabditis elegans* touch receptor neurons transduces mechanical signals. *Nat Neurosci*, 8(1):43–50.
- Okamoto, T., Schlegel, A., Scherer, P. E., and Lisanti, M. P. (1998). Caveolins, a family of scaffolding proteins for organizing ”preassembled signaling complexes” at the plasma membrane. *J Biol Chem*, 273(10):5419–22.

- O’Keeffe, A. H., East, J. M., and Lee, A. G. (2000). Selectivity in lipid binding to the bacterial outer membrane protein OmpF. *Biophysical Journal*, 79(4):2066–74.
- Oliver, D., Lien, C.-C., Soom, M., Baukrowitz, T., Jonas, P., and Fakler, B. (2004). Functional Conversion Between A-Type and Delayed Rectifier K⁺ Channels by Membrane Lipids. *Science*, 304:265–270. 10.1126/science.1094113.
- Opsahl, L. R. and Webb, W. W. (1994). Lipid-glass adhesion in giga-sealed patch-clamped membranes. *Biophysical Journal*, 66(1):75–9.
- Palmer, L. G. and Frindt, G. (1996). Gating of Na channels in the rat cortical collecting tubule: effects of voltage and membrane stretch. *J Gen Physiol*, 107(1):35–45.
- Pande, A. H., Qin, S., and Tatulian, S. A. (2005). Membrane fluidity is a key modulator of membrane binding, insertion, and activity of 5-lipoxygenase. *Biophysical Journal*, 88(6):4084–94.
- Paoletti, P. and Ascher, P. (1994). Mechanosensitivity of NMDA receptors in cultured mouse central neurons. *Neuron*, 13(3):645–55.
- Patel, A. J., Honoré, E., Maingret, F., Lesage, F., Fink, M., Duprat, F., and Lazdunski, M. (1998). A mammalian two pore domain mechano-gated S-like K⁺ channel. *EMBO J*, 17(15):4283–90.
- Perozo, E., Kloda, A., Cortes, D. M., and Martinac, B. (2002). Physical principles underlying the transduction of bilayer deformation forces during mechanosensitive channel gating. *Nat Struct Biol*, 9(9):696–703.
- Posokhov, Y. O., Gottlieb, P. A., Morales, M. J., Sachs, F., and Ladokhin, A. S. (2007). Is lipid bilayer binding a common property of inhibitor cysteine knot ion-channel blockers? *Biophys J*, 93(4):L20–2.
- Powl, A. M., Carney, J., Marius, P., East, J. M., and Lee, A. G. (2005). Lipid interactions with bacterial channels: fluorescence studies. *Biochem Soc Trans*, 33(Pt 5):905–9.
- Ramsey, I. S., Moran, M. M., Chong, J. A., and Clapham, D. E. (2006). A voltage-gated proton-selective channel lacking the pore domain. *Nature*, 440(7088):1213–6.
- Ramu, Y., Xu, Y., and Lu, Z. (2006). Enzymatic activation of voltage-gated potassium channels. *Nature*, 442(7103):696–9.

- Rankin, S. E., Addona, G. H., Kloczewiak, M. A., Bugge, B., and Miller, K. W. (1997). The cholesterol dependence of activation and fast desensitization of the nicotinic acetylcholine receptor. *Biophysical Journal*, 73(5):2446–55.
- Raucher, D. and Sheetz, M. P. (1999). Characteristics of a membrane reservoir buffering membrane tension. *Biophysical Journal*, 77(4):1992–2002.
- Rawicz, W., Olbrich, K. C., McIntosh, T. J., Needham, D., and Evans, E. A. (2000). Effect of chain length and unsaturation on elasticity of lipid bilayers. *Biophysical Journal*, 79(1):328–339.
- Requena, J., Brooks, D., and Haydon, D. A. (1977). van der waals forces in oil-water systems. *J Colloid Interf Sci*, 58(1):26–35.
- Robinson, N. C. (1982). Specificity and binding affinity of phospholipids to the high-affinity cardiolipin sites of beef heart cytochrome c oxidase. *Biochemistry*, 21(1):184–8.
- Romanenko, V. G., Fang, Y., Byfield, F., Travis, A. J., Vandenberg, C. A., Rothblat, G. H., and Levitan, I. (2004). Cholesterol sensitivity and lipid raft targeting of Kir2.1 channels. *Biophysical Journal*, 87(6):3850–61.
- Ruknudin, A., Song, M. J., and Sachs, F. (1991). The ultrastructure of patch-clamped membranes: a study using high voltage electron microscopy. *J Cell Biol*, 112(1):125–34.
- Ruta, V., Jiang, Y., Lee, A., Chen, J., and Mackinnon, R. (2003). Functional analysis of an archaebacterial voltage-dependent K⁺ channel. *Nature*, 422(6928):180–5.
- Ruta, V. and Mackinnon, R. (2004). Localization of the voltage-sensor toxin receptor on KvAP. *Biochemistry*, 43(31):10071–9.
- Sadeghi, A., Doyle, A. D., and Johnson, B. D. (2002). Regulation of the cardiac L-type Ca²⁺ channel by the actin-binding proteins alpha-actinin and dystrophin. *Am J Physiol Cell Physiol*, 282(6):C1502–11.
- Sakmann, B. and Neher, E. (1984). Patch clamp techniques for studying ionic channels in excitable membranes. *Annu Rev Physiol*, 46:455–72.
- Sakmann, B. and Neher, E. (1995). *Single-channel recording*. Plenum Press.

- Samsonov, A. V., Mihalyov, I., and Cohen, F. S. (2001). Characterization of cholesterol-sphingomyelin domains and their dynamics in bilayer membranes. *Biophysical Journal*, 81(3):1486–500.
- Sasaki, M., Takagi, M., and Okamura, Y. (2006). A voltage sensor-domain protein is a voltage-gated proton channel. *Science*, 312(5773):589–92.
- Schmidt, D., Jiang, Q.-X., and Mackinnon, R. (2006). Phospholipids and the origin of cationic gating charges in voltage sensors. *Nature*, 444(7120):775–9.
- Schmidt, D. and Mackinnon, R. (2008). Voltage-dependent K⁺ channel gating and voltage sensor toxin sensitivity depend on the mechanical state of the lipid membrane. *Proceedings of the National Academy of Sciences of the United States of America*, 105(49):19276–81.
- Schoppa, N. E., McCormack, K., Tanouye, M. A., and Sigworth, F. J. (1992). The size of gating charge in wild-type and mutant Shaker potassium channels. *Science*, 255(5052):1712–5.
- Schoppa, N. E. and Sigworth, F. J. (1998a). Activation of shaker potassium channels. i. Characterization of voltage-dependent transitions. *J Gen Physiol*, 111(2):271–94.
- Schoppa, N. E. and Sigworth, F. J. (1998b). Activation of Shaker potassium channels. ii. Kinetics of the V2 mutant channel. *J Gen Physiol*, 111(2):295–311.
- Schoppa, N. E. and Sigworth, F. J. (1998c). Activation of Shaker potassium channels. iii. an activation gating model for wild-type and V2 mutant channels. *J Gen Physiol*, 111(2):313–42.
- Schroeder, H., Leventis, R., Rex, S., Schelhaas, M., Nägele, E., Waldmann, H., and Silvius, J. R. (1997). S-Acylation and plasma membrane targeting of the farnesylated carboxyl-terminal peptide of N-ras in mammalian fibroblasts. *Biochemistry*, 36(42):13102–9.
- Schubert, T. and Akopian, A. (2004). Actin filaments regulate voltage-gated ion channels in salamander retinal ganglion cells. *Neuroscience*, 125(3):583–90.
- Schütz, G. J., Kada, G., Pastushenko, V. P., and Schindler, H. (2000). Properties of lipid microdomains in a muscle cell membrane visualized by single molecule microscopy. *EMBO J*, 19(5):892–901.

- Sens, P. and Turner, M. S. (2004). Theoretical model for the formation of caveolae and similar membrane invaginations. *Biophysical Journal*, 86(4):2049–57.
- Sens, P. and Turner, M. S. (2006). Budded membrane microdomains as tension regulators. *Physical review E, Statistical, nonlinear, and soft matter physics*, 73(3 Pt 1):031918.
- Sharif-Naeini, R., Folgering, J. H. A., Bichet, D., Duprat, F., Lauritzen, I., Arhatte, M., Jodar, M., Dedman, A., Chatelain, F. C., Schulte, U., Retailleau, K., Loufrani, L., Patel, A., Sachs, F., Delmas, P., Peters, D. J. M., and Honoré, E. (2009). Polycystin-1 and -2 dosage regulates pressure sensing. *Cell*, 139(3):587–96.
- Sharma, D. K., Choudhury, A., Singh, R. D., Wheatley, C. L., Marks, D. L., and Pagano, R. E. (2003). Glycosphingolipids internalized via caveolar-related endocytosis rapidly merge with the clathrin pathway in early endosomes and form microdomains for recycling. *J Biol Chem*, 278(9):7564–72.
- Shcherbatko, A., Ono, F., Mandel, G., and Brehm, P. (1999). Voltage-dependent sodium channel function is regulated through membrane mechanics. *Biophysical Journal*, 77(4):1945–59.
- Sidi, S., Friedrich, R. W., and Nicolson, T. (2003). NompC TRP channel required for vertebrate sensory hair cell mechanotransduction. *Science*, 301(5629):96–9.
- Sigworth, F. J. (1980). The variance of sodium current fluctuations at the node of Ranvier. *J Physiol (Lond)*, 307:97–129.
- Sigworth, F. J. (1994). Voltage gating of ion channels. *Q Rev Biophys*, 27(1):1–40.
- Simmonds, A. C., East, J. M., Jones, O. T., Rooney, E. K., McWhirter, J., and Lee, A. G. (1982). Annular and non-annular binding sites on the (Ca²⁺ - Mg²⁺)-ATPase. *Biochim Biophys Acta*, 693(2):398–406.
- Simmonds, A. C., Rooney, E. K., and Lee, A. G. (1984). Interactions of cholesterol hemisuccinate with phospholipids and (Ca²⁺ - Mg²⁺)-ATPase. *Biochemistry*, 23(7):1432–41.
- Simons, K. and Ikonen, E. (1997). Functional rafts in cell membranes. *Nature*, 387(6633):569–72.
- Simons, K. and Toomre, D. (2000). Lipid rafts and signal transduction. *Nat Rev Mol Cell Biol*, 1(1):31–9.

- Simons, K. and van Meer, G. (1988). Lipid sorting in epithelial cells. *Biochemistry*, 27(17):6197–202.
- Singer, S. J. and Nicolson, G. L. (1972). The fluid mosaic model of the structure of cell membranes. *Science*, 175(23):720–31.
- Sokabe, M. and Sachs, F. (1990). The structure and dynamics of patch-clamped membranes: a study using differential interference contrast light microscopy. *J Cell Biol*, 111(2):599–606.
- Solsona, C., Innocenti, B., and Fernández, J. M. (1998). Regulation of exocytotic fusion by cell inflation. *Biophysical Journal*, 74(2 Pt 1):1061–73.
- Somerharju, P., Virtanen, J. A., and Cheng, K. H. (1999). Lateral organisation of membrane lipids. The superlattice view. *Biochim Biophys Acta*, 1440(1):32–48.
- Suchyna, T. M., Tape, S. E., Koeppe, R. E., Andersen, O. S., Sachs, F., and Götterlieb, P. A. (2004). Bilayer-dependent inhibition of mechanosensitive channels by neuroactive peptide enantiomers. *Nature*, 430(6996):235–40.
- Sukharev, S. I., Sigurdson, W. J., Kung, C., and Sachs, F. (1999). Energetic and spatial parameters for gating of the bacterial large conductance mechanosensitive channel, MscL. *J Gen Physiol*, 113(4):525–40.
- Sunshine, C. and McNamee, M. G. (1994). Lipid modulation of nicotinic acetylcholine receptor function: the role of membrane lipid composition and fluidity. *Biochim Biophys Acta*, 1191(1):59–64.
- Swartz, K. J. and Mackinnon, R. (1997a). Hanatoxin modifies the gating of a voltage-dependent K⁺ channel through multiple binding sites. *Neuron*, 18(4):665–73.
- Swartz, K. J. and Mackinnon, R. (1997b). Mapping the receptor site for hanatoxin, a gating modifier of voltage-dependent K⁺ channels. *Neuron*, 18(4):675–82.
- Tabarean, I., Juranka, P. F., and Morris, C. E. (1999). Membrane stretch affects gating modes of a skeletal muscle sodium channel. *Biophysical Journal*, 77(2):758–74.
- Tabarean, I. and Morris, C. E. (2002). Membrane stretch accelerates activation and slow inactivation in Shaker channels with S3-S4 linker deletions. *Biophysical Journal*, 82(6):2982.

- Takimoto, K., Yang, E.-K., and Conforti, L. (2002). Palmitoylation of KChIP splicing variants is required for efficient cell surface expression of Kv4.3 channels. *J Biol Chem*, 277(30):26904–11.
- Tao, X. and Mackinnon, R. (2008). Functional analysis of Kv1.2 and paddle chimera Kv channels in planar lipid bilayers. *J Mol Biol*, 382(1):24–33.
- Tavernarakis, N. and Driscoll, M. (1997). Molecular modeling of mechanotransduction in the nematode *Caenorhabditis elegans*. *Annu Rev Physiol*, 59:659–89.
- Terakawa, S. and Nakayama, T. (1985). Are axoplasmic microtubules necessary for membrane excitation? *J Membr Biol*, 85(1):65–77.
- Tian, L., Coghill, L. S., McClafferty, H., MacDonald, S. H.-F., Antoni, F. A., Ruth, P., Knaus, H.-G., and Shipston, M. J. (2004). Distinct stoichiometry of BKCa channel tetramer phosphorylation specifies channel activation and inhibition by cAMP-dependent protein kinase. *Proceedings of the National Academy of Sciences of the United States of America*, 101(32):11897–902.
- Ursell, T., Phillips, R., Kondev, J., Reeves, D., Wiggins, P., Kamkin, A., and Kiselva, I. (2008). *Mechanosensitivity in Cells and Tissues 1: Mechanosensitive Ion Channels*. Springer Netherlands.
- Valiyaveetil, F. I., Zhou, Y., and Mackinnon, R. (2002). Lipids in the structure, folding, and function of the KcsA K⁺ channel. *Biochemistry*, 41(35):10771–7.
- van den Brink-van der Laan, E., Dalbey, R. E., Demel, R. A., Killian, J. A., and de Kruijff, B. (2001). Effect of nonbilayer lipids on membrane binding and insertion of the catalytic domain of leader peptidase. *Biochemistry*, 40(32):9677–84.
- van Meer, G., Voelker, D. R., and Feigenson, G. W. (2008). Membrane lipids: where they are and how they behave. *Nat Rev Mol Cell Biol*, 9(2):112–24.
- Virtanen, J. A., Cheng, K. H., and Somerharju, P. (1998). Phospholipid composition of the mammalian red cell membrane can be rationalized by a superlattice model. *Proc Natl Acad Sci USA*, 95(9):4964–9.
- Volonte, D., Galbiati, F., Li, S., Nishiyama, K., Okamoto, T., and Lisanti, M. P. (1999). Flotillins/cavatellins are differentially expressed in cells and tissues and form a hetero-oligomeric complex with caveolins in vivo. Characterization and

- epitope-mapping of a novel flotillin-1 monoclonal antibody probe. *J Biol Chem*, 274(18):12702–9.
- Walker, R. G., Willingham, A. T., and Zuker, C. S. (2000). A *Drosophila* mechanosensory transduction channel. *Science*, 287(5461):2229–34.
- Wan, X., Juranka, P., and Morris, C. E. (1999). Activation of mechanosensitive currents in traumatized membrane. *Am J Physiol*, 276(2 Pt 1):C318–27.
- Wang, J. A., Lin, W., Morris, T., Banderali, U., Juranka, P. F., and Morris, C. E. (2009). Membrane trauma and Na⁺ leak from Nav1.6 channels. *Am J Physiol Cell Physiol*, 297(4):C823–34.
- Wang, Y., Roman, R., Lidofsky, S. D., and Fitz, J. G. (1996). Autocrine signaling through ATP release represents a novel mechanism for cell volume regulation. *Proceedings of the National Academy of Sciences of the United States of America*, 93(21):12020–5.
- Wee, C. L., Gavaghan, D., and Sansom, M. S. P. (2008). Lipid bilayer deformation and the free energy of interaction of a Kv channel gating-modifier toxin. *Biophys J*, 95(8):3816–26.
- Wiggins, P. A. and Phillips, R. (2005). Membrane-protein interactions in mechanosensitive channels. *Biophysical Journal*, 88(2):880–902.
- Williamson, I. M., Alvis, S. J., East, J. M., and Lee, A. G. (2002). Interactions of phospholipids with the potassium channel KcsA. *Biophysical Journal*, 83(4):2026–38.
- Wolfe, J. and Steponkus, P. (1983). Mechanical Properties of the Plasma Membrane of Isolated Plant Protoplasts : Mechanism of Hyperosmotic and Extracellular Freezing Injury. *PLANT PHYSIOLOGY*, 71(2):276–285.
- Wong, W. and Schlichter, L. C. (2004). Differential recruitment of Kv1.4 and Kv4.2 to lipid rafts by PSD-95. *J Biol Chem*, 279(1):444–52.
- Wood, S. J. and Slater, C. R. (1998). beta-Spectrin is colocalized with both voltage-gated sodium channels and ankyrinG at the adult rat neuromuscular junction. *J Cell Biol*, 140(3):675–84.
- Wu, L., Bauer, C. S., Guang Zhen, X., Xie, C., and Yang, J. (2002). Dual regulation of voltage-gated calcium channels by Ptdins(4,5)P2. *Nature*, 419(6910):947–52.

- Wymann, M. P. and Schneider, R. (2008). Lipid signalling in disease. *Nat Rev Mol Cell Biol*, 9(2):162–76.
- Xu, Y., Ramu, Y., and Lu, Z. (2008). Removal of phospho-head groups of membrane lipids immobilizes voltage sensors of K⁺ channels. *Nature*, 451(7180):826–9.
- Yarbrough, T. L., Lu, T., Lee, H.-C., and Shibata, E. F. (2002). Localization of cardiac sodium channels in caveolin-rich membrane domains: regulation of sodium current amplitude. *Circulation Research*, 90(4):443–9.
- Yellen, G., Sodickson, D., Chen, T. Y., and Jurman, M. E. (1994). An engineered cysteine in the external mouth of a K⁺ channel allows inactivation to be modulated by metal binding. *Biophysical Journal*, 66(4):1068–75.
- Yifrach, O. and Mackinnon, R. (2002). Energetics of pore opening in a voltage-gated K(+) channel. *Cell*, 111(2):231–9.
- Young, R. M., Holowka, D., and Baird, B. (2003). A lipid raft environment enhances Lyn kinase activity by protecting the active site tyrosine from dephosphorylation. *J Biol Chem*, 278(23):20746–52.
- Zagotta, W. N., Hoshi, T., and Aldrich, R. W. (1994a). Shaker potassium channel gating. iii: Evaluation of kinetic models for activation. *J Gen Physiol*, 103(2):321–62.
- Zagotta, W. N., Hoshi, T., Dittman, J., and Aldrich, R. W. (1994b). Shaker potassium channel gating. ii: Transitions in the activation pathway. *J Gen Physiol*, 103(2):279–319.
- Zhang, L., Lee, J.-K., John, S. A., Uozumi, N., and Kodama, I. (2004). Mechanosensitivity of GIRK channels is mediated by protein kinase C-dependent channel-phosphatidylinositol 4,5-bisphosphate interaction. *J Biol Chem*, 279(8):7037–47.
- Zhang, Y., Gao, F., Popov, V. L., Wen, J. W., and Hamill, O. (2000). Mechanically gated channel activity in cytoskeleton-deficient plasma membrane blebs and vesicles from *Xenopus* oocytes. *J Physiol (Lond)*, 523 Pt 1:117–30.
- Zhang, Y. and Hamill, O. (2000). On the discrepancy between whole-cell and membrane patch mechanosensitivity in *Xenopus* oocytes. *The Journal of Physiology Online*, 523(1):101.

Zhou, J. Y., Potts, J. F., Trimmer, J. S., Agnew, W. S., and Sigworth, F. J. (1991). Multiple gating modes and the effect of modulating factors on the microi sodium channel. *Neuron*, 7(5):775–85.